

---

**Systematic derivation of generalized  
 $t$ - $J$  models from Hubbard models  
in one and two dimensions at and  
away from half-filling**

---

Simone Anke Hamerla

2009



Berichterstatter:

Prof. Dr. G.S. Uhrig

Prof. Dr. W. Weber

# Contents

<b>1. Introduction</b>	<b>6</b>
<b>2. The fermionic Hubbard Model</b>	<b>9</b>
2.1. Generalized $t$ - $J$ model . . . . .	10
<b>3. Continuous Unitary Transformations</b>	<b>12</b>
3.1. Introduction . . . . .	12
3.2. Derivation of the flow equation . . . . .	12
3.3. Generators . . . . .	14
3.3.1. Mielke Knetter Uhrig generator . . . . .	14
3.3.2. Importance of the ROD . . . . .	17
3.3.3. $0n$ generator . . . . .	19
3.3.4. $0n1n$ generator . . . . .	20
3.4. Truncation scheme . . . . .	22
<b>4. Application of the method to the Hubbard model</b>	<b>24</b>
4.1. Quasiparticle description . . . . .	24
4.1.1. MKU generator . . . . .	26
4.1.2. $0n$ generator and $0n1n$ generator . . . . .	26
4.2. Reference ensemble and normal-ordering . . . . .	27
4.3. Truncation schemes . . . . .	29
4.4. Implementation . . . . .	31
4.5. Minimal model . . . . .	36
4.6. NN model . . . . .	40
4.6.1. Results for the NN truncation . . . . .	43
4.7. Results for the one dimensional linear chain at half-filling . . . . .	44
4.7.1. Higher truncation schemes . . . . .	44
4.8. Results for the half-filled two-dimensional square lattice . . . . .	56
4.8.1. Results obtained by the use of the MKU generator . . . . .	56
4.8.2. $0n$ generator and $0n1n$ generator . . . . .	65
4.9. Chapter conclusion . . . . .	79
<b>5. Away from half-filling</b>	<b>80</b>
5.1. Results for the linear chain away from half-filling . . . . .	83
5.2. Results for the two-dimensional square lattice in the case of hole doping . . . . .	86
5.2.1. Results for the MKU generator . . . . .	86

---

5.2.2. Results for the $0n$ and the $0n1n$ generator . . . . .	94
5.3. Chapter conclusion . . . . .	100
<b>6. Charge gap</b>	<b>101</b>
6.1. Charge gap in the half-filled case . . . . .	103
6.2. Charge gap in the case of doping . . . . .	106
6.3. Implementation . . . . .	107
6.4. Results for the charge gap . . . . .	108
6.4.1. One-dimensional linear chain . . . . .	108
6.4.2. Results for the two-dimensional square lattice . . . . .	112
6.5. Chapter conclusion . . . . .	117
<b>7. Summary and outlook</b>	<b>118</b>
<b>8. Abstract</b>	<b>120</b>
<b>A. Additional results for the coupling constants in 2d for different genera-</b> <b>tors</b>	<b>122</b>
<b>Bibliography</b>	<b>124</b>
<b>Danksagungen</b>	<b>128</b>
<b>Erklärung</b>	<b>129</b>

# 1. Introduction

The task of solid state physics is to explain the intrinsic properties of solid state materials. Containing a macroscopic number ( $10^{23}$ ) of electrons and nuclei these materials have to be described by many body theories. For an accurate description of such a many body system a theory based on quantum mechanics is needed.

In solid state physics the full Hamiltonian describing the behavior of the solids is known. Due to the overwhelming number of particles incorporated in these systems a complete solution is impossible as it would result in a flood of details. Consequently one does not aim at treating the Hamiltonian completely but rather at simplifying it.

One possible simplification consists in treating the electrons in the solid as independent particles resulting in single-particle descriptions of the electrons. Although this is the simplest way of treating the electrons it is appropriate to explain the formation of energy bands in crystalline solids.

On the other hand there are many effects which are not explained by this approach. The single-particle picture fails for instance to describe the properties of superconductors. Especially the fascinating features of high- $T_C$  superconductors can only be understood in the context of interacting particles. Another type of material which is not explained by one-particle theories is the Mott insulator. Due to the odd number of electrons the insulating behavior of these materials can not be understood by band theory. Especially the transition of a metal to a Mott insulator [Mot90] is driven by strong correlations. Thus real many body theories are needed to describe these materials.

Materials whose physical properties are determined by correlation effects are specified as strongly correlated electron systems. These correlations induce fascinating phenomena which are not yet fully understood.

A description of these phenomena has to incorporate the kinetics of electrons as well as the interactions between them. The resulting many body problem is too complicated to be solved exactly. To cope with the complexity of this problem approximations have to be made. These lead to simplified models which are restricted to the most important degrees of freedom of the original system.

Finding such a paradigmatic model for a given system is a demanding task itself. An example for such a paradigmatic model is the Hubbard model, which is particularly used in the context of high- $T_C$  cuprate superconductors [Eme87,ZR88]. The properties of cuprates are governed to a large extent by a layered structure of two dimensional copper-oxide planes. The two-dimensional one band Hubbard model serves as a model describing these planes.

The reduction of the full Hamiltonian to the Hubbard Hamiltonian (see chapter 2) is based on restricting the electrons to one orbital and reducing the repulsive interaction between electrons to an on-site interaction. The use of an on-site repulsion instead of the long range Coulomb interaction is justified by screening effects. Due to the fact that it combines a repulsive part with a kinetic part the Hubbard model explains many features. Especially the physics of Mott insulators and antiferromagnets are explained by this model.

Motivated by the great variety of properties, which are governed by strong correlation effects, many new techniques for the solution of this paradigmatic model have been developed.

These techniques include quantum Monte-Carlo methods and exact diagonalization. Both methods lack a description of the thermodynamic limit as they are restricted to small systems. Another group of methods are renormalization group approaches. In the case of strongly correlated electron systems these methods might lead to diverging coupling constants. In addition to these methods perturbative approaches were followed. Problems with these methods are caused by the fact that they are only valid in certain parameter ranges.

In this thesis *self-similar continuous unitary transformations* (sCUT) are used. This method combines renormalization group methods with perturbative approaches. The sCUT method provides the possibility to derive an effective model which can then be used as starting point for further calculations. Another advantage of the sCUT lies in the fact, that it is valid on all energy scales.

Starting from the Hubbard model an effective  $t$ - $J$  model is derived in a systematic fashion. In contrast to work done before on the  $t$ - $J$  model, the results obtained in this thesis are reliable even for larger values of the bandwidth  $W$ . This is due to the self-similar approach.

Beyond the spin interactions the effective  $t$ - $J$  model derived in this thesis provides a systematic treatment of the motion of holes or doubly occupied sites. Moreover it also captures the interaction of holes or doubly occupied sites.

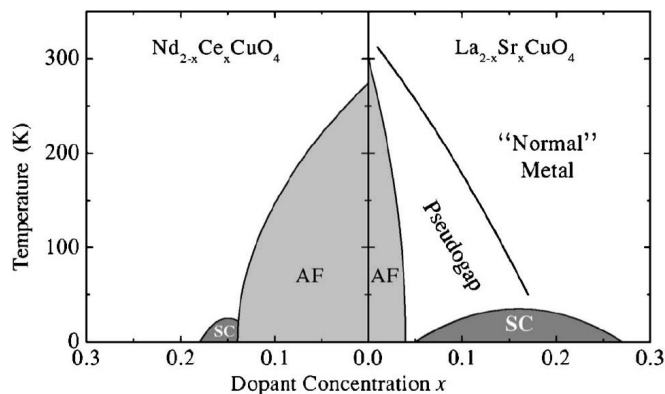


Fig. 1.1.: Doping dependence of the phase diagram for high- $T_C$  cuprate superconductors [DHS03]. AF denotes the antiferromagnetic state and SC stands for the superconducting phase. The doping corresponds to hole doping on the right hand side and to electron doping on the left hand side.

Starting from a doped Hubbard model the sCUT method provides a tool to analyze the influence of doping on the coupling constants of the effective model. As a result the applicability of the approach is significantly enhanced.

In this way the foundations for the quantitative understanding of the doping dependences, for instance in the high- $T_C$  cuprates, is laid. The doping dependence of high- $T_C$  cuprates has been observed by Damascelli et al. [DHS03] (see Fig. 1.1).

## 2. The fermionic Hubbard Model

The Hubbard model was introduced in 1963 independently by J. Hubbard, J. Kanamori and M.C.Gutzwiller [Hub63, Hub64, Kan63, Gut63]. Originally the Hubbard model was intended to describe ferromagnetism and to explain why a system with an odd number of electrons shows insulating behavior. From band theory one would expect that such a system with a partly filled conduction band behaves like a metal. As band theory fails in this case, correlation terms between electrons had to be included. Therefore an on-site repulsion of two electrons was added to the kinetic term. This led to the fermionic Hubbard model.

The Hubbard Hamiltonian describes electrons with spin  $\sigma$  on lattice site  $i$  by the use of their creation  $c_{i\sigma}^\dagger$  and annihilation operators  $c_{i\sigma}$ . It consists of two terms, describing the kinetics ( $H_t$ ) and the correlation effects ( $H_U$ ).

$$H = H_t + H_U \quad (2.0.1)$$

$$H_t = t \sum_{\langle i,j \rangle} (\hat{c}_{i\sigma}^\dagger \hat{c}_{j\sigma} + h.c.) \quad (2.0.2)$$

$$H_U = U \sum_i \left( \hat{n}_{i,\uparrow} - \frac{1}{2} \right) \left( \hat{n}_{i,\downarrow} - \frac{1}{2} \right) \quad (2.0.3)$$

The kinetic part  $H_t$  describes the hopping of an electron with spin  $\sigma$  from site  $j$  to site  $i$  and vice versa. This hopping process can only take place if site  $i$  and  $j$  are nearest neighbors as indicated by the bracket under the sum.

The corresponding hopping element is denoted by  $t$ . The bandwidth of the model is given by  $W = 2zt$  where  $z$  labels the coordination number of the considered lattice. For a one-dimensional linear chain the coordination number takes the value  $z = 2$  and thus  $W = 4t$  whereas in the case of a two-dimensional square lattice the coordination number is  $z = 4$  resulting in the bandwidth  $W = 8t$ . In actual calculations energies are often given in units of the bandwidth.

The second term  $H_U$  determines the repulsion between electrons on the same site. In  $H_U$  the counting operator is given by  $\hat{n}_{i,\sigma} = \hat{c}_{i,\sigma}^\dagger \hat{c}_{i,\sigma}$ . This indicates that putting two electrons with opposite spin on one site costs the energy  $U$ .

In one dimension the Hubbard model can be solved exactly by the use of a Bethe ansatz as has been done by Lieb and Wu [LW68]. For dimensions greater than two a phase diagram can be deduced from various mean-field calculations. A schematic phase diagram at half-filling is shown in Fig. 2.1.

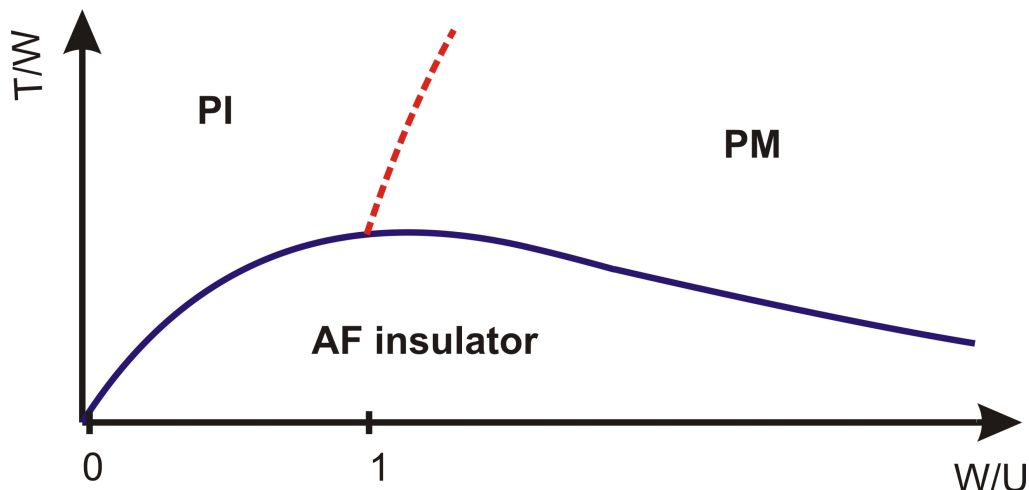


Fig. 2.1.: Schematic phase diagram of the Hubbard model [GKKR96]. PI denotes the paramagnetic insulator. PM stands for the paramagnetic metal and AF denotes the Antiferromagnet with long range order.

In the case of strong interaction and half-filling, which means one electron per site, the system is a paramagnetic insulator as the energy costs for the creation of a doubly occupied site are too high. In the opposite case, where the interaction tends to zero, the Hubbard model describes free electrons.

Including the movement and the interaction of electrons on a lattice the Hubbard model is able to explain the Mott-metal-insulator transition [IFT98]. The model is also applied to transition metal compounds. In the last years the most important field of application is the field of high- $T_C$  cuprate superconductors [BM86, LNW06]. The central part of high- $T_C$  superconductors are two-dimensional copper-oxide planes which are decoupled from each other. According to Anderson these materials can be described by a one-band Hubbard model [And87].

The aim of this thesis is to map the Hubbard model to an effective model by eliminating charge fluctuations.

## 2.1. Generalized $t$ - $J$ model

In the Hubbard model there are four possible configurations at one site. The site may be singly occupied by one electron with spin up or spin down, doubly occupied by two electrons with opposite spin or empty. The last two configurations correspond to charge fluctuations. Both cases are referred to as double occupancies (DO) in this thesis.

Eliminating these charge fluctuations leads to an effective model, which conserves the number of double occupancies. The effective model is a generalized  $t$ - $J$  model which is based on the Heisenberg model. This model describes interactions between spins on neighboring sites. In the effective  $t$ - $J$  model processes that change the number of double occupancies are eliminated but it still contains the spin degrees of freedom of the electrons and the motion and interaction of double occupancies and holes. Moreover the generalized

$t$ - $J$  model contains correlations between two spins with a displacement larger than two and real four spin interaction terms.

In the limit of a half-filled lattice and a large repulsion the effective model reduces to the Heisenberg model.

It is important to take the properties of the initial model into account. If one starts the mapping from a parameter range where the Hubbard model shows metallic properties it is not reasonable to eliminate charge fluctuations as creating them does not cause energy costs in this region. Therefore it is necessary to make sure that the characteristic parameters  $U$  and  $t$  are adjusted to the regime where charge fluctuations are essentially suppressed.

The mapping to the effective  $t$ - $J$  model is done by the method of self-similar continuous unitary transformations which will be explained in the following chapter.

## 3. Continuous Unitary Transformations

### 3.1. Introduction

Starting from a parameter range where the Hubbard model shows insulating behavior the effective  $t$ - $J$  model is derived by eliminating charge fluctuations.

This elimination is done by applying CUT-methods to the original model. In solid state physics continuous unitary transformations are used to derive effective Hamiltonians which are easier to solve than the original one [Weg94, KSU03, Keh06].

The effective model is reached by a systematic change of the basis in which the Hamiltonian is represented. This change is performed by the use of a continuous unitary transformation as will be explained below.

### 3.2. Derivation of the flow equation

The flow equation method was introduced in 1994 by Wegner [Weg94] for solid state problems and independently by Glazek and Wilson [GW93, GW94], who developed this method for problems in high-energy physics. The aim is to convert the original Hamiltonian to an effective Hamiltonian. At best the flow equation method leads to an effective Hamiltonian that is diagonal or at least as close to diagonality as possible. During the transformation the properties of the model must not be changed. That is why a method has to be used that leaves the eigenvalues of the Hamiltonian invariant.

One way to fulfill this constraint is to use unitary transformations  $\hat{U}$  with  $\hat{U}^{-1} = \hat{U}^\dagger$  [Frö52]. The effective Hamiltonian is given by

$$H_{\text{eff}} := \hat{U} H \hat{U}^{-1}.$$

This transformation corresponds to a change of the basis in which the Hamiltonian is represented.

If necessary it is possible to combine multiple unitary transformations  $\hat{U}_1 \dots \hat{U}_i$  by applying them one after another.

This concept of applying several unitary transformations  $\hat{U}_1 \dots \hat{U}_i$  was generalized by Wegner, Glazek and Wilson. They created a continuous unitary transformation based on the use of a continuous flow parameter  $\ell$ .

In this way the Hamiltonian as well as the transformation  $\hat{U}$  become a function of the flow parameter

$$H(\ell) = \hat{U}(\ell) H \hat{U}(\ell)^\dagger. \tag{3.2.1}$$

The associated derivative with respect to  $\ell$  reads

$$\begin{aligned}\frac{dH(\ell)}{d\ell} &= \frac{d\hat{U}(\ell)}{d\ell} H \hat{U}(\ell)^\dagger + \hat{U}(\ell) H \frac{d\hat{U}(\ell)^\dagger}{d\ell} \\ &= \frac{d\hat{U}(\ell)}{d\ell} \hat{U}(\ell)^\dagger \hat{U}(\ell) H \hat{U}(\ell)^\dagger + \hat{U}(\ell) \hat{U}(\ell)^\dagger \hat{U}(\ell) H \frac{d\hat{U}(\ell)^\dagger}{d\ell}.\end{aligned}$$

Now a generator  $\eta(\ell) = \frac{d\hat{U}(\ell)}{d\ell} \hat{U}(\ell)^\dagger$  is introduced leading to

$$\frac{dH(\ell)}{d\ell} = \eta(\ell) H(\ell) + H(\ell) \eta(\ell)^\dagger. \quad (3.2.2)$$

This formula can be simplified using the properties of the generator  $\eta$ . Starting from the unitarity of  $\hat{U}(\ell)$  we can conclude

$$\begin{aligned}\frac{d}{d\ell} \underbrace{\left( \hat{U}(\ell) \hat{U}(\ell)^\dagger \right)}_{\mathbb{1}} &= 0 \\ &= \underbrace{\left( \frac{d}{d\ell} \hat{U}(\ell) \right)}_{\eta(\ell)} \hat{U}(\ell)^\dagger + \hat{U}(\ell) \underbrace{\frac{d}{d\ell} \hat{U}(\ell)^\dagger}_{\eta^\dagger(\ell)} \\ \Rightarrow \eta(\ell) &= -\eta(\ell)^\dagger,\end{aligned}$$

which means that the generator has to be antihermitian.

With this property equation 3.2.2 can be rewritten using a commutator

$$\frac{dH(\ell)}{d\ell} = [\eta(\ell), H(\ell)]. \quad (3.2.3)$$

The transformation of the Hamiltonian is given by this first order differential equation, the so-called *flow equation*. The transformation starts with the initial Hamiltonian  $H(0) = H$ . This continuous unitary transformation corresponds to performing infinitely many infinitesimal transformations of the form  $e^{\eta(\ell)d\ell}$  with the generator  $\eta(\ell)$ . Therefore the transformation can be stopped at an arbitrary value of the flow parameter  $\ell$  but for  $\ell$  equal to infinity we call the corresponding Hamiltonian the effective Hamiltonian  $H(\ell = \infty) = H_{\text{eff}}$ . If the transformation is stopped at a smaller value of  $\ell$  there might still be finite contributions from the terms we wanted to eliminate.

The advantage of the continuous version of the unitary transformation lies in the fact, that the transformation itself is readjusted to the flowing Hamiltonian  $H(\ell)$  for every value of  $\ell$ .

Up to now we just shifted the problem from choosing an appropriate transformation  $\hat{U}$  to choosing a suitable generator  $\eta$ . From equation 3.2.3 it is obvious that the transformation stops when the commutator of the generator with the Hamiltonian vanishes  $[\eta(\ell), H(\ell)] = 0$ . This implies that the generator and the Hamiltonian have a common set of eigenstates. As a consequence of this the structure of the effective Hamiltonian  $H_{\text{eff}}$  is determined by the choice of the generator  $\eta$ . With a given generator predictions concerning the effective model can be made even before the transformation is performed.

### 3.3. Generators

As explained in the previous section the structure of the effective Hamiltonian is governed by the choice of the generator. A famous choice for the generator is the one originally used by Wegner [Weg94]. Trying to diagonalize the Hamiltonian Wegner partitioned the Hamiltonian into a diagonal  $H_d$  and a non-diagonal part  $H_{nd}$

$$H = H_d + H_{nd}. \quad (3.3.1)$$

The generator is constructed by taking the commutator of the diagonal part, which is kept, and the non-diagonal part, which we want to eliminate. This leads to the following expression for the generator

$$\eta_W(\ell) := [H_d(\ell), H_{nd}(\ell)] = [H_d(\ell), H(\ell)] \quad (3.3.2)$$

which defines the matrix element  $\eta(\ell)_{ij}$  of the generator as

$$\eta(\ell)_{ij} = (h_{i,i}(\ell) - h_{j,j}(\ell))h_{i,j}(\ell). \quad (3.3.3)$$

In order to use this generator one has to define which part of the Hamiltonian is seen as the diagonal part. As we use unitary transformations the trace  $tr(H^2)$  does not depend on  $\ell$ . Based on this observation the convergence of a CUT using this generator can be proven [Weg94, KM94]. If the transformation converges  $H$  commutes with its diagonal part  $H_d$ .

In the non-degenerate case a transformation with this generator thus leads to a diagonal effective Hamiltonian [Weg94, DU04]. In the case of degeneracies  $h_{i,i}(\ell) = h_{k,k}(\ell)$  the right hand side of equation 3.3.3 (and consequently the generator) vanishes. In this case one can still deduce an effective model but there is no general argument how the component  $h_{i,k}$  will evolve during the transformation. Thus no predictions about this component of the effective model can be made.

#### 3.3.1. Mielke Knetter Uhrig generator

The MKU generator was introduced in the context of a perturbative approach for the CUT method [KU00]. Starting from a perturbed Hamiltonian with the perturbation parameter  $\lambda$ , the terms are classified according to the order of  $\lambda$  of their prefactors. For this approach the spectrum of the unperturbed part of the Hamiltonian has to be bounded from below.

Mielke [Mie98] introduced a generator whose main advantage is that it benefits from the initial structure of the Hamiltonian. He considered a Hamiltonian in band matrix form. For a band matrix  $H$  it is known that  $h_{i,j}(0) = 0$  for  $|i - j| > \Delta_{max} \in \mathbb{N}$  for some maximal value  $\Delta_{max}$ . Performing a CUT calculation with the MKU generator this structure will be conserved during the flow. During the flow only terms which do not affect this structure can arise. This restricts the amount of new terms. In contrast to this the Wegner generator destroys this structure in general making the calculations more

complicated.

Knetter and Uhrig independently translated this idea for the choice of the generator into the quasiparticle language. This led to the MKU generator. For a treatment with the MKU generator the problem has to be translated into the quasiparticle language. What the quasiparticles look like depends on the system under study.

As a new quantum number we introduce the number of quasiparticles that are present in a certain state. It is useful to introduce an operator  $\hat{Q}$  counting the number of quasiparticles. Now the eigenstates  $\{|i\rangle\}$  of the operator  $\hat{Q}$  are used as new basis vectors. The corresponding eigenvalues are denoted by  $q_i$ . Translating the Hamiltonian into this basis yields

$$h_{ij}(\ell) = \langle i | \hat{H}(\ell) | j \rangle. \quad (3.3.4)$$

The terms in the Hamiltonian can be organized in blocks according to their effect on the number of quasiparticles. As an example we consider the block  $\{i, j\}$ . Terms in this block create  $i$  quasiparticles and destroy  $j$  quasiparticles. The  $\{0, 0\}$ -block takes a special role in this picture. If the system has a unique ground state, this block contains the ground state energy in the effective model, i.e. after the transformation. In the case of the  $t$ - $J$  model the  $\{0, 0\}$  block contains the highly degenerate subspace of magnetically disordered states. This is due to the fact that the quasiparticle vacuum, which is the phase without double occupancies, contains the full spin degrees of freedom of the electrons.

In order to eliminate all changes in the number of quasiparticles we write the generator as

$$\eta(\ell) = \left[ \hat{Q}, \hat{H}(\ell) \right]. \quad (3.3.5)$$

This choice of the generator leads to an effective model in which the number of quasiparticles is conserved (see Section 3). In the basis of the  $|q_k\rangle$  the components of the generator read

$$\begin{aligned} \eta_{ij}(\ell) &= \langle i | \hat{Q} \sum_k |k\rangle \langle k | \hat{H}(\ell) | j \rangle - \langle i | \hat{H}(\ell) \sum_k |k\rangle \langle k | \hat{Q} | j \rangle \\ &= (q_i - q_j) h_{ij}(\ell) \end{aligned}$$

with the eigenvalues  $q_i$  and  $q_j$ . Following Mielke [Mie98] and Knetter/Uhrig [KU00] a signum function is included in the MKU generator

$$\eta_{\text{MKU}}(\ell) = \text{sgn}(q_i - q_j) h_{ij}(\ell). \quad (3.3.6)$$

By the use of this generator we derive an effective model with the property

$$\lim_{\ell \rightarrow \infty} \left[ \hat{Q}, \hat{H}_{\text{eff}}(\ell) \right] = 0.$$

This implies that in the effective model sectors with different numbers of quasiparticles are decoupled from each other. Figure 3.1 provides a diagram of a Hamiltonian, that

changes the number of quasiparticles by at most two, with the terms of the generator coloured in red.

0,0	0,1	0,2	0,3	0,4
1,0	1,1	1,2	1,3	1,4
2,0	2,1	2,2	2,3	2,4
3,0	3,1	3,2	3,3	3,4
4,0	4,1	4,2	4,3	4,4

Fig. 3.1.: The MKU generator contains terms connecting subspaces with different amounts of quasiparticles (coloured in red).

The structure of the Hamiltonian at the end of the calculation is shown in Figure 3.2.

0,0				
	1,1			
		2,2		
			3,3	
				4,4

Fig. 3.2.: After the CUT with the MKU generator the Hamiltonian becomes block diagonal

In the effective model each sector can be treated separately. In this way we have to deal only with a few particles. For the one-particle energies it is sufficient to diagonalize the one-particle sector. In the same way we have to deal with  $r$  instead of  $N \gg r$  quasiparticles if we want to analyze properties of the  $r$  particle sector. Although there are much more terms in the effective model than in the original one, the solution is easier due to the decoupling of the different quasiparticle subspaces.

In the effective model the sectors with a small number of quasiparticles are described most accurately. To decide whether the description with the MKU generator is accurate, we have to check how much weight is included in these sectors. If the sectors with 0,1 or 2 quasiparticles are sufficient to capture most of the weight, the use of the MKU generator is justified.

### 3.3.2. Importance of the ROD

To illustrate the action of the generator, we analyze the effect of the flow equation on the  $ij$ -component of the Hamiltonian. We use again the representation in the eigenbasis of  $\hat{Q}$ . Inserting the definition of the generator 3.3.6 in the flow equation one obtains

$$\begin{aligned}
\frac{dh_{ij}(\ell)}{d\ell} &= \left( \eta(\ell) \hat{H}(\ell) - \hat{H}(\ell) \eta(\ell) \right)_{ij} \\
&= \sum_k \eta_{ik}(\ell) h_{kj}(\ell) - \sum_k h_{ik}(\ell) \eta_{kj}(\ell) \\
&= \sum_k \text{sgn}(q_i - q_k) h_{ik}(\ell) h_{kj}(\ell) - \sum_k \text{sgn}(q_k - q_j) h_{ik}(\ell) h_{kj}(\ell) \\
&= \text{sgn}(q_i - q_j) (h_{jj}(\ell) - h_{ii}(\ell)) h_{ij}(\ell) + \sum_{k \neq i, j} (\text{sgn}(q_i - q_k) + (q_j - q_k)) h_{ik}(\ell) h_{kj}(\ell)
\end{aligned} \tag{3.3.1}$$

At this point it is useful to sort the eigenstates according to their eigenvalue  $q_i$ . This means that  $q_i \geq q_k$  for  $i > k$ .

From this equation we can deduce a differential equation for the sum of the first  $s$  diagonal elements.

$$\frac{d}{d\ell} \sum_{i=1}^s h_{ii} = 2 \sum_{i=1}^s \sum_{k>i} \text{sgn}(q_i - q_k) |h_{ik}(\ell)|^2 \tag{3.3.2}$$

Due to the hermiticity of the Hamiltonian we substituted  $h_{ik} h_{ki}$  for  $|h_{ik}|^2$ .

According to the ordering of the eigenvalues, the right hand side of this equation is always smaller than 0. Thus the sum of the first  $s$  diagonal elements shows a monotonic decrease. Now we assume that the eigenvalues are bounded from below by  $E_0$ . This assumption is justified for realistic systems. As the sum of the eigenvalues is bounded from below the same has to be valid for the sum of the first  $s$  diagonal elements. Consequently the derivative has to vanish for  $\ell \rightarrow \infty$ . For arbitrary values of  $s$  we deduce

$$\lim_{\ell \rightarrow \infty} \text{sgn}(q_i - q_k) |h_{ik}(\ell)|^2 = 0 \quad \forall i, k : i \neq k. \tag{3.3.3}$$

There are two possibilities to fulfill this condition. First, it is possible that degeneracies  $q_i = q_k$  occur. In this case the sign function vanishes. The eigenstates  $i$  and  $k$  have the same number of quasiparticles. Consequently they belong to the same block of the effective Hamiltonian. Second, in the non-degenerate case, the component  $h_{ik}$  vanishes for  $\ell = \infty$ . This component connects different blocks with each other. In summary, there are two types of terms in the Hamiltonian. On the one hand, there are terms  $h_{i',k'}$ , with  $i'$  and  $k'$  belonging to the same block. On the other hand, there are terms  $h_{ik}$  with  $i$  and  $k$  belonging to different blocks, which are eliminated. Thus the effective Hamiltonian is block diagonal with blocks belonging to a certain number of quasiparticles, see Fig. 3.2.

As the whole generator vanishes for  $\ell \rightarrow \infty$ , we obtain a Hamiltonian that commutes with  $\hat{Q}$ . Thus  $\hat{Q}$  and  $\hat{H}$  have a common set of eigenstates. The number of quasiparticles of a certain state is a conserved quantity.

Of course it is not possible to reach the limit  $\ell = \infty$  in realistic calculations. From equation 3.3.3 it is known that all terms connecting different blocks have to vanish. These terms are called off-diagonal elements. For realistic calculations we have to know to what extent the off-diagonal elements have been eliminated for a certain  $\ell'$ . If these terms are not yet eliminated, but have very small values, they can be neglected. In this case we are close to a block diagonal Hamiltonian. The calculation can be stopped at  $\ell = \ell' < \infty$ .

As a measure for the remaining contribution of the off-diagonal terms the *residual off-diagonality* (ROD) is introduced. To calculate the ROD we sum over the squares of the coefficients of all terms in the generator. As explained before these terms are the off-diagonal terms, connecting different blocks. The ROD is the square root of this sum. Note that we already take the square root of the sum in contrast to the work of Reichl [RMHU04].

In a converging transformation the coefficients of terms in the generator decrease exponentially. This can be seen in a quickly decreasing ROD.

These arguments do not hold in cases where sectors with differing numbers of quasiparticles overlap. In this case the ROD diverges, thus terms combining different blocks are not negligible. A mapping to a quasiparticle conserving effective model is not possible anymore. For arbitrary values of  $\ell$  there will still be sizeable contributions from terms changing the number of quasiparticles in the effective Hamiltonian.

### 3.3.2.1. Ordering of energy values

The MKU generator has another important property. It orders the eigenvalues of  $\hat{H}$  according to their quasiparticle number [KU00] [Mie98]. This can be seen in equation 3.3.1. If the limit  $\ell \rightarrow \infty$  is considered, we can neglect the second term. This is justified by the quadratic dependence of this term on  $h_{ik}$ , which takes very small values in this limit

$$\partial_\ell h_{ij} \approx -\text{sgn}(q_i - q_j)(h_{ii} - h_{jj})h_{ij}. \quad (3.3.4)$$

If the transformation converges, the component  $h_{ij}$  has to vanish as seen before. This is only possible if the sign function on the right hand side of equation 3.3.4 is positive. As a result of this the energy values are ordered

$$q_i \leq q_j \Rightarrow h_{ii} \leq h_{jj}.$$

This argument is not valid for blocks which are not connected at all, i.e.  $h_{ij}$  vanishes for all values of  $\ell$  [HU02]. A case like this may result from conserved quantities like the total spin.

The ordering of the energy values may also cause problems. If the initial Hamiltonian contains overlapping multi-particle continua the ordering of the energy values according to the quasiparticle number is more problematic. In this case the different sectors can in general not be separated by this method. The breakdown of the mapping can be seen in a diverging ROD in this case.

### 3.3.3. $0n$ generator

In the quasiparticle picture the description of the sectors with a small quasiparticle number is most accurate. The idea for the use of the  $0n$  generator is that most of the weight is included in the sectors with zero or one quasiparticle. In the  $t$ - $J$  model these sectors are described most accurately. In the  $0n$ -generator we include all terms that couple to the subspace without quasiparticles. For the model under study this subspace is a true subspace and not a single ground state.

A schematic diagram for the  $0n$ -generator is shown in figure 3.3.

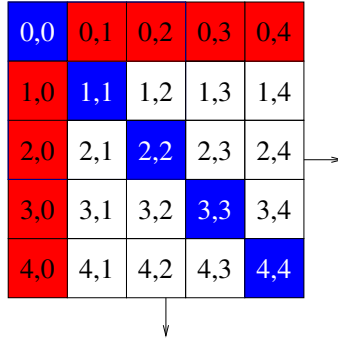


Fig. 3.3.: Schematic diagram for the  $0n$ -generator

In this picture the blocks of terms included in the generator are coloured red. One type of terms contained in the generator are terms that create  $r$  particles out of the 0 quasiparticle sector. These terms belong to the  $\{n, 0\}$  blocks. Besides also terms that annihilate  $r$  quasiparticles from the  $r$  quasiparticle sector are considered. Applying these to the  $r$  quasiparticle sector we end up in the sector without quasiparticles. These terms are found in the  $\{0, n\}$  blocks of the Hamiltonian.

According to Dawson, Eisert and Osborne [DEO08] a variational ansatz can be used to derive the generators. In this ansatz we would start from

$$\langle 0 | [\eta(\ell), \hat{H}(\ell)] | 0 \rangle$$

and minimize this expression under the constraint that the generator has to stay infinitesimal. The derivation of the generator in this work relies on the representation of the generator in matrix form.

In the context of this thesis a description of the  $0n$  generator in matrix form can cause confusion as will be explained below. To avoid this confusion the generator is represented in second quantization [FDU]. In second quantization the Hamiltonian can be written as

$$\hat{H}(\ell) = \sum_{i,j=0}^N H_j^i(\ell). \quad (3.3.1)$$

In this representation upper indices  $i$  denote the number of creation operators contained in a term. Lower indices  $j$  indicate the number of annihilation operators.

By the use of this representation the  $0n$  generator is given by

$$\eta_{0n}(\ell) = \sum_{i>0}^N (H_0^i(\ell) - H_i^0(\ell)) . \quad (3.3.2)$$

Therefore the terms included in the generator contain either only creation or only annihilation operators. In the latter case an additional sign is applied according to the MKU generator. These terms couple to the zero quasiparticle subspace. They can either create  $i$  particles out of the ground state ( $H_0^i(\ell)$ ) or annihilate  $i$  quasiparticles out of the subspace with  $i$  quasiparticles ( $H_i^0(\ell)$ ) thus ending up in the quasiparticle vacuum.

Of course these terms can also couple to other subspaces. Let us consider the term  $H_2^0(\ell)$  as an example. This term creates two quasiparticles and does not annihilate quasiparticles. Consequently this term couples the quasiparticle vacuum to the two quasiparticles subspace. However this term also couples to the subspace with one or more quasiparticles. Applied to the one quasiparticle sector this term creates two additional quasiparticles. Thus the term couples the one quasiparticle subspace to the three quasiparticle subspace and so on.

Due to the fact that the terms in the generator can also couple to other subspaces it is not possible to find a unique matrix representation for the  $0n$  generator. Therefore we restrict ourselves to the description of this generator in second quantization.

A CUT using the  $0n$  generator decouples the zero quasiparticle sector from the other sectors. At the end of the calculation this sector can be treated independently from the others (see Fig. 3.4).

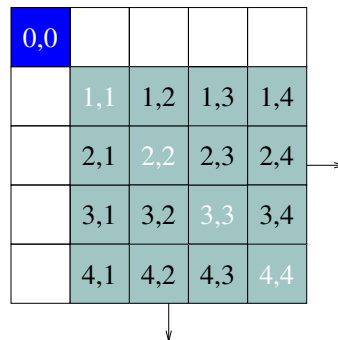


Fig. 3.4.: Hamiltonian at the end of the CUT with the  $0n$  generator

But this is not valid for the other sectors because they are still coupled with one other. Therefore one has to consider all blocks if one is interested in the one-particle energies.

### 3.3.4. $0n1n$ generator

In the  $0n1n$  generator the idea of decoupling only certain sectors from the rest is extended to the one-particle sector. This sector is treated in the same way as the zero particle sector. A diagram for the terms in the Hamiltonian can be found in Fig. 3.5.

0,0	0,1	0,2	0,3	0,4
1,0	1,1	1,2	1,3	1,4
2,0	2,1	2,2	2,3	2,4
3,0	3,1	3,2	3,3	3,4
4,0	4,1	4,2	4,3	4,4

Fig. 3.5.: Hamiltonian at the beginning of the CUT. Terms included in the generator are coloured red.

By the use of this generator the zero particle and the one particle sectors are separated from the rest (see Fig. 3.6).

0,0				
	1,1			
		2,2	2,3	2,4
		3,2	3,3	3,4
		4,2	4,3	4,4

Fig. 3.6.: Hamiltonian at the end of the CUT with the  $0n1n$  generator

After a CUT with this generator the motion of a quasiparticle can be analyzed without considering sectors with two or more quasiparticles.

A CUT using this generator is appropriate if the important processes are included in the zero or the one quasiparticle subspace.

For both generators the ROD is calculated using the terms of the generator. As we do not eliminate the other off-diagonal terms, there is no sense in including these in the measure for the convergence of the method. Hence the ROD depends on the choice of the generator used.

If the ROD vanishes during the calculation with a  $0n1n$  generator, the zero and the one quasiparticle sectors are decoupled from the other sectors, see Fig.3.6.

### 3.4. Truncation scheme

The flow equations are differential equations for the coefficients of the running Hamiltonian. During the flow new terms are arising from the commutators. These have to be included in the Hamiltonian. For  $\ell = 0$  these terms carry the coefficient 0 as they are not part of the initial Hamiltonian  $H(0)$ . In an exact treatment we would have to consider all new terms when setting up the generator and calculating the commutator of the new terms with  $\eta$ . However, there are too many terms to perform an exact calculation except for very small systems.

Thus we have to bound the amount of terms. A truncation scheme has to be defined to decide which of the new terms have to be discarded. This scheme is used to specify the relevance of a term. With the truncation scheme a closed set of differential equations is obtained, which can then be solved numerically.

One possibility is to use a perturbative truncation scheme [KU00, Ste97, KSU03]. In this truncation scheme the terms are specified according to the order of a small expansion parameter.

In this thesis we follow a different approach for the truncation scheme. As truncation criterion we use the locality of a term. This approach has to be justified by the model under study. This means that one has to be able to express the Hamiltonian by the use of local operators.

The local scheme is accurate if the important processes in the model take place on a short range. This is equivalent to a small correlation length as can be found in many strongly correlated electron systems. In the case of a large correlation length, which means in systems with long range interactions, the mapping to the effective model breaks down.

The model under study is a Hubbard model on a linear chain and on a two dimensional square lattice. In the case of half-filling and a large interaction  $U$  the system becomes insulating. The correlation length of the charge degrees of freedom is small indicating that the local approach will be suitable if we start the mapping from the insulating regime.

To apply the truncation a measure for the locality of a term is needed. We use the spatial extension of the terms. Before we define the extension, we need a unique representation for each term. Therefore some kind of normal-ordering has to be applied to the terms. A term is normal-ordered if the expectation value of each of its factors of local operators with respect to the reference ensemble vanishes. The reference ensemble is given by all the states without excitation, which means without double occupancies.

All terms with an extension greater than a predefined maximal extension are neglected during the calculation.

Although we use the extension as truncation criterion we do not observe finite size effects. This is due to the fact, that the model and our approximate treatment is translation invariant. By the use of this symmetry the calculations are extended over the whole lattice and we are not restricted to the sites on which the terms are defined.

Another way of truncating the terms is based on the description of terms by the use of local operators. To bound the number of terms in truncation schemes with large maximal

extensions terms are truncated according to their rank which is given by the amount of local operators the term consists of. Thus we restrict the calculation in the so-called upto4 truncation scheme to terms which consist of at most four local operators .

In actual calculations one proceeds as follows. First new terms are produced by commuting. Then these terms are normal-ordered and the terms that do not fit to the truncation scheme are discarded. The remaining terms are included in the Hamiltonian. This means that the whole transformation is performed in a renormalized fashion. That is why we call the transformation using a truncation like this *self-similar* continuous unitary transformation (sCUT). In contrast to results from other approaches the dependence of the effective coefficients on system parameters is not perturbative.

## 4. Application of the method to the Hubbard model

The sCUT method is used to eliminate double occupancies, which is only possible as long as sectors with a different number of double occupancies are separated in energy. As a result we have to start the transformation from the insulating regime of the Hubbard model. Therefore the interaction  $U$  has to be above a certain threshold as can be seen in the phase diagram 2.1. If  $U$  is smaller, so that the transition to a paramagnetic metal has taken place, a mapping to the  $t$ - $J$  model is not possible anymore. This breakdown of the mapping is accounted for by the vanishing of the energy costs needed to create charge fluctuations. The vanishing of the energy costs results in a sizeable overlap of sectors with different numbers of quasiparticles. This overlap makes the mapping impossible for a too small repulsive interaction.

### 4.1. Quasiparticle description

To derive the effective  $t$ - $J$  model we have to dispose of the charge fluctuations present in the Hubbard model. For this reason it is advisable to restate the problem in the quasiparticle picture. In this context the quasiparticles correspond to double occupancies (DO). These are either sites with two electrons with opposite spins  $|\downarrow\uparrow\rangle$  or empty sites  $|0\rangle$ .

First of all a counting operator for the double occupancies  $\hat{D}$  is needed. In the fermionic language this operator reads

$$\hat{D} = \sum_i (2\hat{n}_{i,\uparrow}\hat{n}_{i,\downarrow} - \hat{n}_{i,\uparrow} - \hat{n}_{i,\downarrow} + 1) \quad (4.1.1)$$

with the counting operator already introduced in section 2. This operator yields one for empty and doubly occupied sites and zero for sites with one electron. Thus it fulfills the task to count the quasiparticles.

It is useful to classify the terms in the Hamiltonian according to their effect on the number of DOs. In this way we obtain

$$\hat{H}_U = \frac{U}{2} \left( \hat{D} - \frac{N}{2} \right) \quad (4.1.2)$$

with  $N$  as the number of sites. The kinetic part can be split up into three terms.

$$\hat{H}_t = \hat{T}_0 + \hat{T}_{+2} + \hat{T}_{-2} \quad (4.1.3)$$

$$\hat{T}_0 = t_0 \sum_{\langle i,j \rangle, \sigma} \left[ (1 - \hat{n}_{i,\sigma}) \hat{c}_{i,\bar{\sigma}}^\dagger \hat{c}_{j,\bar{\sigma}} (1 - \hat{n}_{j,\sigma}) + \hat{n}_{i,\sigma} \hat{c}_{i,\bar{\sigma}}^\dagger \hat{c}_{j,\bar{\sigma}} \hat{n}_{j,\sigma} + h.c. \right] \quad (4.1.4)$$

$$\hat{T}_{+2} = t_{+2} \sum_{\langle i,j \rangle, \sigma} \left[ \hat{n}_{i,\sigma} \hat{c}_{i,\bar{\sigma}}^\dagger \hat{c}_{j,\bar{\sigma}} (1 - \hat{n}_{j,\sigma}) + \hat{n}_{j,\sigma} \hat{c}_{j,\bar{\sigma}}^\dagger \hat{c}_{i,\bar{\sigma}} (1 - \hat{n}_{i,\sigma}) \right] \quad (4.1.5)$$

$$\hat{T}_{-2} = t_{-2} \sum_{\langle i,j \rangle, \sigma} \left[ (1 - \hat{n}_{i,\sigma}) \hat{c}_{i,\bar{\sigma}}^\dagger \hat{c}_{j,\bar{\sigma}} \hat{n}_{j,\sigma} + (1 - \hat{n}_{j,\sigma}) \hat{c}_{j,\bar{\sigma}}^\dagger \hat{c}_{i,\bar{\sigma}} \hat{n}_{i,\sigma} \right]. \quad (4.1.6)$$

In this notation  $T_0$  contains all terms which do not change the number of double occupancies. One example for such a process is the hopping of one electron with spin  $\sigma$  from a doubly occupied site  $i$  to site  $j$  which is occupied by one electron with spin  $\bar{\sigma} = -\sigma$  (figure 4.1).

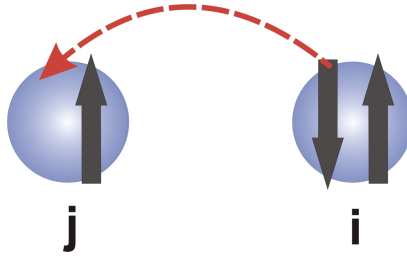


Fig. 4.1.: Hopping processes contained in  $T_0$

In analogy to this  $T_{+2}$  contains all terms that cause an increase of the number of double occupancies by two. Such a process is illustrated in figure 4.2. There one electron hops from one singly occupied site  $i$  to a site  $j$  with one electron of the opposite spin.

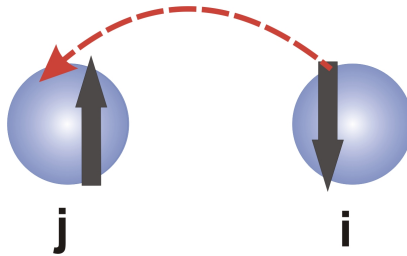


Fig. 4.2.: Hopping processes contained in  $T_{+2}$

The inverse process belongs to  $T_{-2}$ , see Fig. 4.3.

Thus the number of double occupancies can be changed by the initial Hamiltonian by the values 0, +2 and -2.

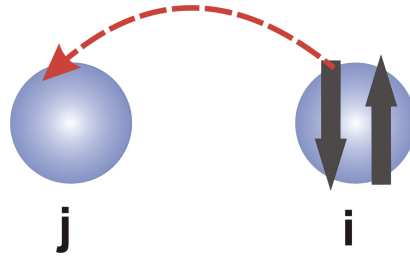


Fig. 4.3.: Hopping processes contained in  $T_{-2}$

#### 4.1.1. MKU generator

As introduced in Section 3.3 the MKU generator is given through the commutator of the quasiparticle counting operator  $\hat{D}$  with the Hamiltonian.

$$\eta(\ell) = [\hat{D}, \hat{H}(\ell)] \quad (4.1.7)$$

Using an eigenstates  $|i\rangle$  of  $\hat{D}$  with  $\hat{D}|i\rangle = d_i|i\rangle$  we obtain the following expression for the  $i, j$  component of the generator.

$$\eta(\ell)_{ij} = (d_i - d_j)H_{ij}(\ell) \quad (4.1.8)$$

As  $H$  changes the eigenvalues of  $\hat{D}$  just by two, this can be re-expressed by

$$\eta(\ell)_{ij} = 2\text{sgn}(d_i - d_j)H_{ij}(\ell) \quad (4.1.9)$$

Compared to the original definition of the MKU generator this definition contains an additional factor of two. As this is a global factor it just represents a renormalization of the flow parameter  $\ell = 2\ell^*$ .

As the MKU generator preserves the block band structure of the initial Hamiltonian no terms are created that change the number of double occupancies by other values than 0, +2, -2. So we can already state that the Hamiltonian will consist of three parts  $H(\ell) = T_0(\ell) + T_{+2}(\ell) + T_{-2}(\ell)$ . Although this imposes a constraint on the new terms, there are still many complicated terms created during the flow.

#### 4.1.2. $0n$ generator and $0n1n$ generator

The  $0n$ -generator consists of all terms that couple the quasiparticle vacuum to the other sectors (see section 3.3.3). Thus a term included in the generator has to change the number of DOs. These terms may be terms contained in  $T_{+2}$ . Terms out of this group create two DOs out of the vacuum coupling to the quasiparticle vacuum.  $T_{-2}$  consists of terms that annihilate two DOs. These terms couple the sector with two double occupancies to the sector without DOs. Thus these terms are also contained in the generator.

Of course these terms will also couple to other sectors. A term from  $T_{+2}$  also couples the sector with two DOs to the sector with four DOs. For the  $0n1n$ -generator also terms coupling to the sector with one DO are considered.

In contrast to the MKU generator a term consisting of four creation operators and two

annihilation operators would neither be included in  $0n$  nor in the  $0n1n$  generator. Such a term couples the two-particle subspace to the subspace with four quasiparticles. It does not couple to subspaces with less than two quasiparticles. Consequently this term does not fit into the schemes for the  $0n$  or the  $0n1n$  generator although it changes the number of DOs.

To keep the results comparable to the ones obtained with the MKU generator, we insert the factor of two into the  $0n$  and the  $0n1n$ -generator.

The initial generator  $\eta(0)$ , which results from the initial Hamiltonian  $\hat{H}(0)$ , is the same for all three types of generators.

$$\eta(0) = [\hat{D}, \hat{H}(0)] \quad (4.1.10)$$

But the generators will evolve in a different way during the flow.

In contrast to the MKU generator a CUT with the  $0n$  or the  $0n1n$  generator will not conserve the block diagonality.

## 4.2. Reference ensemble and normal-ordering

As we have seen before, it is necessary to have a unique representation for the terms to be able to file the contributions to the right term. Following the local approach we express terms as products of local operators. For this some kind of normal-ordering is needed. Normal-ordering is based on tracking fluctuations by the use of the expectation value with respect to some reference ensemble. The reference ensemble consists of a mixture of all states in the quasiparticle vacuum. In our case this means the mixture of all states without double occupancies. In the Hubbard model there are locally two such states namely the states with one electron either with spin up  $|\uparrow\rangle$  or spin down  $|\downarrow\rangle$ . As a result we do not have a single reference state but a whole ensemble given by the statistical operator projecting onto the reference states

$$\hat{\rho}_0 = \prod_i \left( \frac{1}{\#\text{ref-states}} \sum_{\text{ref-states } \alpha} |\alpha\rangle_{ii} \langle \alpha| \right) \quad (4.2.11)$$

$$= \prod_i \frac{1}{2} ( |\uparrow\rangle_{ii} \langle \uparrow| + |\downarrow\rangle_{ii} \langle \downarrow| ) \quad (4.2.12)$$

The product is taken over all sites  $i$  due to the translation symmetry of the model. We do not consider any magnetic ordering. Thus both states carry the same weight and it is guaranteed that the effective model is not biased to any magnetic order.

With the definition of the reference ensemble we can define local normal-ordered operators

bosonic	fermionic
$\mathbb{1}$	$(1 - \hat{n}_\downarrow) \hat{c}_\uparrow$
$\sigma^z = \hat{n}_\uparrow - \hat{n}_\downarrow$	$(1 - \hat{n}_\uparrow) \hat{c}_\downarrow$
$\hat{c}_\uparrow^\dagger \hat{c}_\downarrow$	$\hat{n}_\downarrow \hat{c}_\uparrow$
$\hat{c}_\downarrow^\dagger \hat{c}_\uparrow$	$\hat{n}_\uparrow \hat{c}_\downarrow$
$\hat{c}_\downarrow \hat{c}_\uparrow$	$\hat{n}_\uparrow \hat{c}_\downarrow^\dagger$
$\hat{c}_\uparrow \hat{c}_\downarrow$	$\hat{n}_\downarrow \hat{c}_\uparrow^\dagger$
$\bar{n}_\delta = \hat{n}_\uparrow + \hat{n}_\downarrow - 1 + \delta \mathbb{1}$	$(1 - \hat{n}_\downarrow) \hat{c}_\uparrow^\dagger$
$\hat{D}_\delta = 2\hat{n}_\uparrow \hat{n}_\downarrow - \bar{n}_\delta$	$(1 - \hat{n}_\uparrow) \hat{c}_\downarrow^\dagger$

Table 4.1.: Basis of local operators

as operators whose expectation value with respect to the reference ensemble vanishes

$$\langle \hat{A}_i \rangle_{\text{ref}} = 0 \quad (4.2.13)$$

$$= \text{Tr}(\hat{A}_i \hat{\rho}_0) \quad (4.2.14)$$

$$= \prod_j \frac{1}{2} \left( \langle \uparrow | \hat{A}_i | \uparrow \rangle_j + \langle \downarrow | \hat{A}_i | \downarrow \rangle_j \right) = \frac{1}{2} \left( \langle \uparrow | \hat{A}_i | \uparrow \rangle_i + \langle \downarrow | \hat{A}_i | \downarrow \rangle_i \right). \quad (4.2.15)$$

All normal-ordered operators have to fulfill this constraint. Therefore we create a basis of normal-ordered operators and express terms through these basis operators.

For one lattice site there are four possible states. Therefore the operators may be expressed as  $4 \times 4$  matrices connecting these states. This means that the new basis has to contain 16 normal-ordered operators. The 16 operators used to describe the basis are listed in Table 4.1.

Besides the well known operators the operator  $\bar{n}_\delta$  occurs in this list. In the half-filled case ( $\delta = 0$ )  $\bar{n}_\delta$  reduces to the operator  $\bar{n}$  which counts the amount of electrons compared to the half-filled case. Thus applied to an empty site it yields  $-1$  and applied to a singly occupied site it yields  $0$  whereas a doubly occupied site leads to  $+1$ .

Among these operators the unity operator takes a special role. This operator is not normal-ordered in the sense explained before as the expectation value of this operator would always yield the value one. However, this term is included in the basis of normal-ordered operators as it does not describe charge fluctuations.

The expectation value of the spin operator  $\sigma^z$  vanishes due to the equal weight of  $|\uparrow\rangle$  and  $|\downarrow\rangle$ .

As a unique representation of the terms is required, we have to express each term as a linear combination of these 16 operators. As an example the operator  $\hat{n}_\uparrow(1 - \hat{n}_\downarrow)$ , which projects onto the state with an up electron, is considered. As this operator is not included in the list above, it has to be expressed through other operators

$$\hat{n}_\uparrow(1 - \hat{n}_\downarrow) = \frac{1}{2} \left( (1 - \delta) \mathbb{1} + \sigma^z - \hat{D}_\delta \right). \quad (4.2.16)$$

Due to the fact that the product of normal-ordered operators is also normal-ordered in the sense that the corresponding expectation value vanishes, it is possible to express every term that occurs during the flow using the operators of the normal-ordered basis.

Additionally the operators of a term are ordered according to the sites on which they are acting.

In this way a unique representation for every term as a product of local normal-ordered operators is created.

### 4.3. Truncation schemes

As explained in section 3.4 we follow the local approach. Consequently we use the locality of a term as measure of its relevance for the calculation. The locality is measured through the extension of a term. On the one-dimensional chain the extension of a term is given as the distance between the rightmost and the leftmost site with non-identity operators.

On a two dimensional square lattice we use the taxi cab distance to determine the extension of a term. An example is shown in figure 4.4.

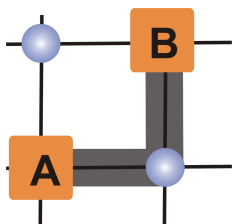


Fig. 4.4.: Illustration of a term with extension 2

In this example the term is represented by the operator  $\hat{A}$  acting on site  $(0,0)$  and operator  $\hat{B}$  on site  $(1,1)$ . The resulting extension for this term is 2. If the extension of a term is greater than a maximal extension, the term will be neglected.

In the two dimensional case the resulting extension of a term is given as the sum over the extension in  $x$ - and the extension in  $y$ -direction. A term which exceeds three lattice sites in the  $x$ -direction and two in the  $y$ -direction thus has an extension of 3 (see figure 4.5).

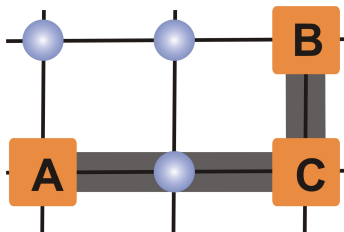


Fig. 4.5.: Illustration of a term with extension 3

There is an additional constraint which occurs in the so called minimal truncation scheme. In this scheme we discard all new terms but the Heisenberg interaction. Be-

sides we neglect contributions originating from the commutator of the generator with the Heisenberg term.

Apart from that the truncation schemes of the one dimensional model are named according to the maximal extension considered in the calculation. In the two dimensional case we have the nearest neighbor (NN) truncation, the plaquette calculation, which corresponds to an extension of two and the double plaquette calculation, where terms with an extension of three are considered. During the double plaquette calculation a vast amount of terms is created so that we introduce another truncation scheme. In the upto4 truncation scheme we consider terms that fit on the double plaquette scheme but additionally we require that these terms consist of at most four local operators. The number of local operators contained in a term is denoted as its rank. This reduces the amount of terms by a factor of 10.

## 4.4. Implementation

With a higher maximal extension more and more terms fulfilling the truncation criteria are created.

As a result of the fast growing number of terms only the calculations belonging to the small truncation schemes like the minimal or the NN-truncation can be performed by hand. For higher truncation schemes the calculations are done by the use of a computer.

The program used in this thesis is implemented using the computer language  $C^{++}$ . The program is divided into two parts. The first part deals with the derivation of the differential equations for the coefficients. In the second part of the program these equations are solved numerically.

The program is based on the classes 'term' and 'operator', see Fig.4.6.

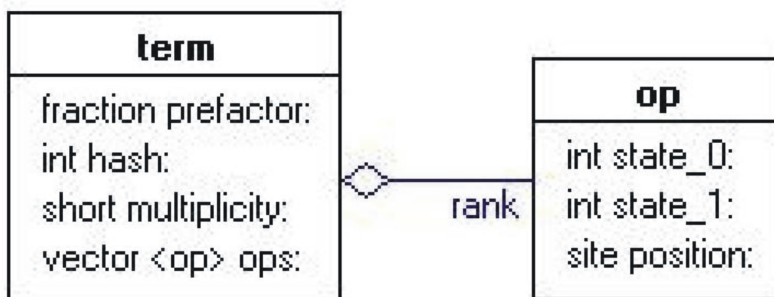


Fig. 4.6.: Schematic diagram for the 0n-generator

Operators are described by two numbers identifying the type of the operator. For each operator there are 16 possibilities as can be seen from the list 4.1. Beyond this the class operator contains a variable for the site on which the operator acts. The class term contains a vector of the type operator, which indicate the local operators, of which the term consists. Additionally the class contains the prefactor of the term. This prefactor is stored as an exact fraction to avoid numerical errors. For practical use this class contains two additional values. The first is the hash value of the term. Keeping this value speeds up the search for a certain term in the list of all terms. The second one is the multiplicity, which will be used in the context of symmetries as explained below.

The Hamiltonian itself is given as a vector of terms.

#### 4.4.0.1. Setting up the differential equations

A structure chart of the first part of the program is shown in figure 4.7.

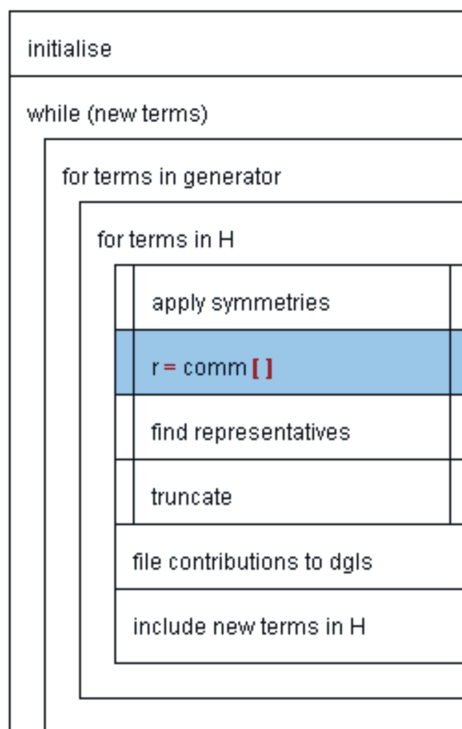


Fig. 4.7.: Structure chart for the used program

First of all the Hamiltonian is initialized. Then the program performs two loops in order to compute the commutator. One runs over all terms of the generator and one runs over all terms in the Hamiltonian. Here we make use of the fact that the generator consists of terms of the Hamiltonian itself. Therefore we just have to check if a certain term contributes to the generator and calculate the right prefactor.

The central part of the program is the calculation of the commutator. In this part we benefit from the representation of terms as products of local operators (see section 3.4). The calculation of commutators of terms can thus be split into calculating commutators of local operators. As there are bosonic as well as fermionic operators in the set of local operators, we have to deal with commutators of two fermions, of two bosons and of a fermion with a boson. Thus we have to express the commutators of terms by commutators or anticommutators of its operators [Fis07]. In the case of two fermionic operators  $\hat{a}_k, \hat{b}_l$ ,

we obtain

$$[\hat{A}, \hat{B}] = \left[ \prod_{i=1}^n \hat{a}_i, \prod_{j=1}^m \hat{b}_j \right] \quad (4.4.1)$$

$$= \sum_{k=1}^n \sum_{l=1}^m (-1)^{(l-1)} \left( \prod_{i=1}^{k-1} \hat{a}_i \right) \left( \prod_{j=1}^{l-1} \hat{b}_j \right) \{ \hat{a}_k, \hat{b}_l \} \left( \prod_{r=l+1}^m \hat{b}_r \right) \left( \prod_{s=k+1}^n \hat{a}_s \right) \quad (4.4.2)$$

with  $m$  even. In this formula  $\{, \}$  stands for the anticommutator of two operators.

The case of two bosonic operators  $\hat{a}_k$  and  $\hat{b}_l$  as well as the case with one bosonic and one fermionic operator are covered by

$$[\hat{A}, \hat{B}] = \left[ \prod_{i=1}^n \hat{a}_i, \prod_{j=1}^m \hat{b}_j \right] \quad (4.4.3)$$

$$= \sum_{k=1}^n \sum_{l=1}^m \left( \prod_{i=1}^{k-1} \hat{a}_i \right) \left( \prod_{j=1}^{l-1} \hat{b}_j \right) [\hat{a}_k, \hat{b}_l] \left( \prod_{r=l+1}^m \hat{b}_r \right) \left( \prod_{s=k+1}^n \hat{a}_s \right) \quad (4.4.4)$$

using the commutators of local operators.

To be able to calculate these commutators it is necessary to implement the algebra of the local operators.

After commuting the terms a unique representation for each term is found by ordering the operators according to the sites on which they are acting. Furthermore the terms are expressed in a normalordered form. Then the truncation scheme is applied as new terms violating this scheme may have been created. The terms that are kept because they fulfill the truncation criteria have to be filed to the right differential equation in the end. If the new terms are not yet considered in the Hamiltonian they have to be included in the vector presenting  $\hat{H}$ .

As we want to consider contributions from these new terms, we have to repeat the steps explained before. As long as there are new terms in  $\hat{H}$  another loop is started, in which commutators of these new terms are calculated.

#### 4.4.0.2. Application of symmetries

Due to the vast number of new arising terms it is advantageous to use symmetries to increase the efficiency of the program. If one term emerges from another term by applying symmetry operations, both terms have to carry the same coefficient.

The model under study inherits many symmetries from the initial Hamiltonian  $H(0)$ . These are the spin flip symmetry, the symmetry of adjoint terms and the whole point

group of the underlying lattice. The two dimensional square lattice is symmetric regarding rotations about  $\frac{\pi}{2}, \pi$  and  $\frac{3}{2}\pi$ . Beyond this it is symmetric regarding reflections about the x-axis, the y-axis and the diagonal. In the one dimensional case this reduces to the reflection about the axis perpendicular to the linear chain itself.

At half-filling we also used the particle-hole symmetry. By applying all symmetry operations in the two dimensional case up to 64 terms are created out of one single representative term. This means that it is sufficient to treat one term instead of 64 thus speeding up the program.

All terms related by symmetry operations with one other are grouped together. For each group one of the terms is chosen to be the representative of this group. The calculation is thus performed for all representatives and not for all terms in the Hamiltonians

$$\sum_{\text{all terms}} H_i = \sum_{\text{symm group}} \sum_{\text{repres.}} R_j. \quad (4.4.5)$$

This leads to a much smaller number of terms and of differential equations.

If a term is chosen to be a representative we eventually have to change its prefactor. As an example we consider the unity operator. Applying the symmetry group to this operator reproduces the unity operator itself several times. This has to be considered in the prefactor of the representatives. How many times a certain operator is reproduced by applying symmetry operations is stored in the variable multiplicity of the class term.

A prefactor might also be changed by sign changes due to the applied symmetry operation. Applying symmetries is also useful for the calculation of the commutators. Instead of commuting all terms of the generator with all terms in the Hamiltonian, we can restrict ourselves to commuting the representatives for the generator terms with the terms in the Hamiltonian.

$$\left[ \eta(\ell), \hat{H} \right] = \sum_{\text{symm group}} \left[ \sum_{\text{repres.}} R_i, \sum_{\text{symm group}} \sum_{\text{repres.}} R_j \right] \quad (4.4.6)$$

This reduces the amount of terms and the size of the set of differential equations. As a result the numerical evaluation can be performed more efficiently. Besides solving the differential equations is more stable as less rounding errors occur if more symmetries are used.

By the use of symmetries the terms in the double plaquette calculation for the  $0n1n$ -generator are reduced from more than 5 million terms to 55049 representatives. At half-filling particle hole symmetries could be used additionally thus reducing the total amount of terms to 28086. This calculation took 1224 hours of CPU time. Storing the corresponding system of coupled differential equations took 10 GB of memory.

The computational effort grows exponentially with the maximal extension used for the calculation. Whereas the calculation mentioned above took 51 days, the NN calculations were done within a few seconds.

Additionally the computational effort depends on the generator used. The double plaquette calculation with the  $0n$  generator took 10 days which has to be compared to the 51 days which were needed for the same calculation with the  $0n1n$  generator.

#### 4.4.0.3. Solving the differential equations

The integration of the differential equation was performed by a Runge-Kutta algorithm. The integration was done for several starting values of the hopping matrix element  $t$  in parallel. As it is not possible to reach  $\ell = \infty$  numerically, we use the residual off-diagonality (ROD) defined in section 3.3.2 to decide when to stop the calculation. The ROD measures to what extent the terms of the generator have been eliminated. In this sense we stop the calculation if the ROD falls below a value of  $10^{-8}$  in units of the Hubbard repulsion  $U$ .

The solution of the differential equations for the small truncation schemes like the NN truncation took less than half an hour of CPU. Even for the double plaquette calculation the integration took less than 40 hours of CPU for the  $0n1n$ -generator.

## 4.5. Minimal model

In a first step we analyze the minimal model (min) as explained in Sect. 3.4. The calculation of this model starts with calculating processes on nearest neighbors. This is equivalent to a maximal extension of  $e = 1$ . To extract the minimal model from these processes all new terms except for the Heisenberg interaction are neglected. Beyond this the Heisenberg interaction will not be considered in the generator. Consequently there are no new contributions to the generators.

As explained before the initial generators for all three types of generators are the same. Starting with the same terms and ignoring all new contributions for the generator all three generators remain the same during the flow in this truncation scheme. According to Eq. 4.1.7 the generator reads

$$\eta(\ell) = \left[ \hat{D}, \hat{H}(\ell) \right] \quad (4.5.1)$$

$$= 2\hat{T}_{+2} - 2\hat{T}_{-2}. \quad (4.5.2)$$

The factor of two in the generator arises from the fact, that one excitation corresponds to two double occupancies. The differential equations can now be determined from the flow equation 3.2.3 which is restated here

$$\frac{d}{d\ell} \hat{H}(\ell) = \left[ \hat{\eta}(\ell), \hat{H}(\ell) \right]. \quad (4.5.3)$$

For the calculation of the flow equation we split the Hamiltonian into the repulsive part  $\hat{H}_U$  and the kinetic part  $\hat{H}_t$ . Then the flow equation

$$\left[ \eta(\ell), \hat{H}_U + \hat{H}_t \right] \quad (4.5.4)$$

yields two contributions which are calculated separately. For the repulsive part we obtain

$$\left[ \eta(\ell), \hat{H}_U \right] = \left[ 2\hat{T}_{+2}(\ell) - 2\hat{T}_{-2}(\ell), \frac{U(\ell)}{2} \hat{D} \right] \quad (4.5.5)$$

$$= -2U(\ell)\hat{T}_{+2}(\ell) - 2U(\ell)\hat{T}_{-2}(\ell). \quad (4.5.6)$$

For the kinetic part we have to calculate

$$\left[ \eta(\ell), \hat{H}_t \right] = \left[ 2\hat{T}_{+2}(\ell) - 2\hat{T}_{-2}(\ell), \hat{T}_0(\ell) + \hat{T}_{+2}(\ell) + \hat{T}_{-2}(\ell) \right]. \quad (4.5.7)$$

As the commutators  $[\hat{T}_{+2}(\ell), \hat{T}_0(\ell)]$  and  $[\hat{T}_{-2}(\ell), \hat{T}_0(\ell)]$  vanish, it remains to calculate the commutator of  $\hat{T}_{+2}(\ell)$  and  $\hat{T}_{-2}(\ell)$

$$\left[ \eta(\ell), \hat{H}_t(\ell) \right] = \left[ 2\hat{T}_{+2}(\ell) - 2\hat{T}_{-2}(\ell), \hat{T}_{+2}(\ell) + \hat{T}_{-2}(\ell) \right] \quad (4.5.8)$$

$$= 4 \left[ \hat{T}_{+2}(\ell), \hat{T}_{-2}(\ell) \right]. \quad (4.5.9)$$

This commutator yields the following expression

$$[\eta(\ell), \hat{H}_t(\ell)] = 4zt_{+2}t_{-2}\hat{D} \quad (4.5.10)$$

$$+ 16t_{+2}t_{-2} \sum_{\langle i,j \rangle} \vec{S}_i \vec{S}_j \quad (4.5.11)$$

$$+ 8t_{+2}t_{-2} \sum_{\langle i,j \rangle} (\hat{c}_{i\uparrow}^\dagger \hat{c}_{i\downarrow}^\dagger \hat{c}_{j\downarrow} \hat{c}_{j\uparrow} + h.c.) \quad (4.5.12)$$

$$- 4t_{+2}t_{-2} \sum_{\langle i,j \rangle} \bar{n}_i \bar{n}_j \quad (4.5.13)$$

$$- 4\mathbb{1}t_{+2}t_{-2} \quad (4.5.14)$$

$$+ \dots \quad (4.5.15)$$

The neglected terms indicated by the three dots are terms that have an extension larger than one.

Here  $\vec{S}_i \vec{S}_j$  stands for

$$\vec{S}_i \vec{S}_j = \frac{1}{2} (\sigma_i^+ \sigma_j^- + \sigma_i^- \sigma_j^+) + \frac{1}{4} \sigma_i^z \sigma_j^z \quad (4.5.16)$$

with

$$\sigma^+ = S_x + iS_y \quad (4.5.17)$$

$$\sigma^- = S_x - iS_y \quad (4.5.18)$$

$$\sigma^z = 2S^z. \quad (4.5.19)$$

In the first term (Eq. 4.5.10)  $z$  denotes the coordination number of the underlying lattice. For the two dimensional square lattice we have  $z = 4$ , whereas the one dimensional linear chain has a coordination number of  $z = 2$ .

Up to this point we performed the full nearest neighbor calculation. For the minimal truncation the last three contributions given in Eqs. 4.5.12 to 4.5.14 are ignored. In the minimal truncation just the Heisenberg interaction on nearest neighbors is included as a new term in the Hamiltonian. The Heisenberg exchange on nearest neighbors

$$H_{\text{NN}} = J_1(\ell) \sum_{\langle i,j \rangle} \vec{S}_i \vec{S}_j \quad (4.5.20)$$

is generated through Eq. 4.5.11. This term is included in the Hamiltonian with the initial condition  $J_1(0) = 0$ . We would have to consider this term in the generator but as the Heisenberg exchange does not change the number of double occupancies it does not contribute to the generator. In the minimal model we also ignore contributions of  $H_{\text{NN}}$  to the flow equation arising from  $[\eta(\ell), H_{\text{NN}}]$ .

The operators belonging to terms in  $T_{+2}$  and  $T_{-2}$  are hermitian conjugates and their coefficients are assumed to be real. Therefore  $t_{+2}(\ell) = t_{-2}(\ell)$  holds.

A comparison of the terms in the second contribution with the terms in the original

Hamiltonian (see Eq. 4.1.2) leads to the differential equation for the Hubbard repulsion  $U$

$$\frac{d}{d\ell} \frac{U(\ell)}{2} = 4zt_{+2}^2(\ell). \quad (4.5.21)$$

$$(4.5.22)$$

The flow equation for the Heisenberg exchange reads

$$\frac{d}{d\ell} J_1(\ell) = 16t_{+2}^2(\ell). \quad (4.5.23)$$

And the remaining equations for the hopping terms are given by

$$\frac{d}{d\ell} t_{+2} = -2U(\ell)t_{+2}(\ell) \quad (4.5.24)$$

$$\partial_\ell t_0(\ell) = 0. \quad (4.5.25)$$

Taking the second derivative of Eq. 4.5.21 and inserting Eq.4.5.24 leads to

$$\frac{d^2 U(\ell)}{d\ell^2} = 16zt_{+2} \frac{dt_{+2}}{d\ell} \quad (4.5.26)$$

$$= -32zt_{+2}^2 U(\ell) \quad (4.5.27)$$

$$= -4U(\ell) \frac{dU(\ell)}{d\ell}. \quad (4.5.28)$$

This differential equation is solved by

$$U(\ell) = \frac{A}{2} \tanh(A\ell + B) \quad (4.5.29)$$

with the constants A and B. The constant B is given by the initial value  $U(0) = U_0$  as

$$B = \operatorname{arctanh}\left(\frac{2U_0}{A}\right). \quad (4.5.30)$$

From Eq. 4.5.21 we obtain  $t_{+2}$

$$\begin{aligned} t_{+2}(\ell) &= \sqrt{\frac{1}{8z} \frac{d}{d\ell} U(\ell)} \\ &= \sqrt{\frac{1}{8z} \frac{A^2}{2} (1 - \tanh^2(A\ell + B))} \\ &= \frac{A}{4} \sqrt{\frac{1}{z} (1 - \tanh^2(A\ell + B))}. \end{aligned} \quad (4.5.31)$$

Combining Eq. 4.5.29 and 4.5.31 and using  $t_0(0) = t_{+2}(0)$  the constant A is given by

$$A = \sqrt{4U(\ell)^2 + 16zt_{+2}^2} = \sqrt{4U_0^2 + 16zt_0^2}. \quad (4.5.32)$$

These results are used to solve the initial value problem for  $J_1$  with  $J_1(0) = 0$ . Integrating Eq. 4.5.23

$$\frac{d}{d\ell} J_1(\ell) = 16t_{+2}(\ell)^2 = \frac{2}{z} \frac{dU(\ell)}{d\ell} \quad (4.5.33)$$

leads to

$$J_1(\ell) = \frac{2}{z}U(\ell) - \frac{2}{z}U_0 \quad (4.5.34)$$

$$= \frac{A}{z}\tanh(A\ell + B) - \frac{2}{z}U_0. \quad (4.5.35)$$

The constant  $\frac{2}{z}U_0$  ensures that the initial condition for  $J_1$  is fulfilled.

The effective coefficients which can be determined in the limit  $\ell = \infty$  are given in the following equations

$$t_{0,\text{eff}} = t_0 \quad (4.5.36)$$

$$t_{+2,\text{eff}} = 0 \quad (4.5.37)$$

$$U_{\text{eff}} = \frac{1}{2}\sqrt{4U_0^2 + 16zt_0^2} \quad (4.5.38)$$

$$J_{1,\text{eff}} = \frac{A}{z} - \frac{2}{z}U_0 \quad (4.5.39)$$

$$= \frac{1}{z}\sqrt{4U_0^2 + 16zt_0^2} - \frac{2}{z}U_0. \quad (4.5.40)$$

For simplicity we rename the initial values  $t_0 = t$  and  $U_0 = U$  in further calculations.

Thus the minimal model contains in leading order the second order perturbation theory result for  $J_1^{(2)} = \frac{4t^2}{U}$ .

In the case of a two dimensional square lattice we have  $z = 4$  in these formulas. The derived effective coefficients for the two dimensional square lattice are in agreement with the results obtained by Reischl [RMHU04] and Lorscheid [Lor].

For other lattices one just has to insert a different value of  $z$ . The formulas stay valid.

With these values the effective  $t$ - $J$  Hamiltonian is given as

$$H_{\text{eff}} = U_{\text{eff}}\frac{1}{2}\hat{D} + \hat{T}_0 + J_{1,\text{eff}}\sum_{\langle i,j \rangle}\vec{S}_i\vec{S}_j. \quad (4.5.41)$$

## 4.6. NN model

The NN model is an extension of the minimal model discussed before. In the NN truncation all terms with a maximal extension of one are considered. This means that we consider all processes on nearest neighbors (NN). In section 4.5 we already derived the flow equation for the nearest neighbor truncation

$$[\eta(\ell), \hat{H}_t(\ell)] = 4zt_{+2}(\ell)t_{-2}(\ell)\hat{D} \quad (4.6.1)$$

$$+ 16t_{+2}(\ell)t_{-2}(\ell) \sum_{\langle i,j \rangle} \vec{S}_i \vec{S}_j \quad (4.6.2)$$

$$+ 8t_{+2}(\ell)t_{-2}(\ell) \sum_{\langle i,j \rangle} \left( \hat{c}_{i\uparrow}^\dagger \hat{c}_{i\downarrow}^\dagger \hat{c}_{j\downarrow} \hat{c}_{j\uparrow} + h.c. \right) \quad (4.6.3)$$

$$- 4t_{+2}(\ell)t_{-2}(\ell) \sum_{\langle i,j \rangle} \bar{n}_i \bar{n}_j \quad (4.6.4)$$

$$- 4t_{+2}(\ell)t_{-2}(\ell) \mathbf{1} \quad (4.6.5)$$

$$+ \dots \quad (4.6.6)$$

The only point where the geometry of the lattice enters is the coordination number  $z$ . As long as the coordination number  $z$  is known, there are no limitations on the geometry of the lattice. Thus universal expressions for the effective coupling constants can be derived [HDU]. These expressions are also valid for dimers and even in the limit of infinite dimensions as will be seen below.

For a derivation of the NN model all terms in the Eqs. 4.6.1 to 4.6.4 have to be considered. Besides the Heisenberg exchange this equation contains the term

$$H_V(\ell) = V(\ell) \sum_{\langle i,j \rangle} \bar{n}_i \bar{n}_j. \quad (4.6.7)$$

Again the brackets under the sum indicate that site  $i$  and site  $j$  are nearest neighbors. The operator  $\bar{n} = \hat{n}_\uparrow + \hat{n}_\downarrow - 1$  counts the amount of electrons compared to the half-filled case. Thus  $H_V$  describes the interaction of two neighboring DOs.

Equation 4.6.3 contains an additional term in the third line. This term is given by

$$H_p(\ell) = V_p(\ell) \sum_{\langle i,j \rangle} \left( \hat{c}_{i\uparrow}^\dagger \hat{c}_{i\downarrow}^\dagger \hat{c}_{j\downarrow} \hat{c}_{j\uparrow} + h.c. \right). \quad (4.6.8)$$

$H_p$  describes the hopping of two DOs. Two electrons hop from a doubly occupied site to another empty site. Sites with two electrons as well as empty sites are labeled as DOs. Consequently  $H_p$  does not change the number of quasiparticles. Both new terms act on neighboring sites thus fitting to the truncation scheme.  $H_V$  and  $H_p$  are included in the Hamiltonian. But they do not change the number of quasiparticles and so they are not part of the generator. Apart from the contributions already determined in the minimal model there are additional contributions to the differential equations arising from the commutator

$$[\eta(\ell), H_{\text{NN}}(\ell) + H_p(\ell) + H_V(\ell)] \quad (4.6.9)$$

In analogy to the previous calculations a  $z$  dependent differential equation for the Hubbard repulsion  $U$  is obtained

$$\frac{d}{d\ell}U = 8zt_{+2}^2(\ell). \quad (4.6.10)$$

A comparison of the coefficients yields the remaining differential equations

$$\frac{dt_{+2}(\ell)}{d\ell} = \left( -2U(\ell) + 2V(\ell) - 2V_p(\ell) - \frac{3}{2}J_1(\ell) \right) t_{+2}(\ell) \quad (4.6.11)$$

$$\frac{dJ_1(\ell)}{d\ell} = 16t_{+2}^2(\ell) = \frac{2}{z} \frac{dU(\ell)}{d\ell} \quad (4.6.12)$$

$$\frac{dV(\ell)}{d\ell} = -4t_{+2}^2(\ell) = \frac{-1}{2z} \frac{dU(\ell)}{d\ell} \quad (4.6.13)$$

$$\frac{dV_p(\ell)}{d\ell} = 8t_{+2}^2(\ell) = \frac{1}{z} \frac{d}{d\ell}U(\ell). \quad (4.6.14)$$

The initial conditions for the coefficients of the new terms are  $J_1(0) = 0$ ,  $V(0) = 0$  and  $V_p(0) = 0$ . With these conditions and the Eqs. 4.6.11 to 4.6.14 the following relations between the coefficients are obtained

$$J_1(\ell) = \frac{2}{z}U(\ell) - \frac{2}{z}U_0 \quad (4.6.15)$$

$$V(\ell) = -\frac{1}{2z}U(\ell) + \frac{1}{2z}U_0 \quad (4.6.16)$$

$$V_p(\ell) = \frac{1}{z}U(\ell) - \frac{1}{z}U_0 \quad (4.6.17)$$

$$\Rightarrow \frac{d}{d\ell}t_{+2}(\ell) = t_{+2}(\ell) \left( \frac{-2}{z}U(\ell)(z+3) + \frac{6}{z}U_0 \right). \quad (4.6.18)$$

The second derivative of the differential equation for  $U(\ell)$  reads

$$\frac{d^2U}{d\ell^2} = 16zt_{+2}(\ell) \frac{dt_{+2}}{d\ell}, \quad (4.6.19)$$

which can be rewritten as

$$\frac{d^2U}{d\ell^2} = \frac{dU}{d\ell} \left( \left( -\frac{12}{z} - 4 \right) U(\ell) + \frac{12}{z}U_0 \right). \quad (4.6.20)$$

For the solution of this equation we use the ansatz

$$U(\ell) = \frac{z}{6+4z}A \tanh(A\ell + B) + \frac{\frac{3}{z}}{\frac{3}{z}+4}U_0 \quad (4.6.21)$$

with  $A$  and  $B$  constant. Again the constant  $B$  can be derived from the initial conditions to be  $B = \operatorname{artanh}\left(\frac{2U_0}{A}\right)$ . By the use of

$$t_{+2}^2 = \frac{dU}{d\ell} \frac{1}{8z} \quad (4.6.22)$$

$$= A^2 \frac{1}{16(3+z)} (1 - \tanh^2(A\ell + B)) \quad (4.6.23)$$

an expression for  $A$  is obtained, it is defined by

$$A = 2\sqrt{U^2 + 4(3+z)t^2} \quad (4.6.24)$$

where we again used  $t$  and  $U$  to denote the initial values  $t_0(0)$  and  $U_0(0)$ . From the expression for  $U(\ell)$  and Eq. 4.6.15 we can derive the  $\ell$  dependence for all the other coefficients

$$V(\ell) = -\frac{2}{3+4z}\sqrt{U^2 + 4(3+z)t^2} \tanh(A\ell + B) + \frac{2}{3+4z}U_0 \quad (4.6.25)$$

$$V_p(\ell) = \frac{4}{3+4z}\sqrt{U^2 + 4(3+z)t^2} \tanh(A\ell + B) + \frac{4}{3+4z}U_0. \quad (4.6.26)$$

$$J_1(\ell) = \frac{2}{3+z} \left( \sqrt{U_0^2 + 4(3+z)t_0^2} \tanh(A\ell + B) - U_0 \right) \quad (4.6.27)$$

In the limit  $\ell \rightarrow \infty$  the effective coupling constants read

$$V_{\text{eff}}(\ell) = -\frac{2}{3+4z}\sqrt{U^2 + 4(3+z)t^2} + \frac{2}{3+4z}U_0$$

$$V_{p,\text{eff}}(\ell) = \frac{4}{3+4z}\sqrt{U^2 + 4(3+z)t^2} + \frac{4}{3+4z}U_0.$$

The effective Heisenberg interaction is given as

$$J_{1,\text{eff}} = \frac{2}{3+z} \left( \sqrt{U_0^2 + 4(3+z)t_0^2} - U_0 \right),$$

where  $z$  is again the coordination number of the lattice.

For a linear chain we set  $z = 2$ . The two dimensional square lattice yields  $z = 4$  and a three dimensional square lattice corresponds to  $z = 6$ . A dimer can be captured by setting  $z = 1$ . To analyze the limit of infinite dimensions it is useful to replace  $t$  and  $J_1$  by scaled values

$$t_0 = \frac{\bar{t}_0}{\sqrt{z}}$$

$$= z \frac{2}{3+z} U_0 \left( \sqrt{1 + 4(3+z) \frac{\bar{t}_0^2}{zU_0^2}} - 1 \right).$$

For  $z \rightarrow \infty$  we obtain

$$\bar{J} = 2U_0 \left( \sqrt{1 + 4 \frac{\bar{t}_0^2}{U_0^2}} - 1 \right).$$

The expression for the Heisenberg exchange contains the perturbation results for leading order of  $\frac{t}{U}$ .

### 4.6.1. Results for the NN truncation

In a first step we compare the analytical result to the numerical one for the NN calculation. As a cross check the result for the Heisenberg exchange  $J_1$  obtained by a numerical treatment is compared to the analytical one for the two-dimensional square lattice. Additionally we show the results for the minimal model. The curves are shown in Fig. 4.8.

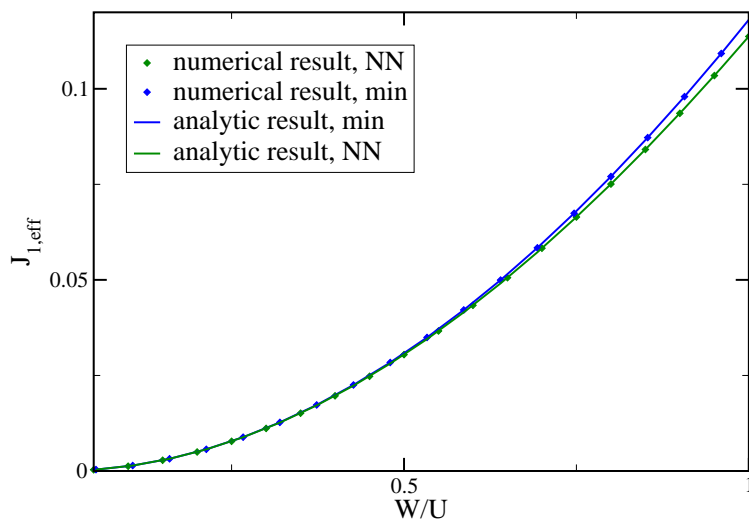


Fig. 4.8.: Results for the nearest neighbor Heisenberg exchange  $J_1$  for the NN calculation

In both cases the curves show perfect agreement of the numerical and the analytical result.

The minimal model leads to slightly larger values for the nearest neighbor Heisenberg exchange.

## 4.7. Results for the one dimensional linear chain at half-filling

### 4.7.1. Higher truncation schemes

Now we consider results for higher truncation schemes. With a larger maximal extension more and more terms are considered in the calculation. Thus we expect to reach exact results for the coupling constants in the limit of an extension  $e \rightarrow \infty$ . In this limit the effective coupling constants are converged. If an effective coupling constant converges for finite values of  $e$  we can conclude that all processes which influence this coupling constant are already contained in the considered truncation scheme. Thus including terms with higher maximal extensions does not improve the result anymore.

The schemes considered in the case of the one-dimensional linear chain are the ones with maximal extension of three or four (see Sect.3.4). The results for various truncation schemes are compared to one other. In this way it is possible to analyze how the coupling constants develop when more extended terms are included. With more extended terms included more reliable results are expected.

During the CUT the coupling constants of all appearing terms are calculated but we restrict the discussion to a few exemplary results. The coupling constants are shown in dependence of  $W/U$  for different truncation schemes where  $W$  denotes the bandwidth  $W = 2zt$ . The results shown in this section correspond to calculations which were stopped at a value of  $10^{-10}$  for the ROD.

Before we show effective coupling constants we discuss the behavior of the ROD. As the ROD decreases exponentially with the flow parameter  $l$  it is shown in a logarithmic plot in Fig. 4.9 for the large value of  $W/U = 1.1$ .

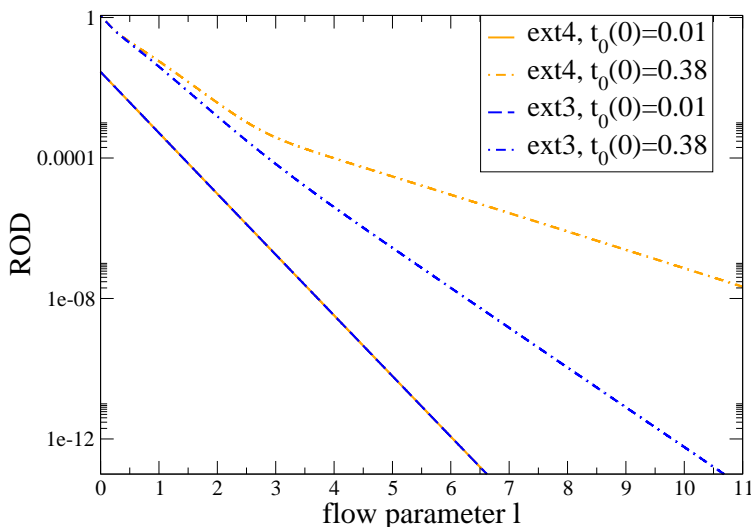


Fig. 4.9.: Behavior of the ROD for different starting values of the hopping parameter  $t$ .

For  $\ell = 0$  the only terms contributing to the ROD are the terms  $T_{+2}$  and  $T_{-2}$  of the original Hamiltonian. Each of these terms includes a sum running over two possible spin directions and one sum for the nearest neighbors. Therefore the ROD starts at a value of  $4zt^2$  where  $t$  denotes the starting value of the hopping parameter and  $z$  denotes the coordination number of the lattice.

In the one-dimensional case the ROD shows convergent behavior for all values of  $W/U$  for all truncation schemes with a maximal extension  $\leq 4$ .

As will be seen in Sect.6.4 the mapping to the effective model is valid up to  $W/U$  of about 0.8 in the one-dimensional case. Therefore the coupling constants are shown in dependence of  $W/U$  for values of  $W/U \leq 0.8$ .

#### 4.7.1.1. Spin terms

Having analyzed the ROD we now study the spin interactions. The most important spin interaction is the Heisenberg exchange between nearest neighbors

$$H_{\text{NN}} = J_1 \sum_{\langle i,j \rangle} \vec{S}_i \vec{S}_j. \quad (4.7.1)$$

The coefficients of the spin terms as well as of the interaction terms are compared to the second order result of perturbation theory  $J_1^{(2)} = \frac{4t^2}{U}$ .  $J_1$  was determined in fourth order perturbation theory to be

$$J_1 = \frac{4t^2}{U} - \frac{24t^4}{U^3} + O\left(\frac{t^6}{U^5}\right)$$

with the hopping element  $t$  and the repulsion  $U$  [Tak77] [MGY88].

The effective value of the coupling constant  $J_1$  compared to  $J_1^{(2)}$  is shown in Fig. 4.10. In the limit  $W/U \rightarrow 0$  the results correspond to  $J_1^{(2)}$ .

Compared to the other truncation schemes the minimal model leads to much higher values whereas the NN calculation yields smaller values. The results for the other truncation schemes lie close together. This observation implies that the terms, which are important to determine the value of  $J_1$ , are already contained in the calculation with a maximal extension of two. However even the results obtained in a NN calculation are close to the ones obtained by calculations with higher schemes.

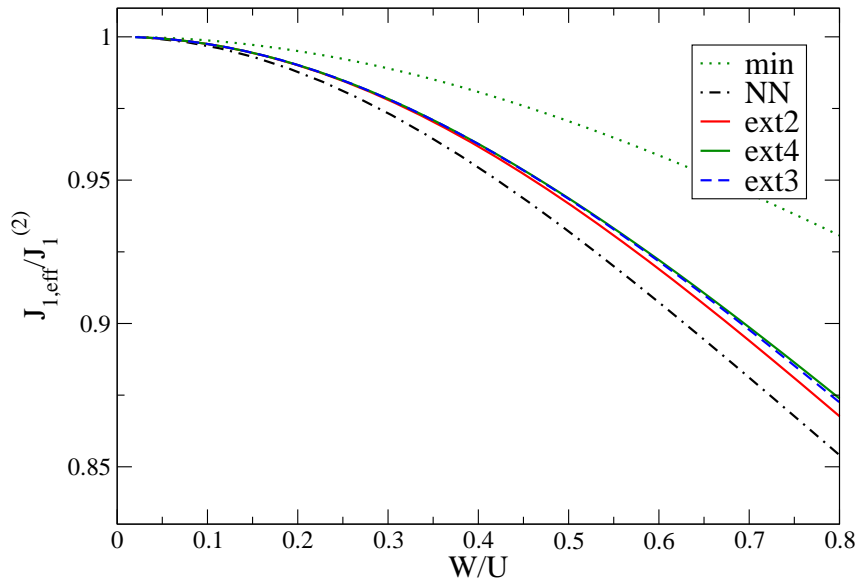


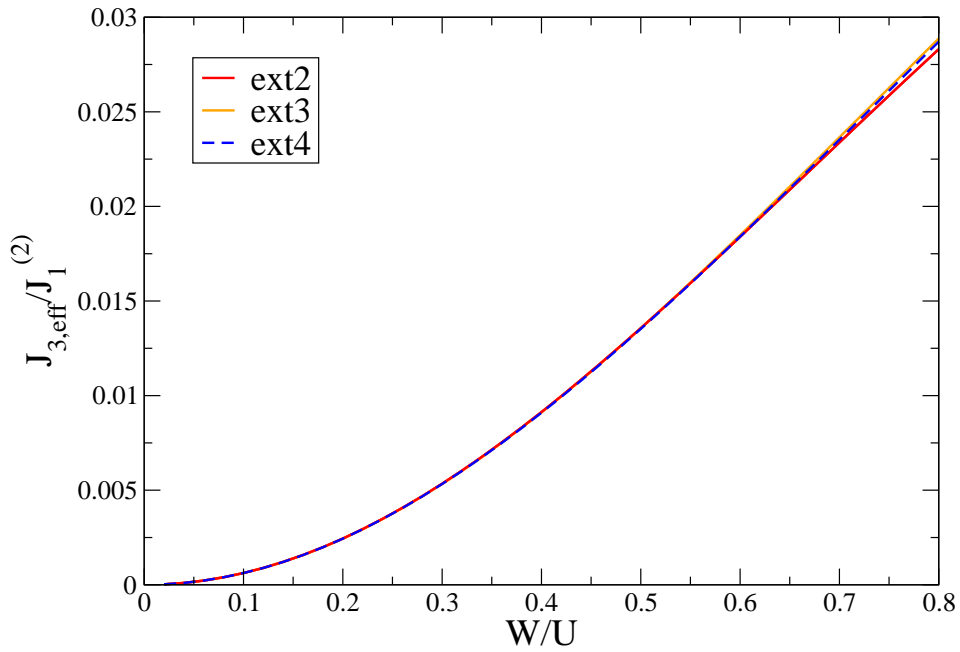
Fig. 4.10.: Dependence of the coupling constant  $J_1$  for the nearest neighbor Heisenberg interaction on the linear chain.

Heisenberg interaction terms between two spins with a greater distance occur as well. The interaction between to spins at a distance of  $2a$  with the lattice constant  $a$  is given by

$$H_{3NN} = J_3 \sum_{\langle\langle i,j \rangle\rangle} \vec{S}_i \vec{S}_j \quad (4.7.2)$$

where the sum runs over next to nearest neighbors on a linear chain. The results for this coupling are shown in Fig. 4.11.

All curves shown in this figure show the same behavior. The spin interaction  $J_3$  is proportional to  $\frac{t^4}{U^3}$  in leading order, which explains its relative small values. Differences in the results for different truncation schemes can only be seen for larger values of  $W/U$ .  $J_3$  turns out to be much smaller than  $J_1$ . For  $W/U = 0.4$  the value of  $J_3$  is one percent of the one for  $J_1$ . Therefore the coupling between spins at a distance of  $2a$  may be safely neglected in a simplified model.

Fig. 4.11.: Results for the Heisenberg term  $J_3$ 

#### 4.7.1.2. Hopping terms

The first hopping term we consider belongs to  $T_0$  which was explained before

$$\hat{T}_0 = t_0 \sum_{\langle i,j \rangle, \sigma} \left[ (1 - \hat{n}_{i,\sigma}) \hat{c}_{i,\bar{\sigma}}^\dagger \hat{c}_{j,\bar{\sigma}} (1 - \hat{n}_{j,\sigma}) + \hat{n}_{i,\sigma} \hat{c}_{i,\bar{\sigma}}^\dagger \hat{c}_{j,\bar{\sigma}} \hat{n}_{j,\sigma} + h.c. \right]. \quad (4.7.3)$$

This term represents hopping without an effect on the number of DOs and it is already included in the initial Hamiltonian. The results for the minimal and the NN model do not depend on  $W/U$  (see Fig. 4.12).

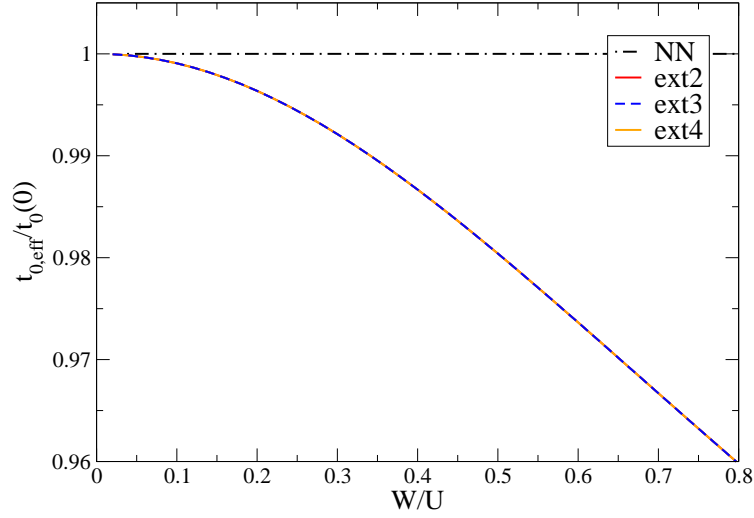


Fig. 4.12.:  $W/U$  dependence of the hopping element  $t_0$

Besides  $T_0$  the effective Hamiltonian also contains spin dependent hopping processes. One of this processes is described by

$$T''_{\text{spin}} = t''_{\text{spin}} \sum_{\alpha, \beta} \sum_{\langle\langle i, k, j \rangle\rangle} \left\{ \left[ \left( 1 - \hat{n}_{i, \alpha} \hat{c}_{i, \alpha}^\dagger \right) \vec{\sigma}_{\bar{\alpha}, \bar{\beta}} \hat{c}_{j, \bar{\beta}} (1 - \hat{n}_{j, \beta}) \right] \vec{S}_k \right. \\ \left. + \left[ \hat{n}_{i, \alpha} \hat{c}_{i, \alpha}^\dagger \vec{\sigma}_{\bar{\alpha}, \bar{\beta}} \hat{c}_{j, \bar{\beta}} \hat{n}_{j, \beta} \right] \vec{S}_k + h.c. \right\} \quad (4.7.4)$$

where the bracket under the sum indicates that this process takes place between sites  $i$  and  $j$  with a distance  $2a$  and  $k$  in the middle of  $i$  and  $j$ .  $\vec{\sigma}_{\alpha, \beta}$  represents the vector of the Pauli matrices. One possible process described by  $T''_{\text{spin}}$  is the hopping of an electron with spin  $\bar{\beta}$  from a singly occupied site  $j$  to site  $i$ . During the hopping the electron changes its spin. To conserve the total spin another spin flip has to appear on site  $k$ .

The results for the corresponding coupling constant coincide for the extension2 and the extension3 calculations (see Fig.4.13). A calculation with maximal extension of four yields smaller values for large  $W/U$ .

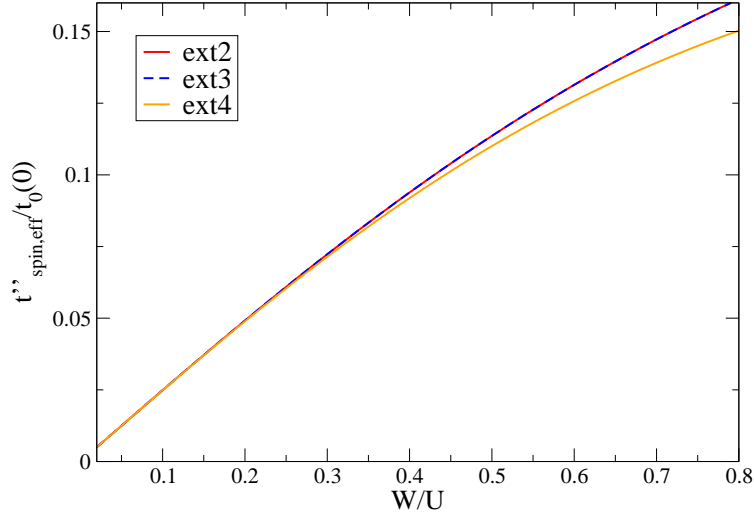


Fig. 4.13.: Results for the spin dependent hopping element on a linear chain.

#### 4.7.1.3. Interaction terms

An interaction term which has already been introduced is the hopping of a DO

$$H_{pair} = V_p \sum_{\langle i,j \rangle} \left( \hat{c}_{i,\uparrow}^\dagger \hat{c}_{i,\downarrow}^\dagger \hat{c}_{j,\downarrow} \hat{c}_{j,\uparrow} + h.c. \right). \quad (4.7.5)$$

A process described by this term is the hopping of two electrons from site  $j$  to an empty site  $i$ . The results for the effective coupling constant  $V_p$  for truncation schemes with a maximal extension  $e \geq 2$  coincide (see Fig. 4.14). Thus  $V_p$  seems to be converged in a calculation with a maximal extension of two. Figure 4.14 shows the coefficient of the operator

$$H''_{pair} = V''_{pair} \sum_{\sigma} \sum_{\langle\langle i,j \rangle\rangle} \left[ \hat{c}_{k,\sigma}^\dagger \hat{c}_{k,\bar{\sigma}}^\dagger \hat{c}_{i,\bar{\sigma}} \hat{n}_{i,\sigma} \hat{c}_{j,\sigma} (1 - \hat{n}_{j,\bar{\sigma}}) + \hat{c}_{k,\sigma}^\dagger \hat{c}_{k,\bar{\sigma}}^\dagger \hat{c}_{i,\bar{\sigma}} (1 - \hat{n}_{i,\sigma}) \hat{c}_{j,\sigma} \hat{n}_{j,\bar{\sigma}} + h.c. \right]. \quad (4.7.6)$$

This operator describes processes similar to  $H_p$  on three sites. One possible action of this term is to move an electron with spin up from a doubly occupied site  $i$  to an empty site  $k$ . Additionally an electron with spin down hops from the singly occupied site  $j$  to site  $k$ . Conclusively the total effect of this term is to destroy a DO on site  $i$  and create one on site  $j$ .

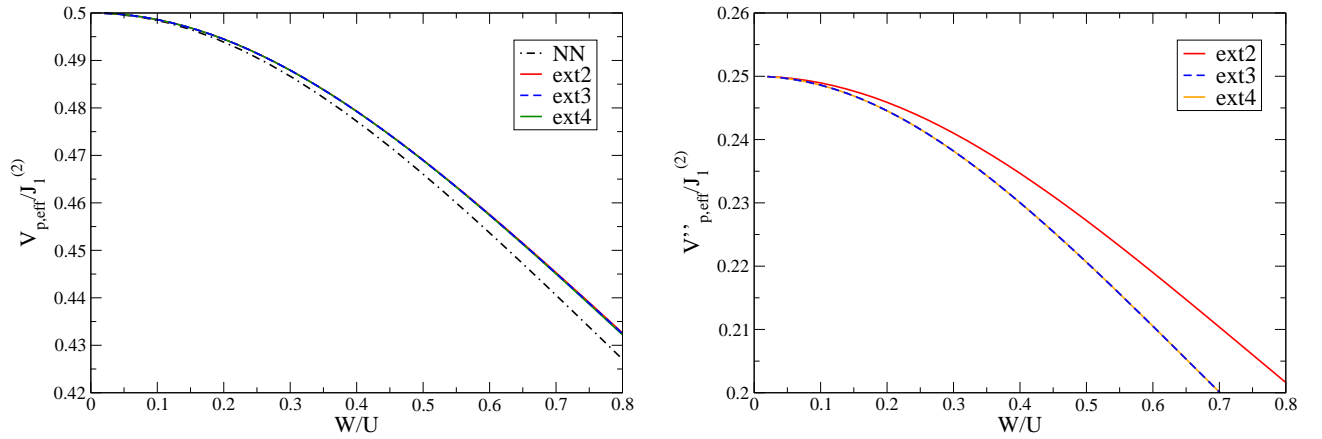


Fig. 4.14.: Results for the pair interaction terms  $V_p$  and  $V_p''$

Another type of interaction terms are density density interactions. The density-density interaction between two nearest neighbouring DOs is given by

$$H_V = V \sum_{\langle i,j \rangle} \bar{n}_i \bar{n}_j. \quad (4.7.7)$$

The corresponding coupling constant is shown in Fig. 4.15.

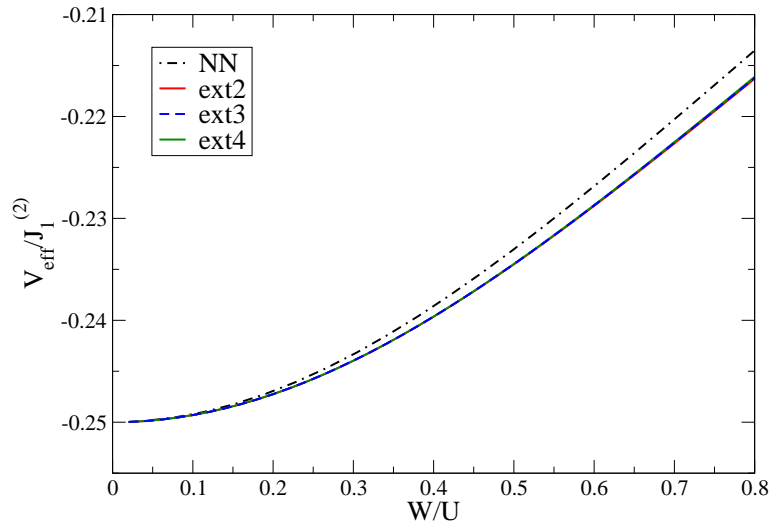


Fig. 4.15.: Behavior of the density density interaction in dependence of  $W/U$

For this constant all but the NN calculation yield similar results.

#### 4.7.1.4. Results for the $0n$ generator and the $0n1n$ generator

After presenting the results for the MKU generator we now compare these results to the ones obtained by the use of the other generators.

Before discussing the effective coupling constants we will have a look at the behavior of the off-diagonal terms as these visualize the differences between the different generators. Note that these off-diagonal elements do not correspond to the ROD for the  $0n$  generator. In the ROD only those terms are included which are considered in the generator. For the  $0n$  generator this means that only terms which consist of either only creation operators or only annihilation operators are considered in the ROD.

Figure 4.16 depicts the off-diagonal terms for a calculation with a maximal extension of four.

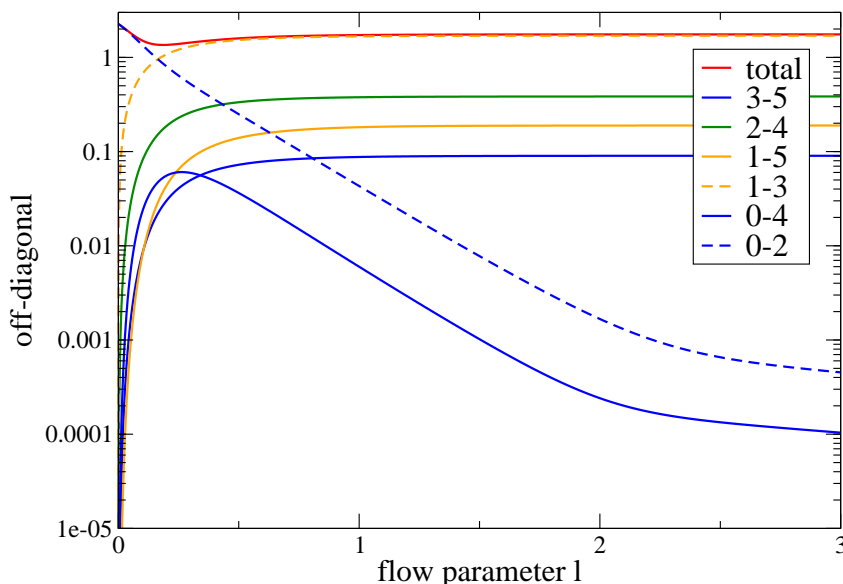


Fig. 4.16.: Behavior of the off-diagonal terms for the  $0n$  generator and a maximal extension of four

The off-diagonal terms are denoted according to the quasiparticle sectors they connect. Thus 0-2 denotes terms that create two quasiparticles without annihilating any quasiparticle as well as terms which annihilate two quasiparticles without creating any quasiparticle. Note that these terms may couple to the groundstate as well as to other subspaces.

At the beginning the Hamiltonian consists of terms combining the zero and the two quasiparticle sector. The contributions from these terms start at  $4zt^2$  as explained before. As these terms are included in the generator they are rotated away by the CUT. Thus their coefficients decrease exponentially. During the flow there are new terms arising among which the 1-3 terms yield the most important contributions. These terms are not included

in the  $0n$  generator, thus their contribution stays finite. The same argument pertains for the 2-4, 3-5, 1-5 and the 1-3 terms.

Additionally there are terms arising denoted by 0-4. As these terms may couple to the ground state sector they are rotated away leading to exponentially decreasing contributions.

An analogous consideration concerning the off-diagonal terms in the case of the  $0n1n$  generator is shown in Fig. 4.17. The terms coupling to the ground state sector show the same behavior as in the case of the  $0n$  generator. Additionally also terms coupling to the one quasiparticle sector are included in the  $0n1n$  generator. This leads to an exponential decrease of contributions from 1-3 terms. The terms 2-4 are not part of the generator thus their contributions stay finite.

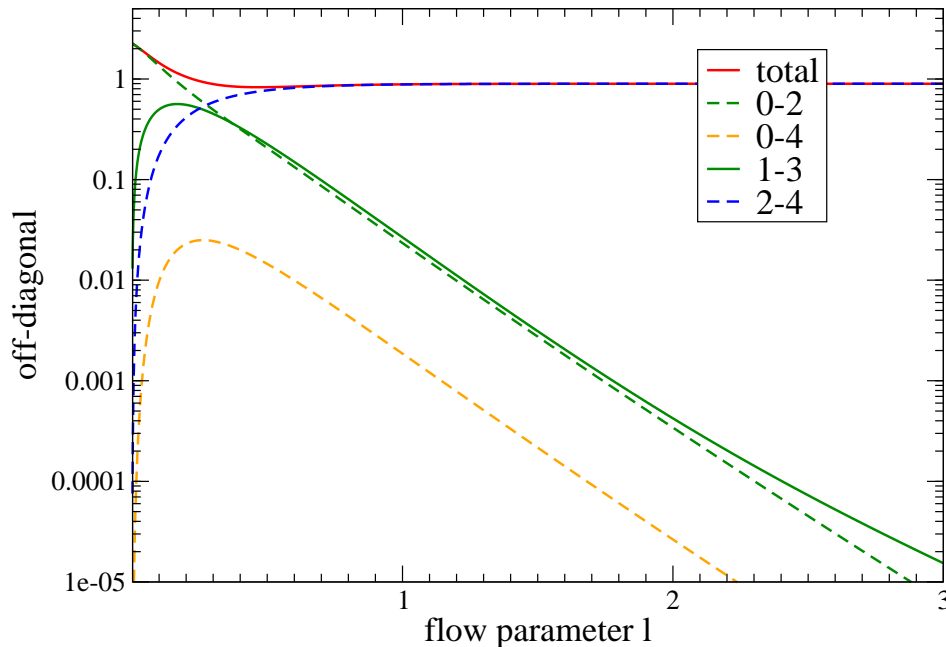


Fig. 4.17.: Behavior of the off-diagonal terms for the  $0n1n$ -generator

By the use of these generators we calculated all effective coupling constants for various truncation schemes. The following figures present a few exemplary results obtained for a calculation with a maximal extension of four.

We skip the spin terms in this context as the coupling constants obtained with different generators lie perfectly above each other. As the  $0n$  generator yields similar values for the nearest neighbor Heisenberg exchange as the MKU generator we assume that for the dominant Heisenberg interactions all important terms are already included in the ground state sector. Therefore we start the discussion with the hopping terms.

The behavior of the hopping parameter  $t_0$  for the various generators is depicted in Fig. 4.18.

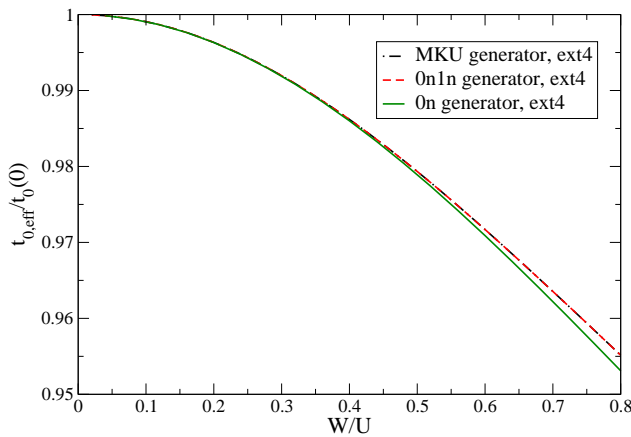


Fig. 4.18.: Results for the hopping element  $t_0$  for different generators

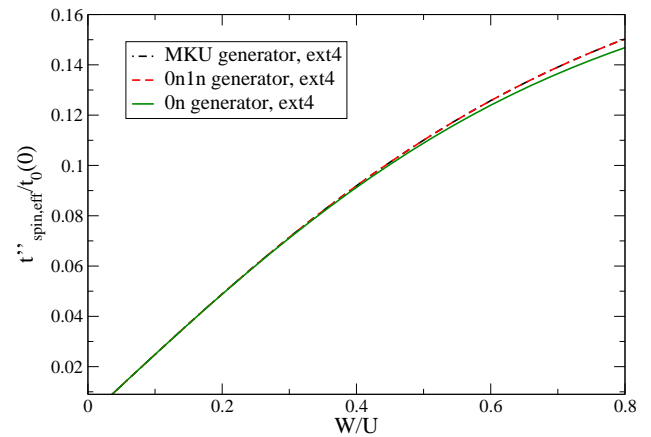


Fig. 4.19.: Results for the spin dependent hopping term (Eq. 4.7.4)

The results for the hopping element  $t_0$  obtained with the  $0n1n$  generator and the ones obtained with the MKU generator lie above each other whereas the  $0n$  generator leads to slightly smaller values for  $W/U \geq 0.3$  (see Fig. 4.18).

The same behavior can be observed for the spin dependent hopping terms (see Fig. 4.19).

In a next step we discuss the results for the interaction terms in Figs. 4.20 and 4.21. As the  $0n$  generator only contains terms of the ground state sector, we would expect that the deviation of the results for the interaction terms are rather large. In fact the results for the pair interaction describing the interaction of a hole with a doubly occupied site (see Eq. 4.6.8) do not show large deviations for the  $0n$  generator from the result for the MKU and the  $0n1n$  generator.

As can be seen in Fig. 4.21 the deviation increases with  $W/U$ . Even for larger values of  $W/U$  the deviation compared to the perturbative result for  $J_1$  is smaller than 0.003. For the  $0n1n$  generator the deviations are negligible.

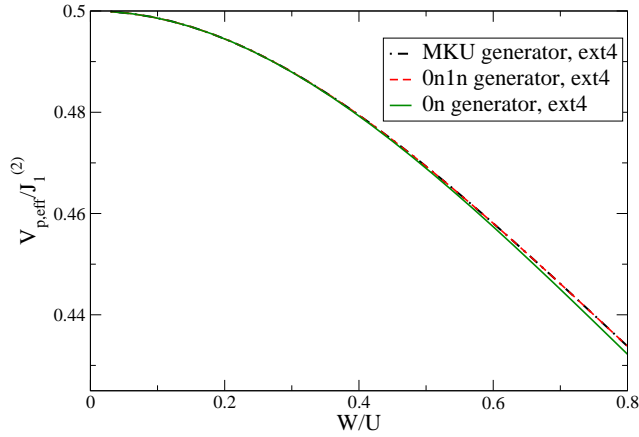


Fig. 4.20.: Results for the pair interaction obtained with different generators

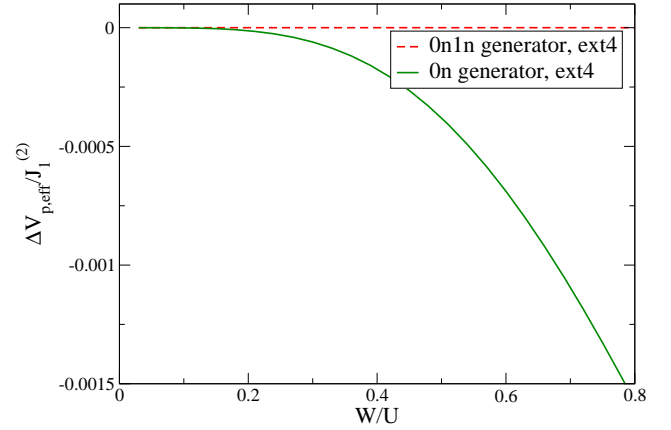


Fig. 4.21.: Deviation of the results from the MKU results

Figure 4.22 shows the pair interaction (see Eq. 4.7.5) between next nearest neighbors on a linear chain. For this coupling constant the results for the  $0n$  generator show larger deviations than for the nearest neighbor interaction. This is caused by the fact that these terms are extended over a larger distance.

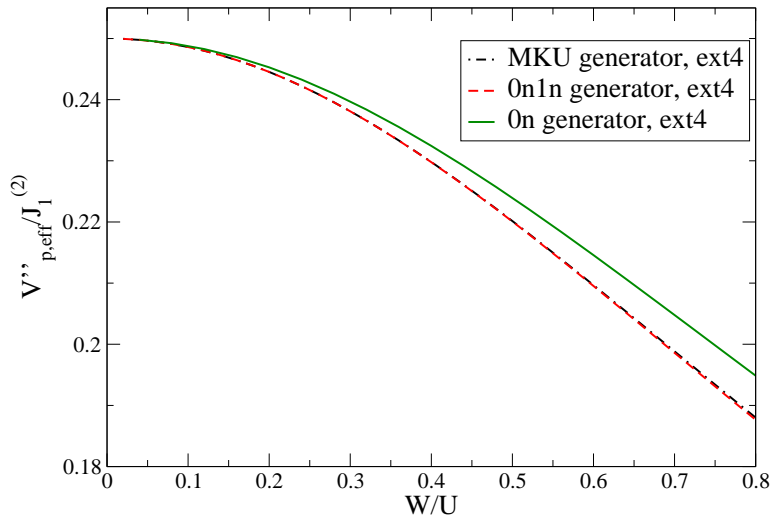


Fig. 4.22.:  $W/U$  dependence of  $V''_p$  as defined in Eq. 4.7.6 for different generators

For the density density interaction between nearest neighbors (Eq. 4.7.7) we obtain a similar result for all three types of generators. The results for this term are depicted in Fig. 4.23. Surprisingly the results of a CUT with the  $0n$  generator show a better agreement with the MKU generator for this coupling constant than the results obtained

by the use of the  $0n1n$  generator.

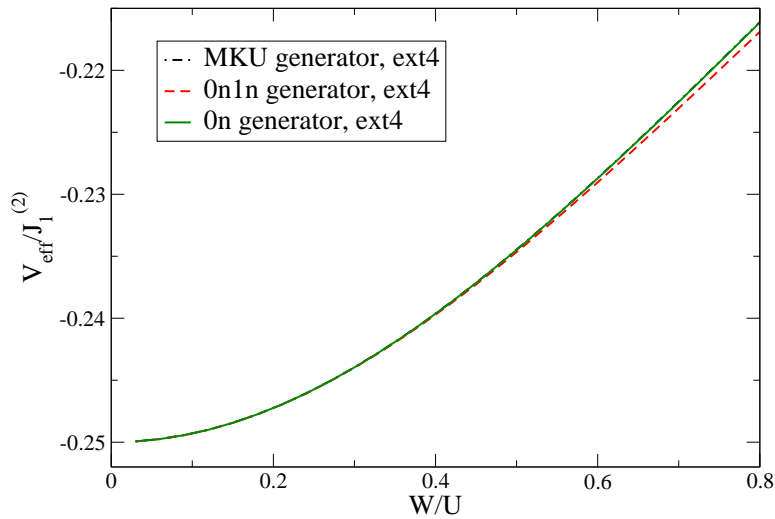


Fig. 4.23.: Results for the density density interaction for different generators

All three generators lead to similar results for the coupling constants. Especially the pure spin terms  $J_1$  and  $J_3$  lead to a good agreement of the results for different generators. As a result of this it is advantageous to use the  $0n$  generator in further calculation as the calculations performed with this generator show a better convergence and lead to less computational effort.

## 4.8. Results for the half-filled two-dimensional square lattice

### 4.8.1. Results obtained by the use of the MKU generator

For the two-dimensional case we directly show the results for the higher truncation schemes like the plaquette calculation (see Fig. 4.24) or the upto4 calculation. In the upto4 calculation all terms are considered which fit onto the double plaquette scheme (see Fig. 4.25) and consist of at most four local operators.

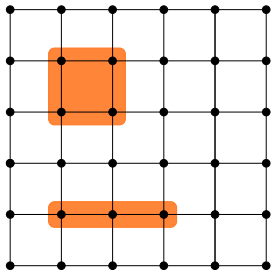


Fig. 4.24.: Plaquette scheme

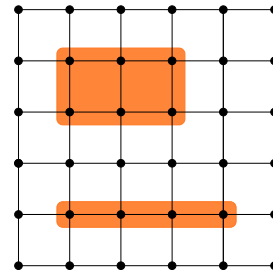


Fig. 4.25.: Double plaquette scheme

As will be seen in Sect. 6.4 the mapping to the effective model is restricted to values  $W/U \leq 1$ . Therefore we show the coupling constant depending on  $W/U$  for  $W/U \leq 1$ .

#### 4.8.1.1. Results for the spin interactions

The most important spin term is the Heisenberg exchange between nearest neighbors  $J_1$ . The behavior of this coupling constant compared to the second order perturbation theory result is shown in figure 4.26.

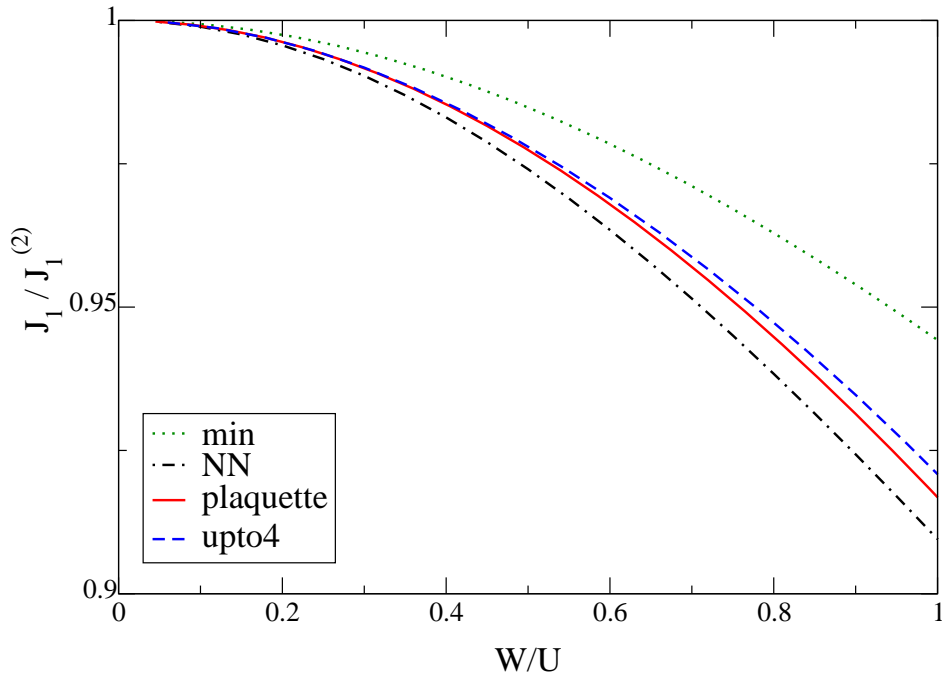


Fig. 4.26.: Heisenberg exchange term  $J_1$  in dependence of  $W/U$

This coupling constant shows the same behavior in the two-dimensional case as in the one-dimensional case. The nearest neighbor coupling  $J_1$  is reduced for larger  $W/U$ . The minimal truncation scheme yields higher values for  $J_1$  than the other calculations. The plaquette calculation already includes all important terms thus the results obtained in the plaquette calculation and the one obtained in the upto4 calculation almost coincide.

In addition to the coupling  $J_3$ , which was introduced for the one-dimensional case in Eq. 4.7.2, we introduce the Heisenberg exchange between diagonal neighbors. The corresponding coupling constant is denoted by  $J_2$ . The corresponding results are shown in Figs. 4.27 and 4.28.

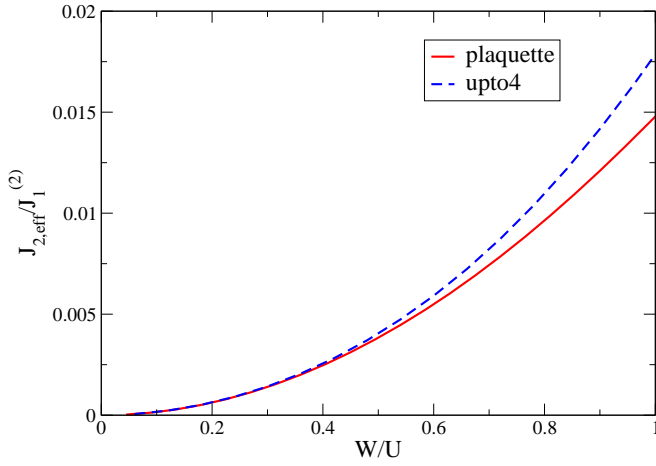


Fig. 4.27.: Spin interaction between diagonal neighbors

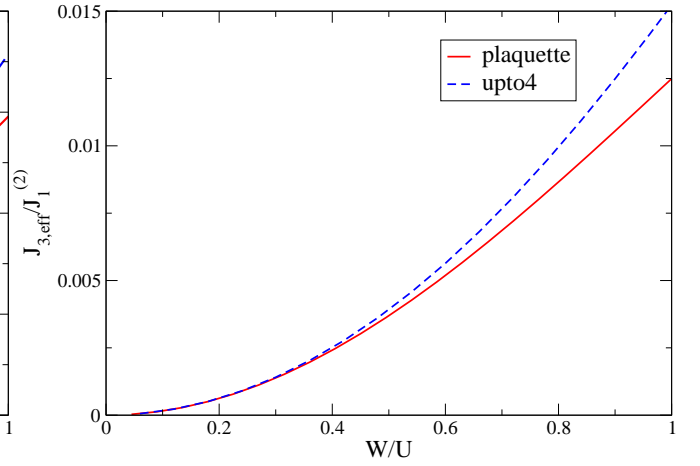


Fig. 4.28.: Spin interaction  $J_3$  as defined in Eq. 4.7.2

Both coupling constants yield much smaller values than  $J_1$  and can thus be neglected in simplified models. In contrast to  $J_1$  the results for  $J_2$  and  $J_3$  for the plaquette calculation differ significantly from the results of the upto4 calculation. The plaquette calculation is the first truncation scheme in which these terms can occur. Thus the corresponding coupling constants change if more extended terms are considered as it is the case in the upto4 calculation.

Besides spin interactions between two spins the two-dimensional case also yields four spin interactions. One of these terms is the ring exchange term [Tak77, KK02]

$$H_{\square} = J_{\square} \sum_{\langle i,j,k,l \rangle} \left[ (\vec{S}_i \vec{S}_j) (\vec{S}_k \vec{S}_l) + (\vec{S}_i \vec{S}_l) (\vec{S}_j \vec{S}_k) - (\vec{S}_i \vec{S}_k) (\vec{S}_j \vec{S}_l) \right]. \quad (4.8.1)$$

This term presents a spin interaction between four spins on a plaquette as presented in Fig. 4.29.

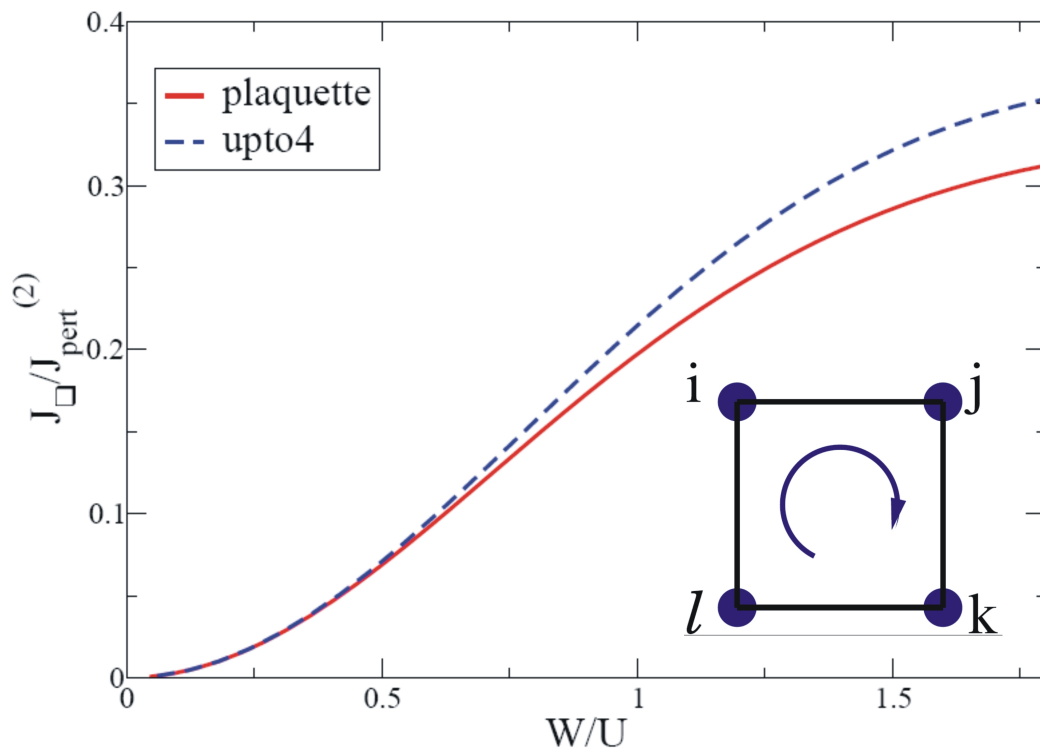


Fig. 4.29.: Results for the ring exchange  $J_{\square}$  dependent on  $W/U$

This coupling constant takes values of up to 43 percent of  $J_1$  for  $W/U = 1.5$ . Consequently the ring exchange may not be neglected in an effective model for the spins. This observation is in agreement with the results obtained by A. Reischl [RMHU04].

The importance of this term was assumed before [Tak77] and already observed in  $\text{La}_2\text{CuO}_4$  [KK02]. The ring exchange turned out to be necessary to explain the IR data for high- $T_C$  cuprates. Without this term it is not possible to explain the additional peaks in the spectrum [LES99, MVM04].

Besides this term there is another four spin interaction the so-called cross interaction

$$H_{\times} = J_{\times} \sum_{\langle i,j,k,l \rangle} (\vec{S}_i \vec{S}_k) (\vec{S}_j \vec{S}_l). \quad (4.8.2)$$

The interacting sites are aligned in the same way as for the ring exchange. In contrast to the ring exchange the interaction shown here takes place between diagonal neighbors. Figure 4.30 shows results for the effective coupling constant  $J_{\times}$ . Compared to the ring exchange this interaction is much smaller.

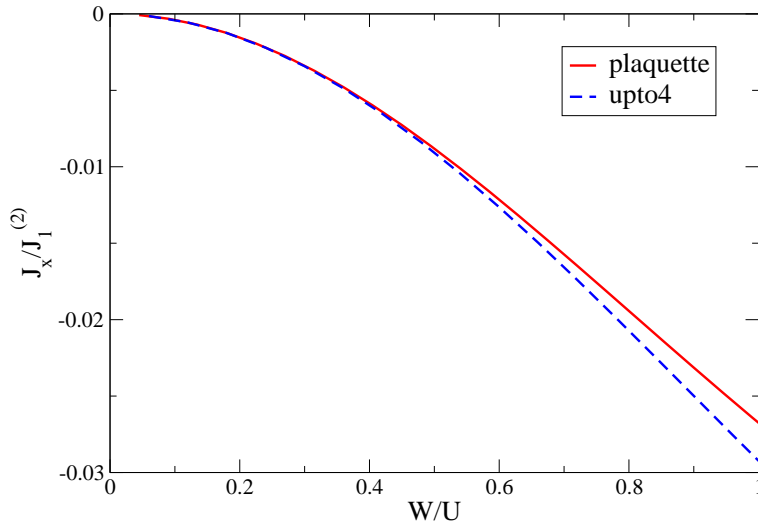


Fig. 4.30.: Results for the cross exchange  $J_x$  dependent on  $W/U$

The results obtained in this thesis coincide with the results obtained by A. Reischl [RMHU04] within the scope of the computer precision.

#### 4.8.1.2. Results for the hopping terms

This section deals with the behavior of the hopping terms. The first term to be considered belongs to  $T_0$  which was introduced before (Eq. 4.7.3). This term presents hopping processes without a change of the number of DOs. The corresponding parameter is compared to its initial value  $t_0(0)$ . As can be seen in Fig. 4.31 the results for this constant obtained in the plaquette calculation differ from the results for the plaquette calculation. The hopping parameter is influenced by terms which are considered in the upto4 calculation but not in the plaquette calculation.

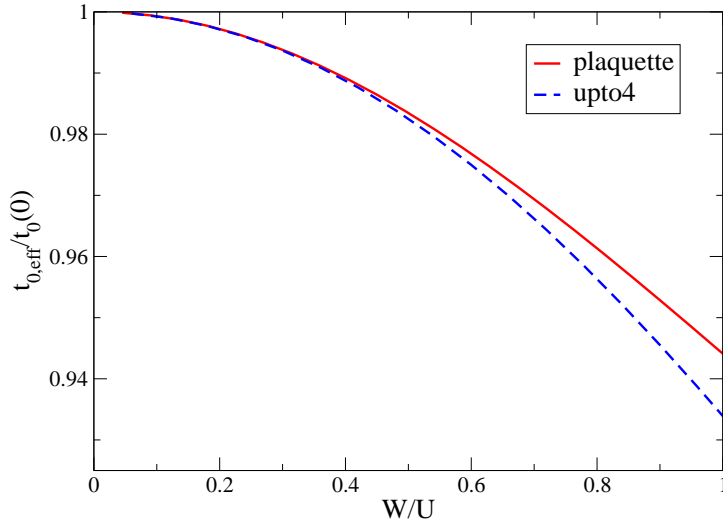


Fig. 4.31.: Results for the coupling constant  $t_0$  for the MKU generator.

Hopping terms can also be defined between diagonal neighbors  $T'_0$ .

$$T'_0 = t' \sum_{\sigma} \sum_{\langle\langle i,j \rangle\rangle} \left[ (1 - \hat{n}_{i,\sigma}) \hat{c}_{i,\sigma}^{\dagger} \hat{c}_{j,\sigma} (1 - \hat{n}_{j,\sigma}) + \hat{n}_{i,\sigma} \hat{c}_{i,\sigma}^{\dagger} \hat{c}_{j,\sigma} \hat{n}_{j,\sigma} + h.c. \right] \quad (4.8.3)$$

The operator  $T''_0$  includes the same terms but for this operator the sum runs over two sites with a distance of  $2a$  with the lattice constant  $a$ .

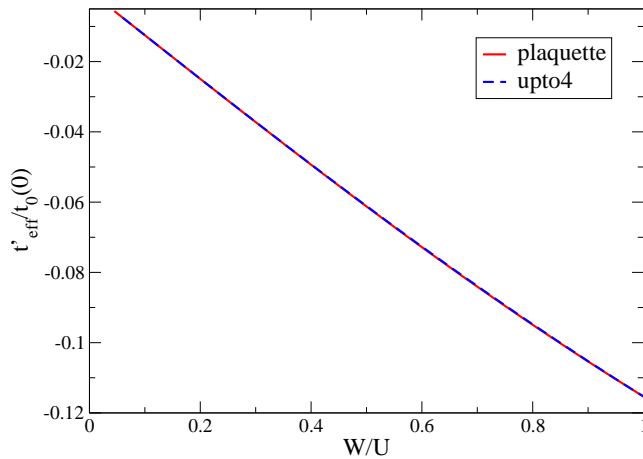


Fig. 4.32.: Results for the hopping parameter  $t'$

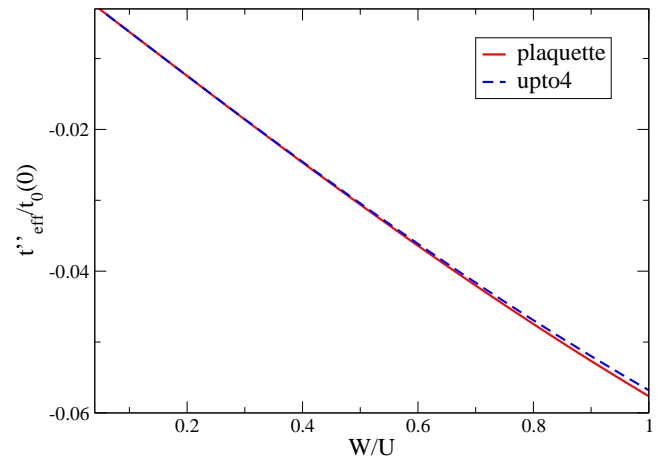


Fig. 4.33.: Results for the hopping parameter  $t''$

Both hopping parameters are much smaller than  $t_0$ . This can be understood from the larger distance of the corresponding sites.

Besides these terms the effective model also contains spin dependent hopping terms for the two dimensional case. These terms read

$$T'_{spin} = t'_{spin} \sum_{\alpha\beta} \sum_{\langle i,k,j \rangle} \left\{ \left[ (1 - \hat{n}_{i,\alpha}) \hat{c}_{i,\alpha}^\dagger \vec{\sigma}_{\alpha,\beta} \hat{c}_{j,\beta} (1 - \hat{n}_{j,\beta}) + \hat{n}_{i,\alpha} \hat{c}_{i,\alpha}^\dagger \vec{\sigma}_{\alpha,\beta} \hat{c}_{j,\beta} \hat{n}_{j,\beta} + h.c. \right] \vec{S}_k \right\} \quad (4.8.4)$$

where the sum runs over two diagonal neighbors  $i$  and  $j$  which have a common nearest neighbor  $k$ .

For the term  $T''_{spin}$  we just have to replace the sum by a sum running over  $ijk$  which are aligned along one coordinate axis.

As the parameters behave similarly we restrict the discussion to  $t'_{spin}$  which is shown in Fig. 4.34.

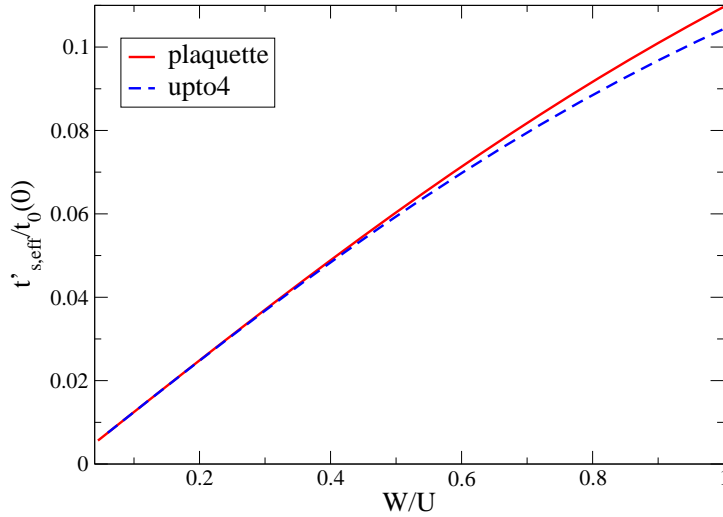


Fig. 4.34.: Results for the spin dependent hopping parameter  $t'_{spin}$  as defined in Eq. 4.8.4

The spin dependent parameters have the same size as the hopping parameter between diagonal neighbors  $t'_{eff}$ . Thus spin dependent hopping terms can not be neglected in a  $t'$  model.

### 4.8.1.3. Results for the interaction terms

In agreement with the one-dimensional case we consider density density interactions expressed in the coupling constant  $V$

$$H_V = V \sum_{\langle i,j \rangle} \bar{n}_i \bar{n}_j.$$

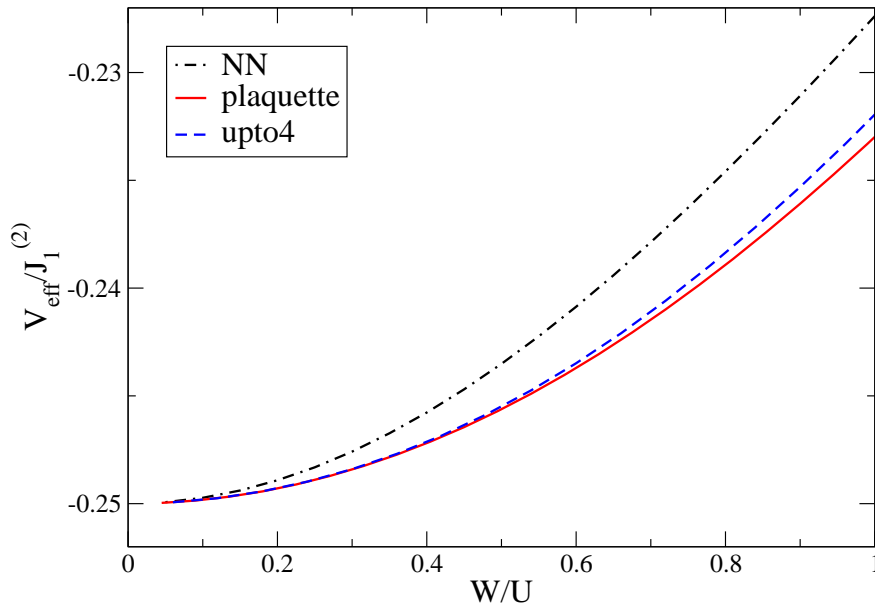


Fig. 4.35.: Density density interaction term dependent on  $W/U$

The effective value  $V_{\text{eff}}$  is proportional to  $\frac{t^2}{U}$ . This dependency is accounted for by the fact that the interaction is mediated by hopping processes. For this interaction two hopping processes are needed. Each of these processes is proportional to  $t$  which leads to the quadratic dependence.

Another type of interactions included in the effective model are pair interactions, between two DOs. These terms may be extended over nearest neighbors like  $V_p$  which was defined in Eq. 4.7.5 or over more terms. Besides the term  $H_p''$ , which was considered for the one-dimensional case, there exists another pair interaction term  $V_p'$  between three spins on a plaquette.

$$H'_{\text{pair}} = V'_{\text{pair}} \sum_{\sigma} \sum_{\langle i,j \rangle} \left[ \hat{c}_{k,\sigma}^{\dagger} \hat{c}_{k,\bar{\sigma}}^{\dagger} \hat{c}_{i,\bar{\sigma}} \hat{n}_{i,\sigma} \hat{c}_{j,\sigma} (1 - \bar{n}_{j,\bar{\sigma}}) + \hat{c}_{k,\sigma}^{\dagger} \hat{c}_{k,\bar{\sigma}}^{\dagger} \hat{c}_{i,\bar{\sigma}} (1 - \hat{n}_{i,\sigma}) \hat{c}_{j,\sigma} \bar{n}_{j,\bar{\sigma}} + h.c. \right]. \quad (4.8.5)$$

In this case  $i$  and  $j$  represent diagonal neighbors.

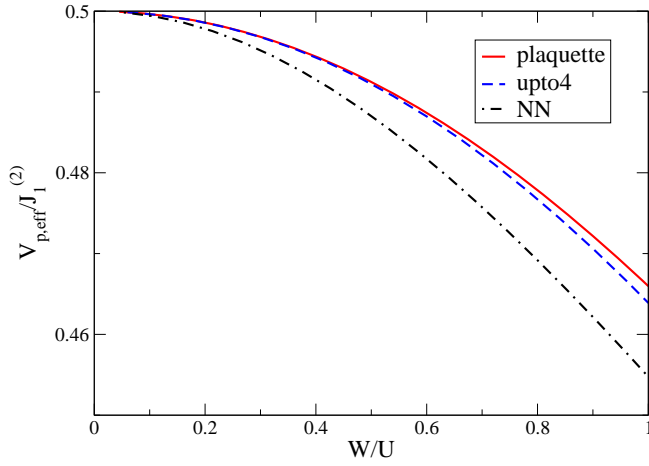


Fig. 4.36.: Coefficient of the pair interaction between nearest neighbor sites

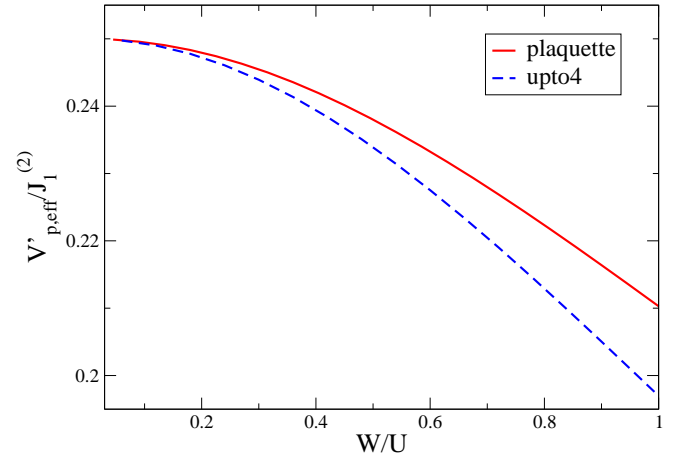


Fig. 4.37.: Coefficient of the pair interaction between diagonal neighboring sites

The coupling  $V'_p$  is as half as big as  $V_p$ . The operator corresponding to  $V'_p$  imposes an additional constraint on site  $k$ . Thus the coupling  $V'_p$  is smaller than the one for  $V_p$  for which only site  $i$  and site  $j$  have to be in a certain state.

We skipped  $V''_p$  as this coupling constant shows a similar behavior as the coupling  $V'_p$  which is shown in Fig. 4.37. This is due to the fact that both terms originate from hopping processes over three sites.

The last interaction terms considered here are correlated hopping terms. These terms describe processes where an electron hops from a singly occupied site  $j$  to an empty site  $i$  under the condition that there is a DO on site  $k$ . A process like this which takes place between diagonal neighbors  $i$  and  $j$  is described by

$$H'_{Vn} = V'_n \sum_{\alpha,\beta} \sum_{\langle i,j \rangle} \left\{ (1 - \hat{n}_{i,\alpha}) \hat{c}_{i,\alpha}^\dagger \hat{c}_{j,\beta} (1 - \hat{n}_{j,\beta}) \bar{n}_k + \hat{n}_{i,\alpha} \hat{c}_{i,\alpha}^\dagger \hat{c}_{j,\beta} \hat{n}_{j,\beta} \bar{n}_k + h.c. \right\}. \quad (4.8.6)$$

The prefactor  $V''_n$  denotes the effective coefficient for such a process taking place between three sites which are aligned along one direction.

The effective coefficients of these terms are shown in the Fig. 4.38 and 4.39.

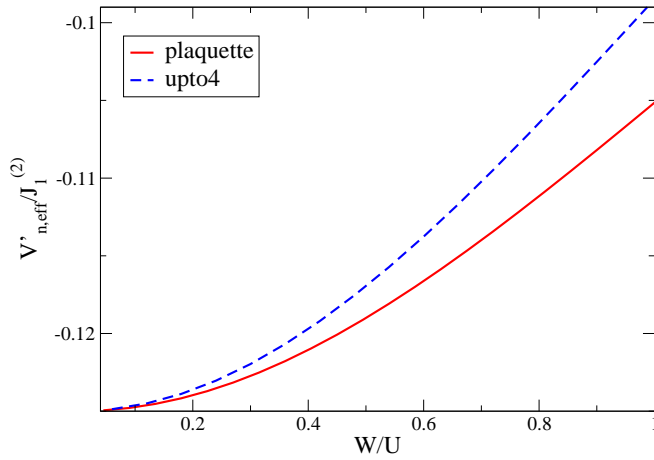


Fig. 4.38.: Coefficient of the density density interaction between diagonal neighbors

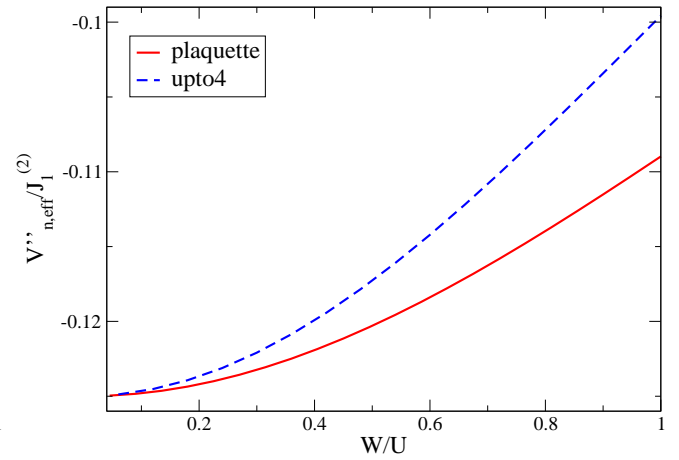


Fig. 4.39.: Coefficient of the density density interaction between third nearest neighbors on a square lattice

The results obtained in this context coincide with the results of the work done by A. Reischl [RMHU04]. The results of this work agree with our results within the computer precision.

#### 4.8.2. $0n$ generator and $0n1n$ generator

In this section we analyze the effects of the use of different generators on the effective coupling constants. With the use of these generators we calculated all coupling constants for various truncation schemes in dependence of  $W/U$ .

In contrast to the calculations done with the MKU generator we are able to perform the double plaquette calculation with the  $0n$  as well as with the  $0n1n$  generator. Figure 4.40 shows the ROD for these calculations in dependence of the flow parameter  $\ell$ . For the  $0n$  generator the ROD converges for all values of  $W/U$ . In contrast to this the ROD for the  $0n1n$  generator shows divergencies for larger values of  $W/U$ . Thus for larger values of  $W/U$  the terms in the  $0n1n$  generator can not be transformed away. Consequently the mapping breaks down.

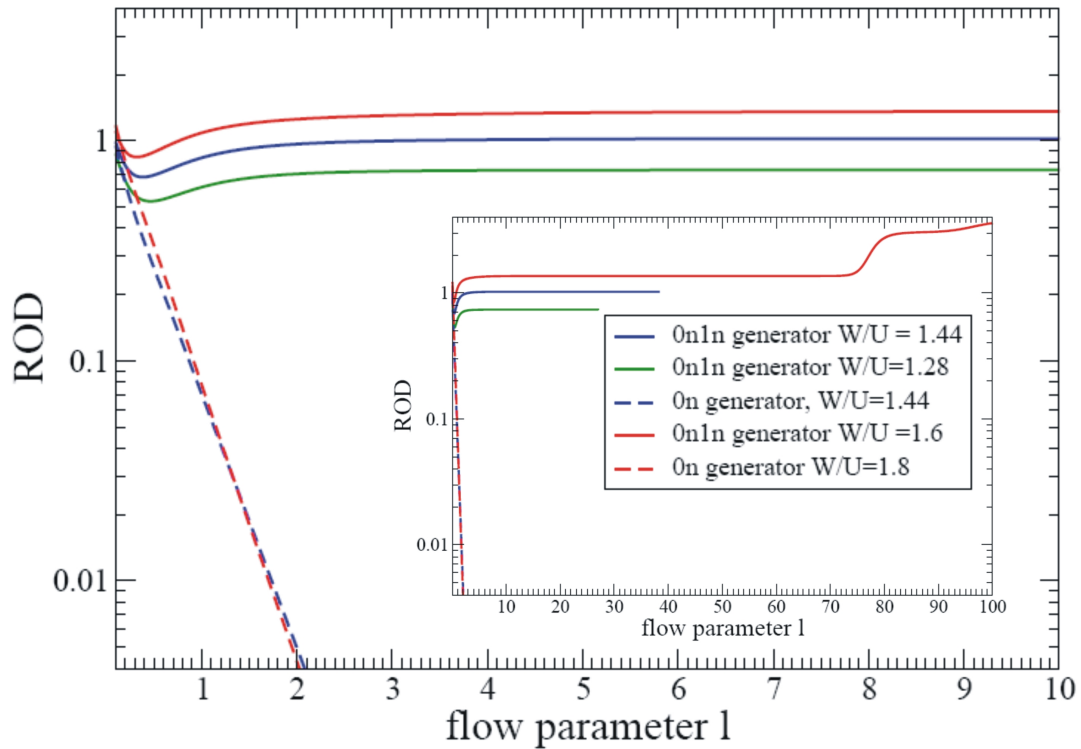


Fig. 4.40.: Behavior of the ROD for various starting values and generators

We study the effects of the choice of the generators on the coupling constants starting with the spin terms. A few exemplary results for the upto4 truncation scheme are shown.

#### 4.8.2.1. Spin terms

The most important spin coupling is the Heisenberg interaction  $H_{\text{NN}}$  between nearest neighbors as defined in Eq. 4.7.7. The corresponding coupling constant is shown in Fig. 4.41. As the curves lie nearly above each other we additionally show the deviation of the results for the  $0n$  and the  $0n1n$  generator from the results obtained with the MKU generator in Fig. 4.42.

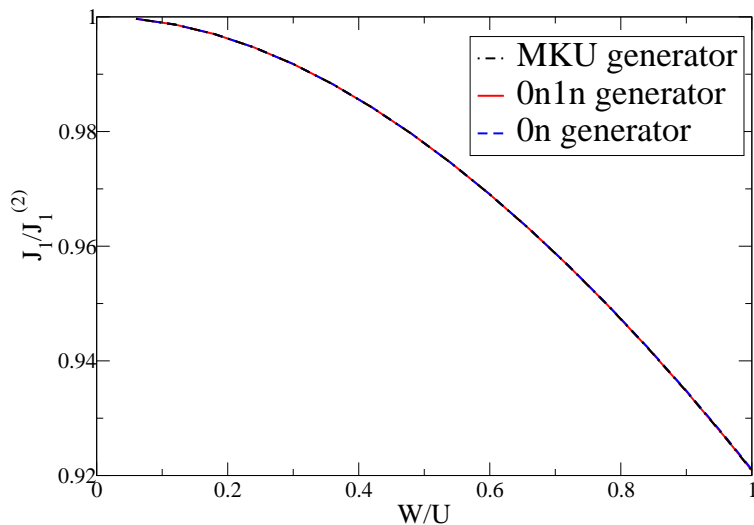


Fig. 4.41.: Behavior of nearest neighbor Heisenberg coupling for different generators.

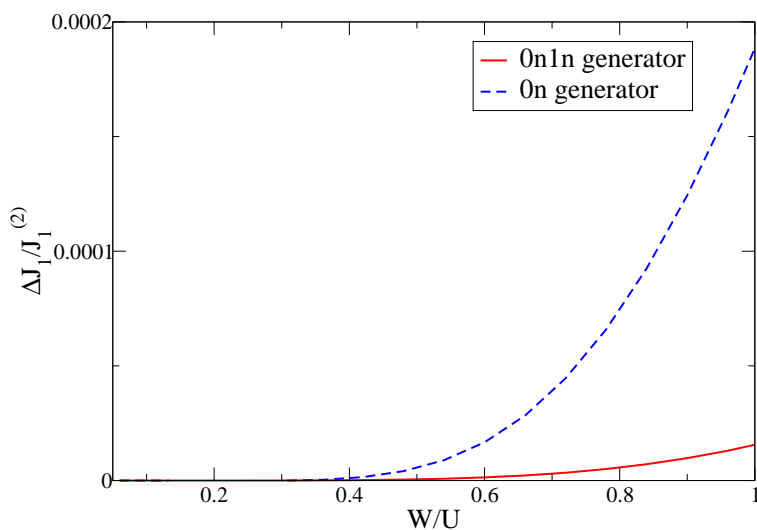


Fig. 4.42.: Deviation of the results for different generators from the MKU result.

The relative deviation of the coupling constant obtained with the  $0n$  generator from the one obtained by the use of the MKU generator stay below 0.006% for  $W/U \leq 1.5$ . For the  $0n1n$  generator the deviation is even smaller.

The  $0n$  generator only decouples the sector without quasiparticles from the other sectors. Thus this result supports the assumption that all processes which are important for the nearest neighbor Heisenberg interaction are already contained in this sector. As the  $0n1n$  generator additionally considers the one-particle sector the deviations for this generator

are even smaller.

For the coupling constants  $J_2$  and  $J_3$  (Eq. 4.7.2) we observe a similar behavior. Therefore we show the relative deviation of these constants in Fig. 4.43 and Fig. 4.44.

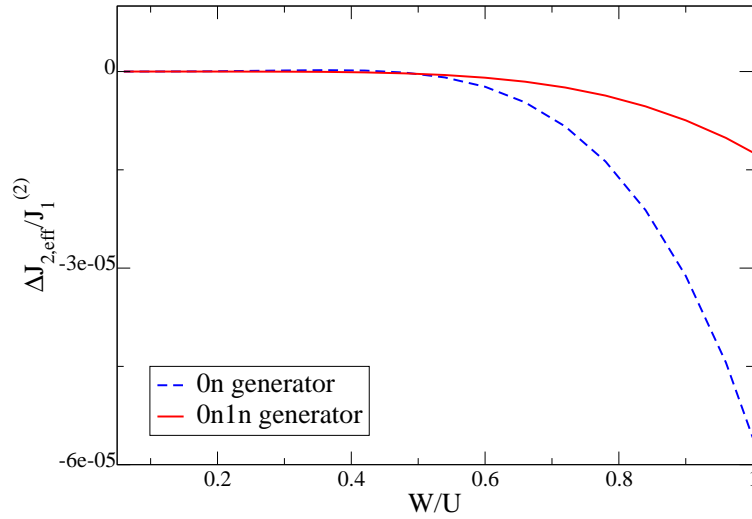


Fig. 4.43.: Deviation of the results for  $J_2$  for different generators from the MKU result.

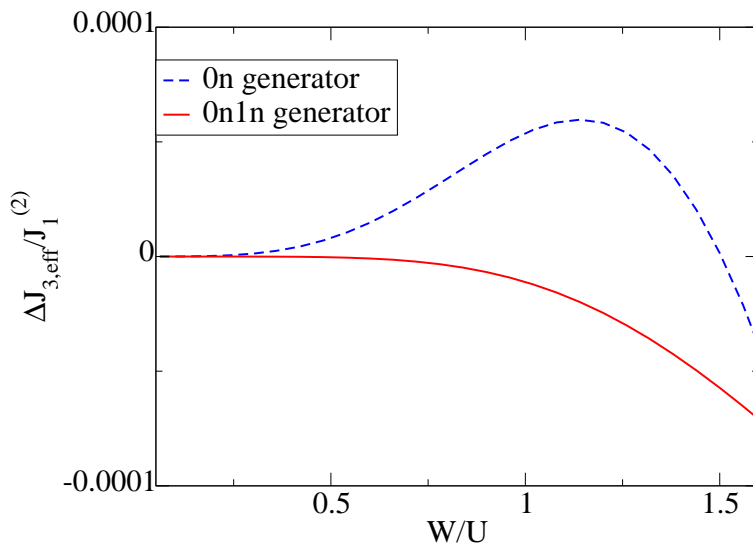


Fig. 4.44.: Deviation of the results for  $J_3$  as defined in Eq. 4.7.2 for different generators from the MKU result.

For very large values of  $W/U$  the deviation of the results from the  $0n$  generator become smaller.

Even the coupling constant  $J_4$  which describes the Heisenberg interaction between a spin

on site  $(0,0)$  and a spin on site  $(2,1)$  shows a good agreement of the results for the different generators even for larger values of  $W/U$ . This interaction takes place between fourth nearest neighbors on a two-dimensional square lattice.

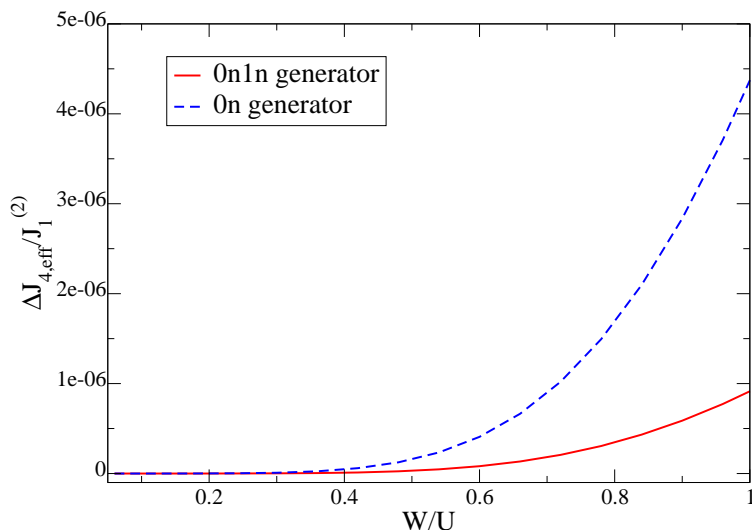


Fig. 4.45.: Deviation of the results for different generators from the MKU result.

As explained before the ring exchange defined in Eq. 4.8.1 is one of the most important spin interactions. Also for this term the results for different generators show very similar behavior, see Fig. 4.46.

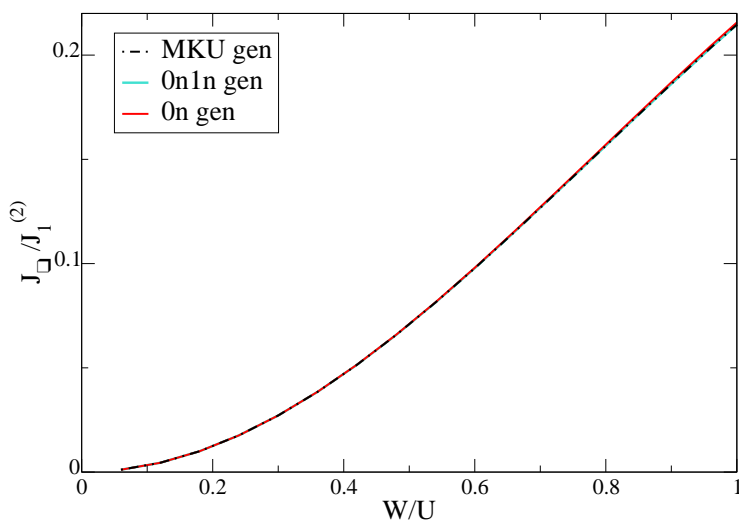


Fig. 4.46.: Ring exchange for different generators

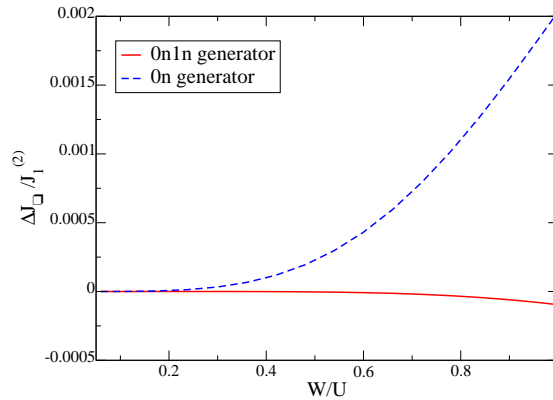


Fig. 4.47.: Deviation of the results for different generators from the MKU result.

The deviation for the  $0n$  generator, which is shown in Fig. 4.47, is less than 0.8 percent. For the  $0n1n$  generator the deviations are negligible. For the cross interaction, which is defined in Eq. 4.8.2, the same result is obtained (see appendix A).

Conclusively we can state that for a determination of the important spin terms it is sufficient to use the  $0n$  generator instead of the MKU or the  $0n1n$  generator in this model. The use of the  $0n$  generator instead of the others leads to a considerable reduction in the amount of terms that have to be considered during the calculation.

Besides the use of this generator leads to a convergent ROD for all values of  $W/U$  even for the double plaquette calculation as shown in Fig. 4.40.

#### 4.8.2.2. Hopping terms

The results for the hopping element  $t_0$  are shown in Fig. 4.48. The results for the MKU and the  $0n1n$  generator almost coincide whereas the  $0n$  generator leads to slightly smaller values for  $t_0$ .

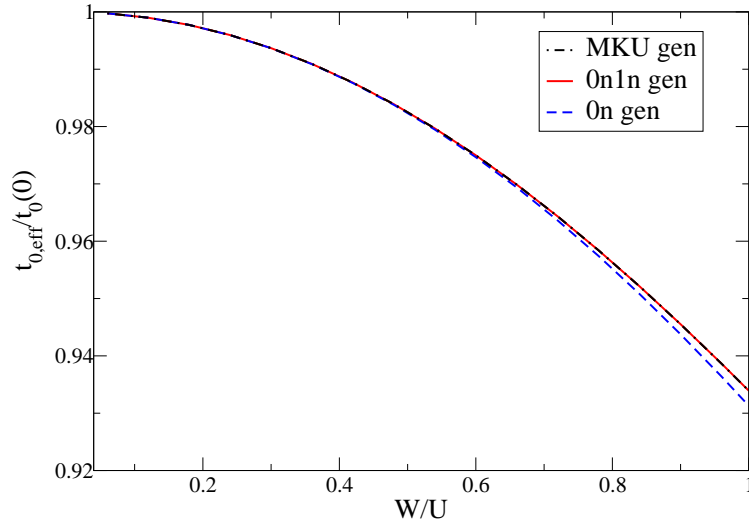


Fig. 4.48.: Results for the hopping element  $t_0$  for different generators

Figure 4.49 shows the coefficient for the hopping between sites with a distance of  $2a$  where  $a$  denotes the lattice constant. The results obtained with the MKU generator and the one obtained with the  $0n1n$  generator lie on top of each other. The  $0n$  generator leads to slightly smaller values of the hopping parameter. The deviation grows with  $W/U$ .

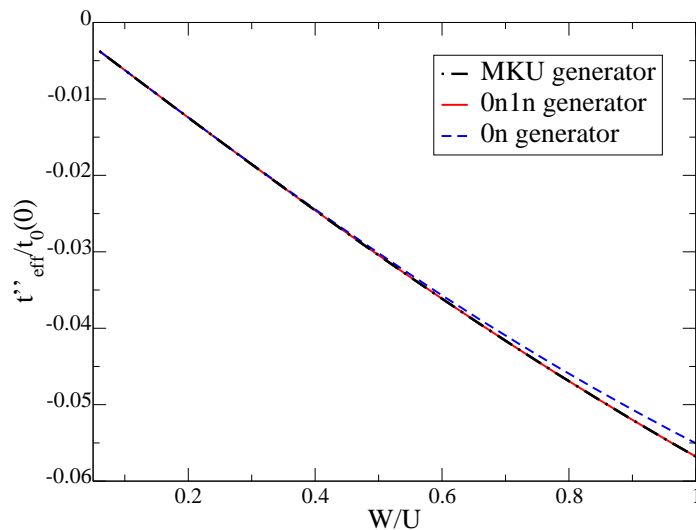


Fig. 4.49.: Deviation of the results for different generators from the MKU result.

Analogous behavior is found for the spin dependent hopping over diagonal neighboring sites on a plaquette, which means two spin situated at  $(0, 0)$  and  $(1, 1)$  (see figure 4.50).

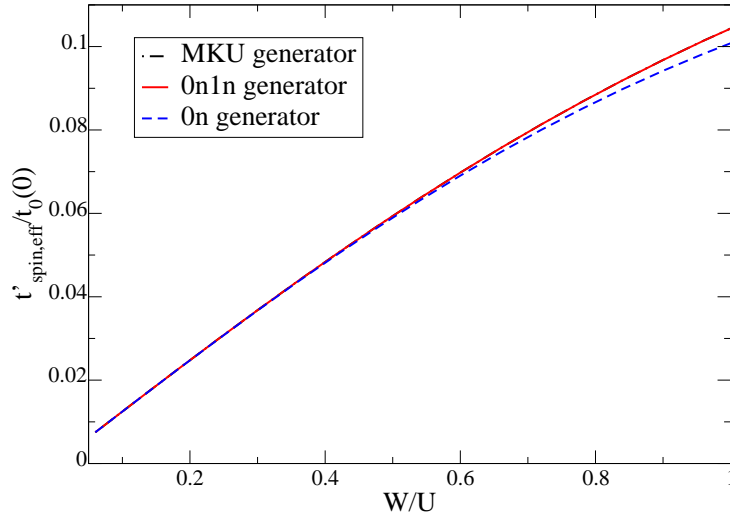


Fig. 4.50.: Deviation of the results for different generators from the MKU result.

The spin dependent hopping over a distance of  $2a$  shows the same results. Thus we directly show the deviations compared to the perturbative result for  $J_1$  in Fig. 4.51.

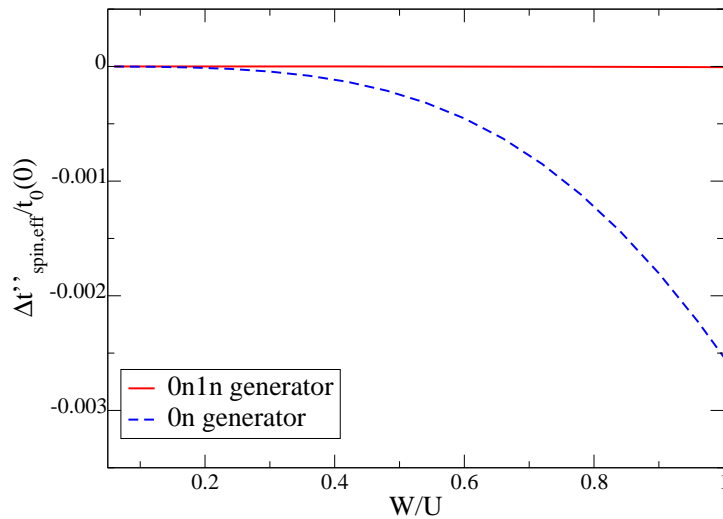


Fig. 4.51.: Deviation of the results for different generators from the MKU result.

The use of the  $0n$  generator leads to smaller values for the spin dependent hopping than the other generators. It should be highlighted again that there is no sizeable difference in the results of the MKU generator and the  $0n1n$  generator. And even the deviations for the  $0n$  generator are small.

### 4.8.2.3. Interaction terms

Differences between the MKU generator and the  $0n1n$  generator can be seen in the coefficients of the interaction terms.

Although the  $0n$  generator does not consider terms of the sectors with two DOs it led to similar results in the one-dimensional case. Therefore we also show the results obtained with this generator for the two-dimensional case.

The coefficient of the density density interaction

$$H_V = V \sum_{\langle i,j \rangle} \bar{n}_i \bar{n}_j. \quad (4.8.7)$$

shows larger deviations for the  $0n1n$  generator for larger  $W/U$  than for the  $0n$  generator.

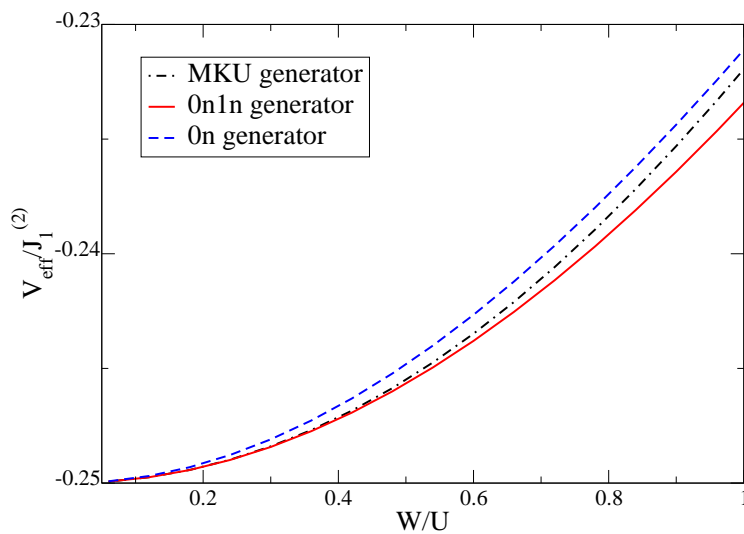


Fig. 4.52.: Density-density interaction  $V$  for different generators

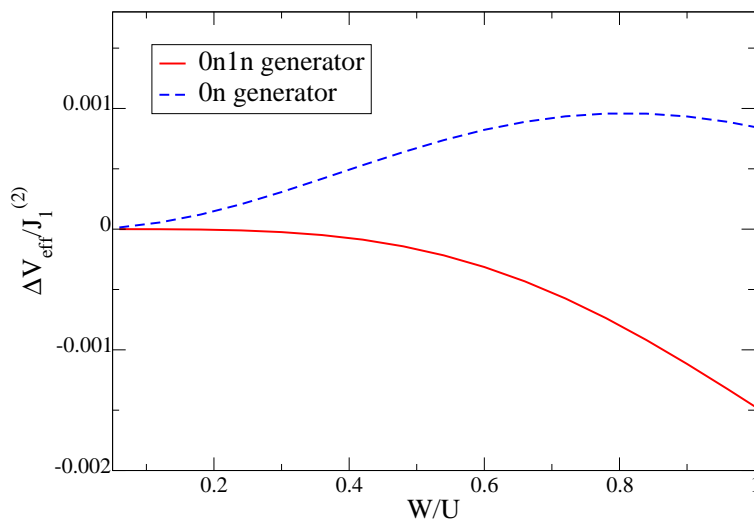


Fig. 4.53.: Deviation of the results for different generators from the MKU result.

However the deviation of the  $0n1n$  generator is smaller than 1.5 percent even for  $W/U = 1.6$ .

The coefficient of the density-density interaction between third nearest neighbors on a square lattice  $V_n''$  shows the expected result. The MKU and the  $0n1n$  generator produce a very similar behavior of the coefficient. The  $0n$  generator leads to a slight deviation of up to 7 percent.

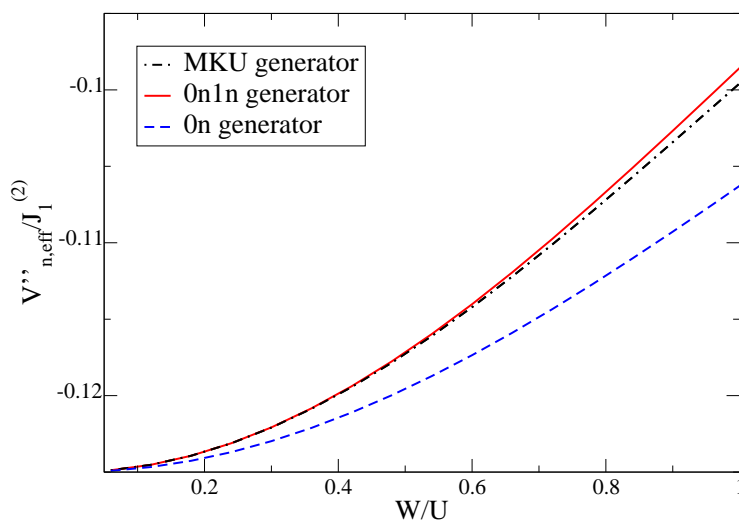


Fig. 4.54.: Results for the coupling constant  $V_n''$

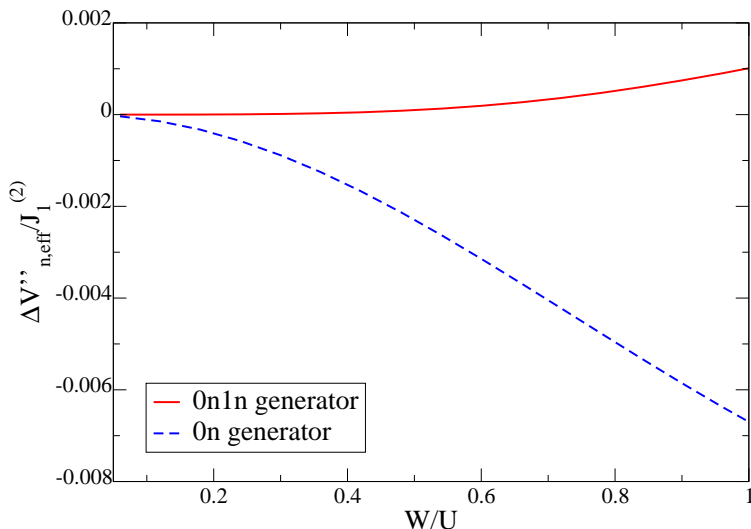


Fig. 4.55.: Deviation of the results for different generators from the MKU result.

The same result is obtained for the density-density interaction between next nearest neighbors (see Eq. 4.8.6).

Another interaction term of interest is the interaction between a hole and a doubly occupied site on diagonal neighbors given by  $V'_p$  which is defined in Eq. 4.8.5. The results for this coupling show deviations for both generators. The deviations for the  $0n$  generator reach a value of about 6.8 percent. This deviation is accounted for by the fact that the  $0n$  generator does not decouple the sector with two quasiparticles from the other sectors. Thus results for the interaction terms for this generator have to be treated cautiously.

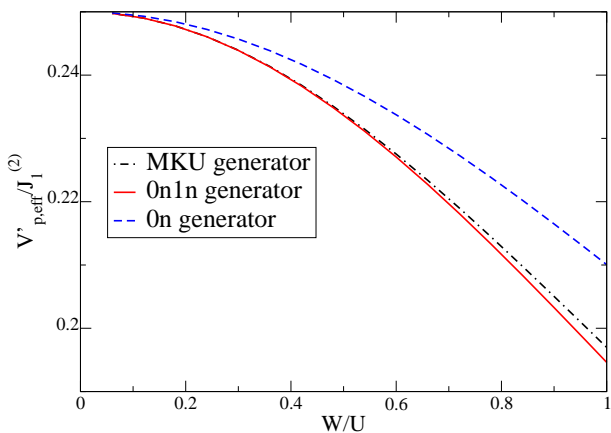


Fig. 4.56.: Pair interaction between diagonal neighbors

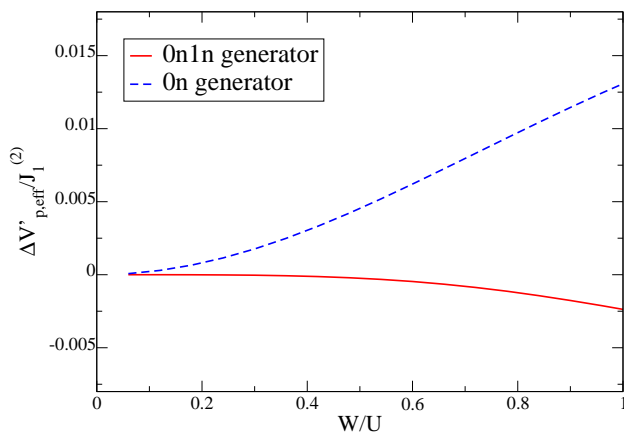


Fig. 4.57.: Deviation of the results from the MKU results

For the pair interaction between third nearest neighbors  $V_p''$ , which is defined in Eq. 4.7.6, we obtain the same behavior.

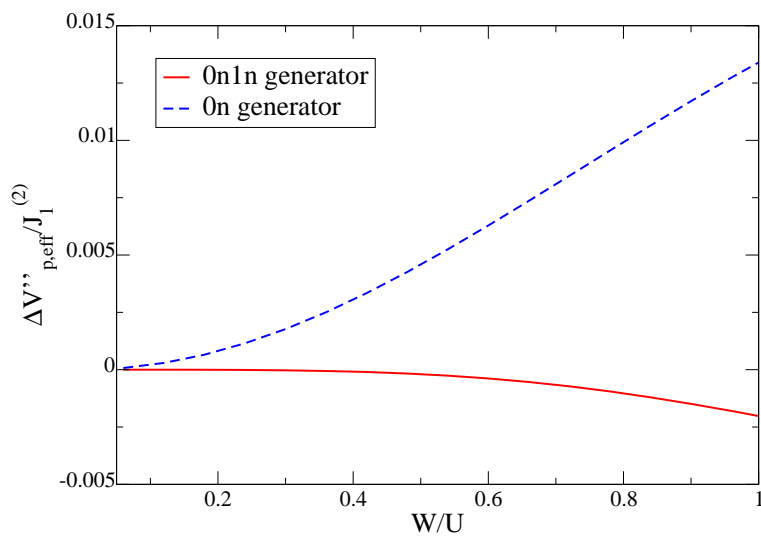


Fig. 4.58.: Deviation of the results for  $V_p''$  for different generators from the MKU result.

## 4.8.2.4. Results for the double plaquette

As explained before the double plaquette calculation was feasible with the  $0n$  and the  $0n1n$  generator. With the MKU generator this calculation could not be performed up to now due to time constraints. Therefore we showed the coupling constants for the upto4 calculation.

The results presented above show that a CUT with the  $0n1n$  generator leads to similar results as a CUT using the MKU generator. As a consequence of this we can use the results for the  $0n1n$  generator to analyze the effects of terms which are included in a double plaquette calculation but not in the upto4 calculation.

Therefore we show some results for the double plaquette calculation with the  $0n1n$  generator.

The only coupling constants which show a change in the results due to the higher truncation scheme are the four spin terms. As we have seen before the results for these coupling constants obtained with the  $0n1n$  generator show good agreement with the results of the MKU generator.

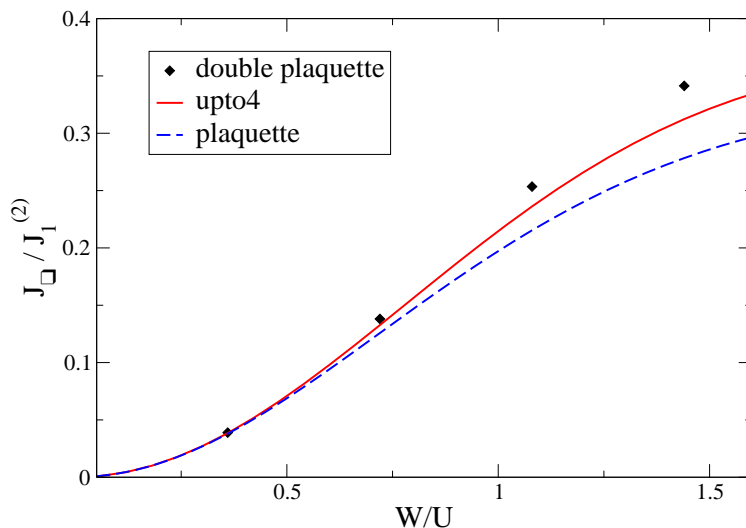


Fig. 4.59.: Results for  $J_{\square}$  obtained with the  $0n1n$  generator

In the case of the ring exchange the double plaquette calculation leads to slightly higher values than the upto4 calculation.

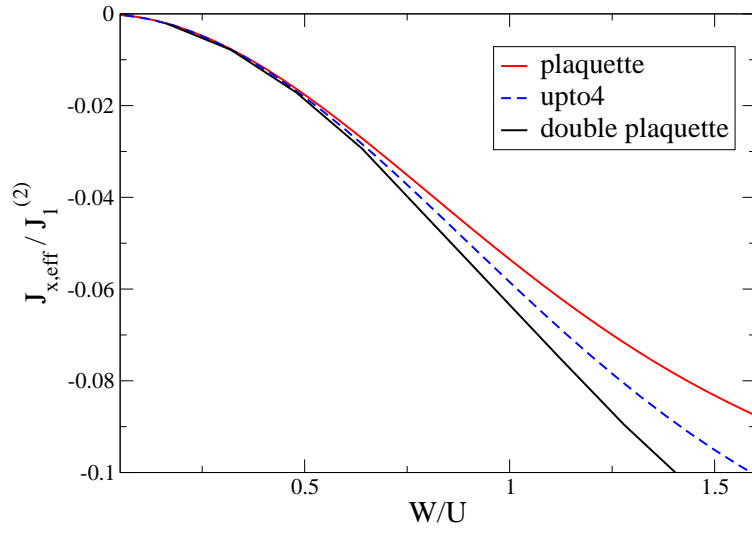


Fig. 4.60.: Results for  $J_{\times}$  obtained with the  $0n1n$  generator

The value for the cross interaction is renormalized to smaller values for the double plaquette calculation.

Both coupling constants show a significant change for larger values of  $W/U$ . Thus for both interactions terms included in the double plaquette calculation but not in the upto4 calculation lead to slight changes of the coupling constants.

## 4.9. Chapter conclusion

In a first step we calculated the coefficients for a nearest neighbor calculation analytically. This lead to a formula which can be used for all lattices and all coordination numbers. In the second step the effective coefficients for higher truncation schemes were obtained numerically.

In the half-filled case we observe that in the one-dimensional case as well as in the two dimensional case the Heisenberg interaction between nearest neighbors  $J_1$  is the most important spin interaction term. Heisenberg interactions between next to nearest neighbors or third nearest neighbors are negligible compared to  $J_1$ . In the one-dimensional case all calculations show a convergent behavior of the ROD. Even in the extension4 calculation the ROD decays rapidly for all values of  $W/U$ . Except for the spin dependent hopping between two spins at a distance  $2a$  with lattice constant  $a$  the results for the coefficients obtained in a extension3 calculation are covered by the results of the extension4 calculation.

Comparing the results for the different generators it can be observed that except for  $V_p''$  all coefficients are described accurately by the  $0n$  generator. Although the  $0n$  generator does not include interactions of DOs it seems to be sufficient to describe the most important effects on the interaction terms. In a CUT using the  $0n$  generator instead of the MKU generator less terms are created. Thus the calculations take less time.

For the two-dimensional square lattice the double-plaquette calculation performed with the  $0n$  generator lasts less than 10 days, whereas the same calculation with the  $0n1n$  generator took 51 days. In the two-dimensional case the ring exchange turns out to be one of the most important subleading spin terms. The size of the corresponding coefficient is almost comparable to  $J_1$ . As a result the ring exchange must not be neglected. In the same way the spin dependent hopping between diagonal neighbors  $t'_{\text{spin}}$  takes values as high as its spin independent equivalent  $t'$ . Thus  $t'_{\text{spin}}$  has to be included in an effective model containing  $t'$ . For terms describing the interaction between nearest neighbor sites the plaquette calculation already covers the important processes. The constants of the four spin terms show a significant change in the results obtained in an upto4 calculation from the ones of the double plaquette calculation.

For the double-plaquette calculation with the  $0n1n$  generator we observe divergencies in the ROD for values of  $W/U \geq 1.6$ . A. Reischl observed a similar behavior for a double plaquette calculation using the MKU generator. In this case the ROD shows divergencies for values of  $W/U \geq 1.2$  [RMHU04]. The use of the  $0n1n$  generator leads to a similar behavior as for the MKU generator for all coupling constants. In contrast, the  $0n$  generator leads in the two-dimensional case to noticeable changes in the description of interactions between next nearest neighbors or third nearest neighbors. The values of the coupling constants differ by about 10% for the two generators.

## 5. Away from half-filling

Up to now we considered the Hubbard model in the half-filled case. This section deals with the influence of doping on the effective  $t$ - $J$  model.

We analyze the case of hole doping. One could also dope the system by inserting electrons, thus creating doubly occupied sites  $|\uparrow\downarrow\rangle$  due to particle-hole symmetry. For a Hubbard model on a bipartite lattice like the ones studied in this thesis this yields the same results.

Let us first consider how the reference ensemble changes under hole doping. In the half-filled case the reference ensemble consists of the two equally weighted states  $|\uparrow\rangle$  and  $|\downarrow\rangle$ . In the doped case, we have to consider besides these two states also the empty state  $|0\rangle$  in the reference ensemble. Consequently this state has to be incorporated in the reference ensemble. The probability for the empty state is given by the doping constant  $\delta$ . As the effective model should not exhibit any magnetic order, there should be no favored direction for the spin. From this fact we can conclude that the singly occupied states carry the same weight, which is given through  $\frac{1-\delta}{2}$ . Knowing the weights for the states in the reference ensemble, we can write down the statistical operator for the new reference ensemble

$$\hat{\rho}_\delta = \prod_i \left\{ \delta |0\rangle_i \langle 0|_i + \frac{1-\delta}{2} [ |\uparrow\rangle_i \langle \uparrow|_i + |\downarrow\rangle_i \langle \downarrow|_i ] \right\}. \quad (5.0.1)$$

As in the half-filled case the product over  $i$  extends over the whole lattice.

The 16 local operators in Table 4.1 used as basis in the half-filled case, where chosen in such a way that they are all normal-ordered (except for the unity operator). As the normal-ordering is based on taking the expectation value of the operators with respect to the reference ensemble, we have to check if this condition is still fulfilled. Regarding the doped reference ensemble (Eq. 5.0.1) the condition for normal-ordered operators reads

$$\langle A_i \rangle_{\text{ref}} = \delta \langle 0|_i A_i |0\rangle_i + \frac{1-\delta}{2} (\langle \uparrow|_i A_i | \uparrow\rangle_i + \langle \downarrow|_i A_i | \downarrow\rangle_i).$$

From the operators used in the half-filled case all but the operators  $\hat{D}$  and  $\bar{n}$  fulfill this condition. As the expectation values of  $\hat{D}$  and  $\bar{n}$  yield finite values, these operators have to be replaced by new normal-ordered operators  $\hat{D}_\delta$  and  $\bar{n}_\delta$ . The new operators should still perform the same task. Thus we replace the operator  $\bar{n}$ , which counts the number of electrons on a site compared to the half-filled case, by

$$\bar{n}_{\delta,i} = \bar{n}_i + \delta \mathbf{1}_i$$

This operator is constructed such that it counts the number of electrons on one site compared to the mean value of the filling in the doped case  $1 - \delta$ . As  $\hat{D} = 2\hat{n}_{i\uparrow}\hat{n}_{i\downarrow} - \bar{n}$  holds, the counting operator  $\hat{D}$  is replaced by

$$\hat{D}_\delta = \hat{D} - \sum_i \delta \mathbf{1}_i.$$

Having thus created a new set of normal-ordered basis operators, all terms have to be expressed in this basis. This is true for the Hamiltonian itself as well as for all arising terms during the CUT. The repulsive part of the Hamiltonian is rewritten as

$$\hat{H}_U = \frac{U}{2} \hat{D}_\delta + \frac{UN}{4} (2\delta - 1)$$

where  $N$  denotes the total number of sites. In contrast to  $\hat{H}_U$  the kinetic part  $\hat{H}_t$  neither contains  $\bar{n}$  nor  $\hat{D}$ . Thus it takes the same form as in the half-filled case at  $\ell = 0$ . This implies that also the generator  $\eta$  which contains only terms from  $\hat{H}_t$  stays invariant.

#### 5.0.0.5. Results for the NN model

In analogy to the procedure in the half-filled case we first consider the NN model as an example. We will not consider the minimal model in this case as the results for this model are not changed by doping. All new arising contributions due to the doping are neglected in the minimal model.

For the NN model we have to calculate the commutator  $[\eta(\ell), \hat{H}_U]$ . As  $\hat{D}$  and  $\hat{D}_\delta$  only differ by a multiple of the unity operator this commutator yields the same results as before. The same holds for the commutator of the kinetic part of  $\hat{H}$  with the generator  $[\eta, \hat{H}_t(\ell)]$ . From this commutator we obtain contributions containing the operators  $\bar{n}$  and  $\hat{D}$ . As a result the contributions have to be expressed by the use of the new operators  $\hat{D}_\delta$  and  $\bar{n}_\delta$ . Inserting the definitions of these operators leads to the following expression

$$4 [\hat{T}_{+2}(\ell), \hat{T}_{-2}(\ell)] = 4t_{+2}^2(\ell) z \hat{D}_\delta \tag{5.0.2}$$

$$+ 16t_{+2}^2(\ell) \sum_{\langle i,j \rangle} \vec{S}_i \vec{S}_j \tag{5.0.3}$$

$$8t_{+2}^2(\ell) \sum_{\langle i,j \rangle} (\hat{c}_{i\uparrow}^\dagger \hat{c}_{i\downarrow}^\dagger \hat{c}_{j\downarrow} \hat{c}_{j\uparrow} + h.c.) \tag{5.0.4}$$

$$- 4t_{+2}^2(\ell) \sum_{\langle i,j \rangle} \bar{n}_{\delta,i} \bar{n}_{\delta,j} \tag{5.0.5}$$

$$+ 4t_{+2}^2(\ell) z \sum_i \delta \bar{n}_{\delta,i} \tag{5.0.6}$$

$$+ \dots \tag{5.0.7}$$

$\langle i, j \rangle$  denotes a pair of nearest neighbor sites and the dots indicate that we ignored contributions from the unity operator and from terms with extensions larger than one. Note

that we used  $t_{+2} = t_{-2}$  in this formula.

Comparing this result to the half-filled case, there is no change in the differential equations for the coupling constants we already discussed. Thus the results obtained for these constants in the half-filled case stay valid. But in the doped case a new contribution occurs in the differential equations (see Eq. 5.0.6). This contribution corresponds to the term

$$\hat{H}_\mu = \mu \sum_i \bar{n}_{i,\delta}$$

which represents the chemical potential. As this term does not create or destroy double occupancies it is not part of the generator. However the commutator  $[\eta, \hat{H}_\mu]$  has to be calculated. As  $\eta$  preserves the total number of DOs it commutes with  $\hat{H}_\mu$ . Thus the commutator vanishes and the term  $\hat{H}_\mu$  does not influence the differential equations of the other terms. In this way we can adopt the expressions for these terms from the half-filled case.

The differential equation for  $\hat{H}_\mu$  itself reads

$$\frac{d}{d\ell} \mu(\ell) = 4z\delta t_{+2}^2$$

with the initial condition  $\mu(0) = 0$ . Using the relation between  $U(\ell)$  and  $t_{+2}(\ell)$

$$\frac{dU(\ell)}{d\ell} = 8zt_{+2}(\ell)^2 = 2\frac{d}{d\ell} \mu(\ell) \frac{1}{\delta}$$

we obtain

$$\mu(\ell) = \left( \frac{U(\ell)}{2} - \frac{U_0}{2} \right) \delta.$$

We now insert the known solution for  $U(\ell)$  (Eq. 4.6.21) to derive the expression

$$\mu(\ell) = \frac{\delta z}{12 + 4z} A \tanh(A\ell + B) - \frac{z}{2(3+z)} \delta U_0. \quad (5.0.8)$$

In this formula  $z$  denotes the coordination number of the lattice. The constants  $A = 2\sqrt{U^2 + 4(3+z)t^2}$  and  $B = \operatorname{artanh}(\frac{2U_0}{A})$  can be adopted from the half-filled case.

In the limit  $\ell = \infty$  the effective model is reached, with the effective chemical potential given by

$$\mu_{\text{eff}} = \frac{\delta z}{2(3+z)} U \sqrt{1 + 4(3+z) \frac{t^2}{U^2}} - \frac{z}{2(3+z)} U \delta \quad (5.0.9)$$

where we used  $t$  and  $U$  to denote the starting values  $t_0(0)$  and  $U(0)$ .

In leading order in  $\frac{t}{U}$  this yields a chemical potential which depends linearly on the doping constant  $\delta$  and on the coordination number of the lattice

$$\mu^{(2)} = \delta z \frac{t^2}{U}. \quad (5.0.10)$$

## 5.1. Results for the linear chain away from half-filling

In this section we study the influence of hole doping on the effective coefficients in one dimension. The coupling constants have been calculated for all truncation schemes and various doping concentrations. A few exemplary results for the most important terms of an extension4 calculation are shown here.

Before we discuss the behavior of the coupling constants we present results for the ROD for various doping concentrations  $\delta$ .

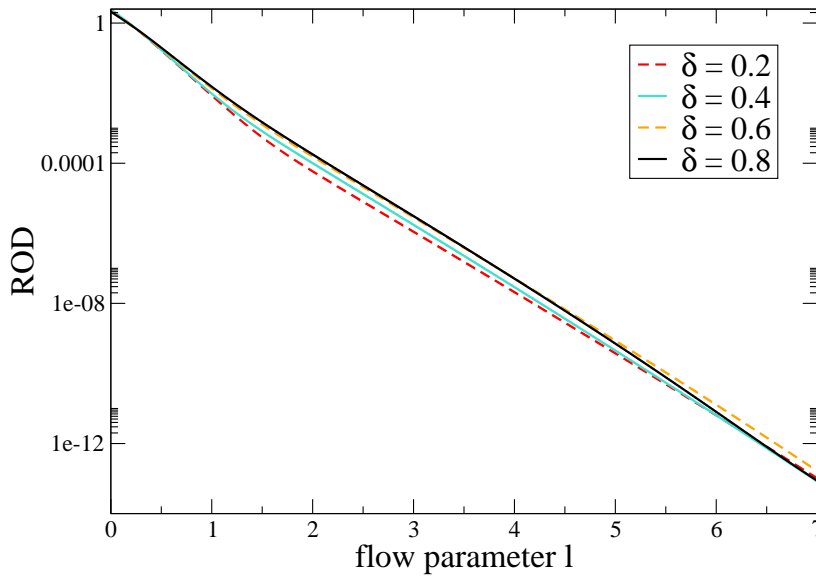


Fig. 5.1.: Behavior of the ROD for different doping concentrations for the extension4 calculation and  $W/U = 1.2$

Even for the large value  $\delta = 0.8$  the ROD decreases rapidly. The first coupling constant under study is the one for the nearest neighbor Heisenberg exchange  $J_1$  (see Fig. 5.2). The Heisenberg interaction between nearest neighbors  $J_1$  increases with the doping concentration  $\delta$ . But the difference lies in a range of about 1 percent.

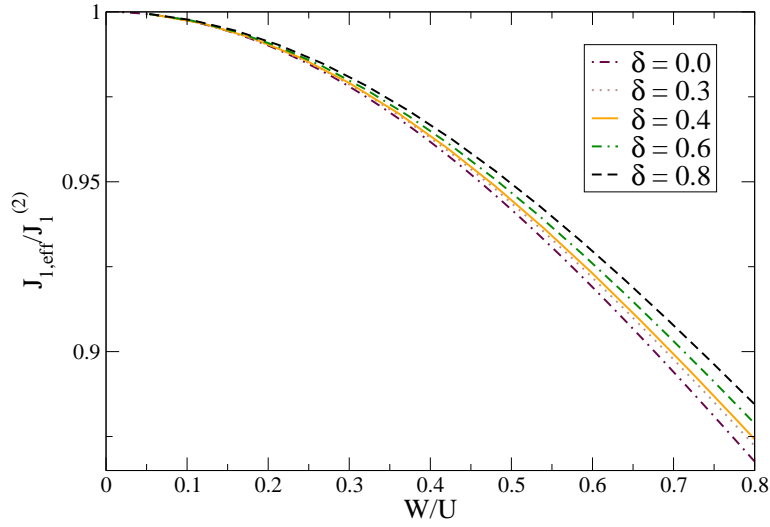


Fig. 5.2.: Coupling constant  $J_1$  in dependence on  $W/U$  for different values of the doping concentration  $\delta$

The hopping element  $t_0$  seems to be more influenced by the effects of the doping (see Fig. 5.3). The results obtained for the half-filled case and the ones obtained for  $\delta = 0.8$  differ about 7 percent.

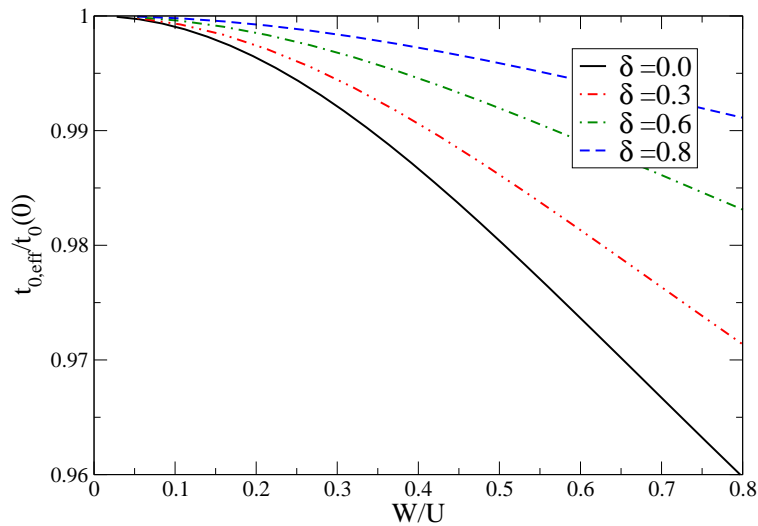


Fig. 5.3.: Doping dependence of the hopping element  $t_0$

The corresponding results for the spin dependent hopping over diagonal neighboring sites  $t''_{\text{spin}}$  which is defined in Eq. 4.7.4 are shown in Fig. 5.4.

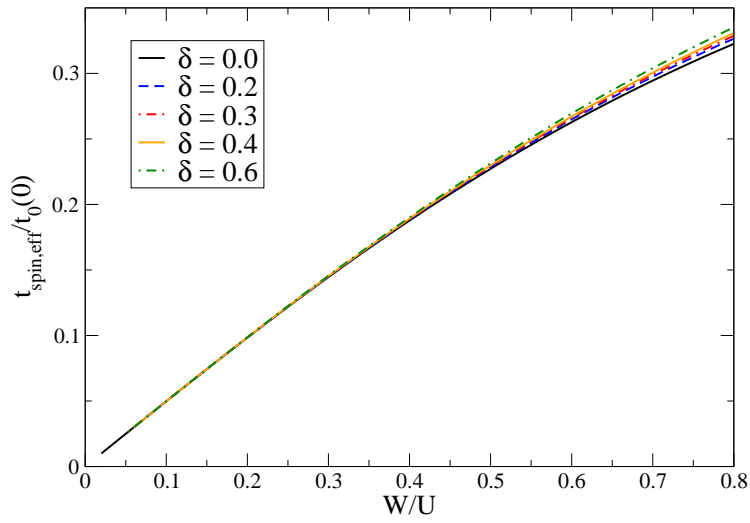


Fig. 5.4.: Results for the spin dependent hopping term

For large values of  $W/U$  this parameter shows a linear dependence on the doping concentration  $\delta$ .

Conclusively we can say that there is hardly any doping dependence.

## 5.2. Results for the two-dimensional square lattice in the case of hole doping

For the two-dimensional square lattice we start the discussion with the effective chemical potential  $\mu$ . The corresponding term is given by

$$\hat{H}_\mu = \mu \sum_i \tilde{n}_{i,\delta}.$$

As explained before this coupling constant is in leading order proportional to  $\delta$ . Therefore we show this constant compared to  $\delta J_1^{(2)}$  in Fig. 5.5.

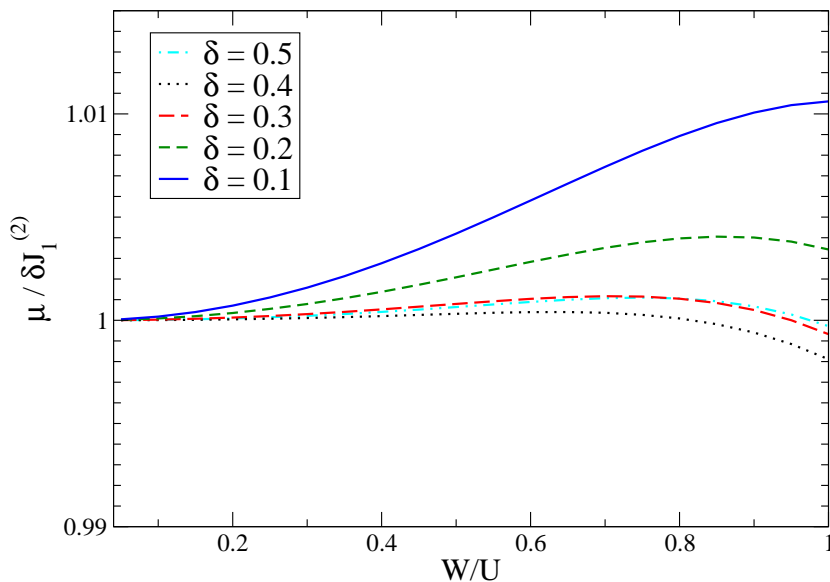


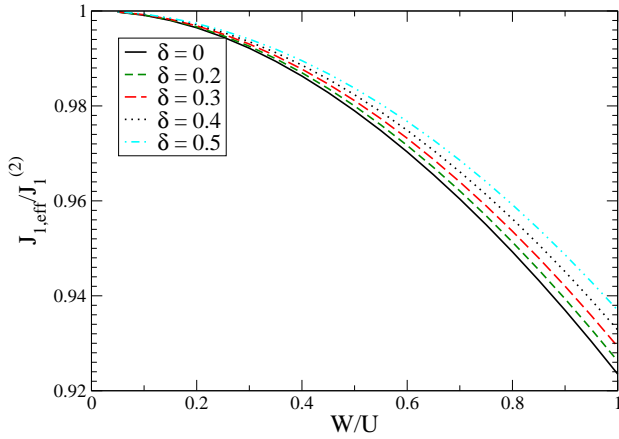
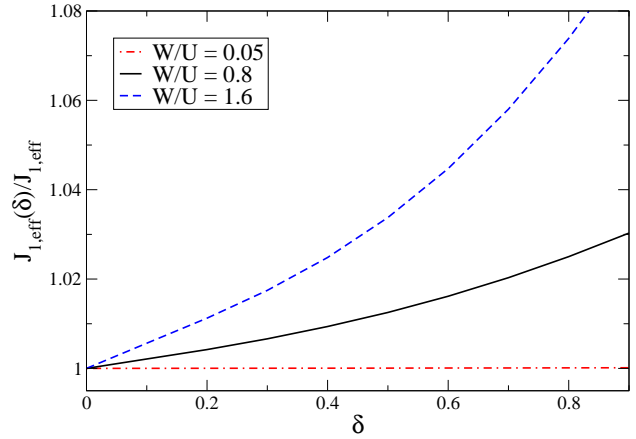
Fig. 5.5.: Results for the chemical potential for different doping concentrations  $\delta$

### 5.2.1. Results for the MKU generator

The results presented in this section are obtained in an upto4 calculation using the MKU generator.

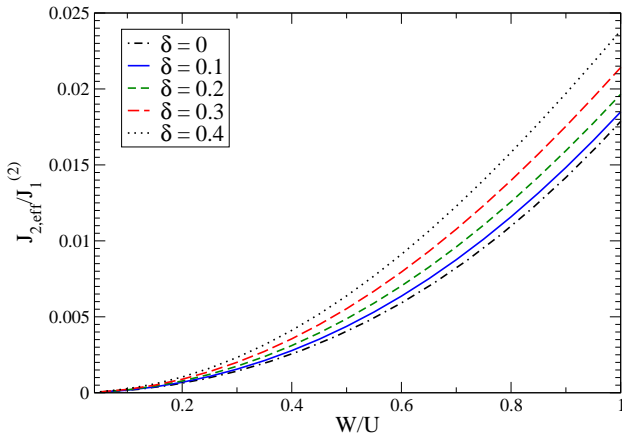
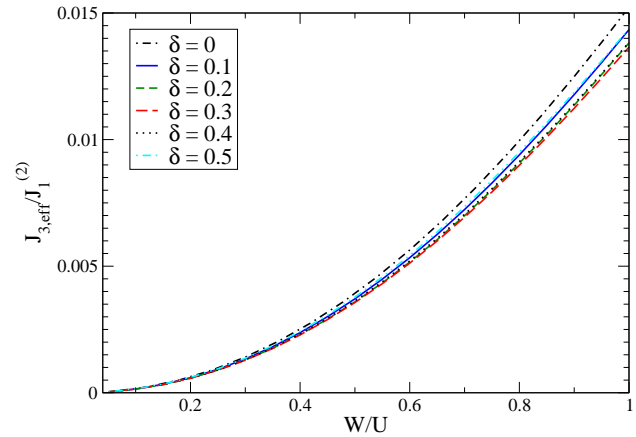
#### 5.2.1.1. Spin terms

In Fig. 5.6 the coupling constant  $J_1$  is shown dependent on  $W/U$  for different doping concentrations. Additionally we show the change of  $J_1$  for a doping concentrations  $\delta$  compared to  $J_1$  for the undoped system. The resulting curves are shown in Fig. 5.7 for different values of  $W/U$ .


 Fig. 5.6.:  $J_1$  for different values of  $\delta$ 

 Fig. 5.7.:  $J_1$  in dependence of  $\delta$ 

These curves indicate that the doping has a greater influence on  $J_1$  for larger values of  $W/U$ . However the changes due to doping effects are small. For  $W/U = 0.8$  the doping causes a change in  $J_1$  of about 3%.

The coefficients  $J_2$  and  $J_3$  (see Eq. 4.7.2) both show a dependence on the doping concentration. For  $\delta = 0.4$   $J_2$  shows an increase of about 8%.


 Fig. 5.8.: Effective  $J_2$  for different doping concentrations

 Fig. 5.9.: Effective  $J_3$  for different doping concentrations

The coupling constant of the Heisenberg exchange between third nearest neighbors first decreases with  $\delta$  but starts to increase at a value of  $\delta = 0.3$  again, as can be seen in Fig. 5.10.

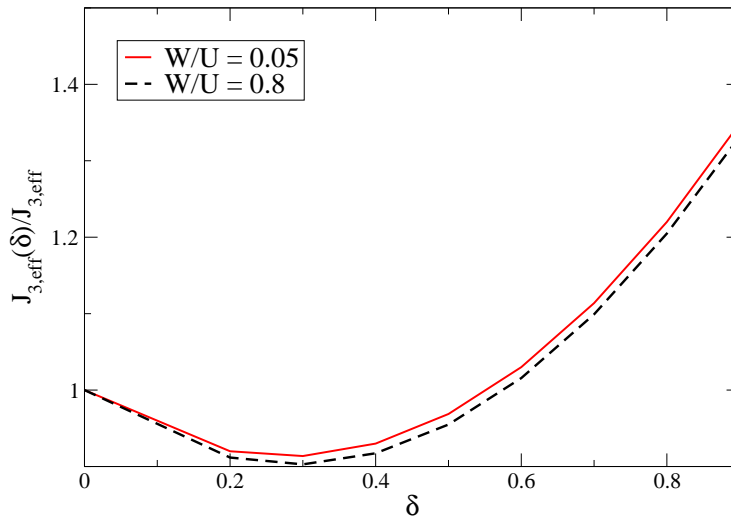


Fig. 5.10.: Dependence of the effective  $J_3$  as defined in Eq. 4.7.2 on the doping concentration  $\delta$

The ring exchange (Eq. 4.8.1) shows nearly no dependence on the doping constant  $\delta$ . Even for the large doping concentration  $\delta = 0.8$  the change in the coefficient is less than 1.12 percent. For smaller doping concentration the change in the coefficient is much smaller as can be seen in Fig. 5.12.

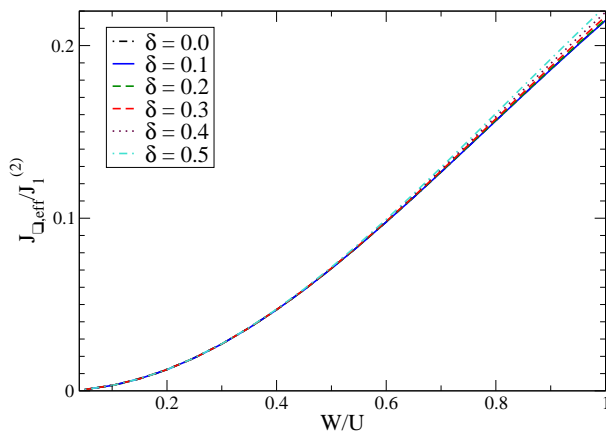


Fig. 5.11.: Results for the ring interaction

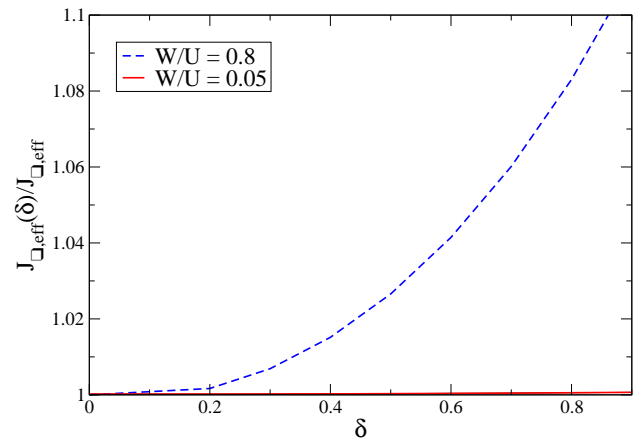


Fig. 5.12.: Doping dependence of  $J_{\square}$

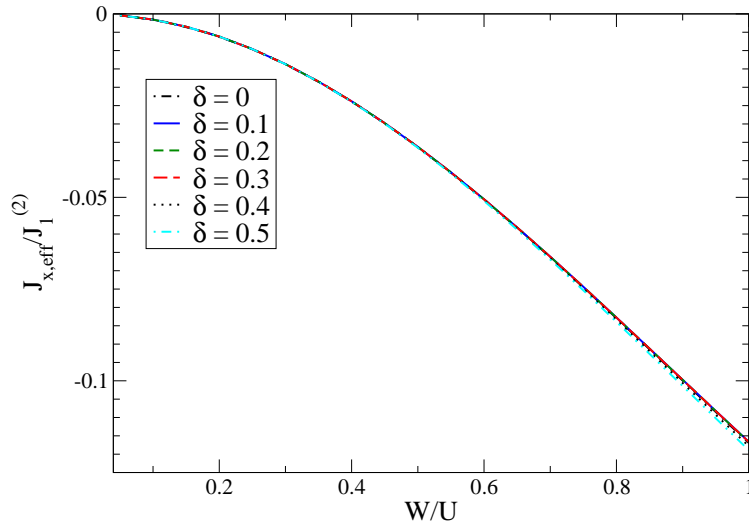


Fig. 5.13.: Effective  $J_x$  as defined in Eq. 4.8.2 for various doping concentrations  $\delta$

### 5.2.1.2. Interaction terms

The Hubbard repulsion  $U$  shows nearly no effect depending on the doping constant  $\delta$ . Even for  $W/U = 0.8$  the change is less than 0.05% (see Fig. 5.14).

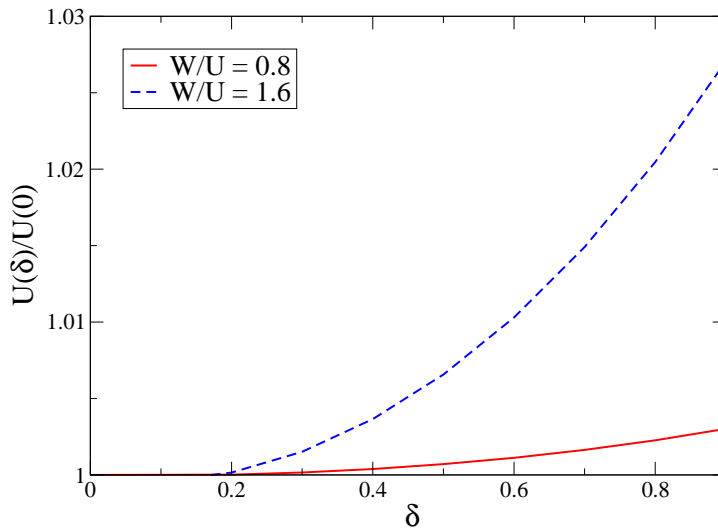


Fig. 5.14.: Results for the Hubbard repulsion  $U$

The influence of doping on the interaction between two electrons on the same site is negligible.

The density-density interaction  $H_V$  which is defined in Eq. 4.7.7 shows an increase in the

coupling constant of about 1 percent under the influence of doping for  $W/U = 0.8$ .

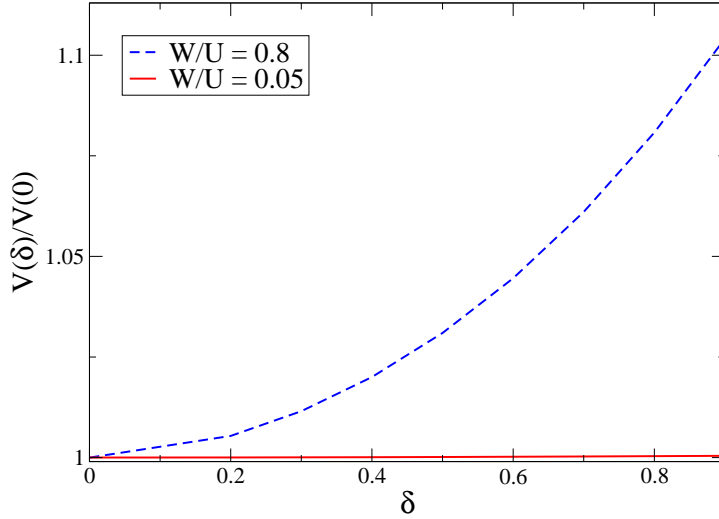
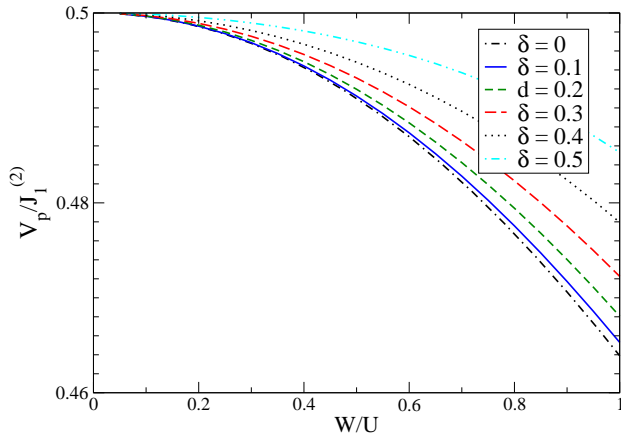
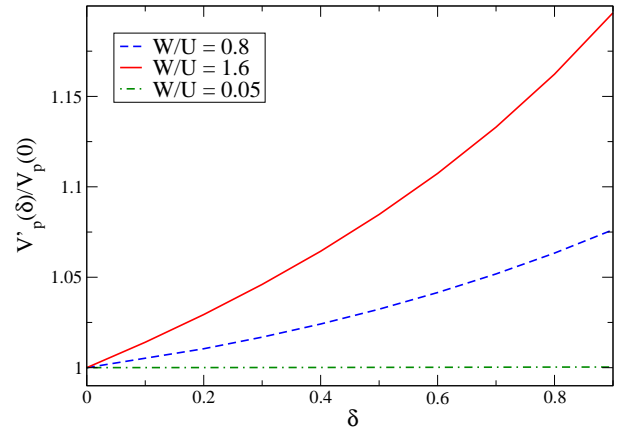


Fig. 5.15.: Result for the interaction term  $V$

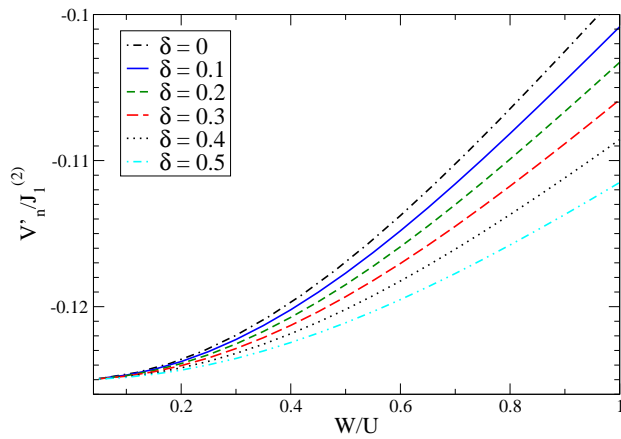
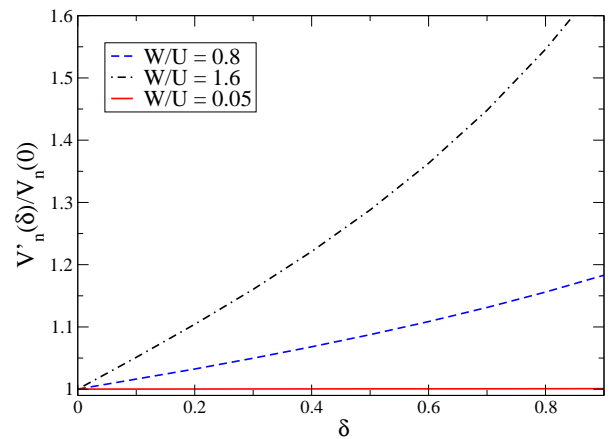
The coefficients of the pair interaction  $V_p$ ,  $V'_p$  and  $V''_p$  show a similar behavior. The pair interaction between two spins at a distance of  $2a$  with the lattice constant  $a$  is given by

$$H''_{pair} = V''_{pair} \sum_{\sigma} \sum_{\langle\langle i,j \rangle\rangle} \left[ \hat{c}_{k,\sigma}^{\dagger} \hat{c}_{k,\bar{\sigma}}^{\dagger} \hat{c}_{i,\bar{\sigma}} \hat{n}_{i,\sigma} \hat{c}_{j,\sigma} (1 - \hat{n}_{j,\bar{\sigma}}) + \hat{c}_{k,\sigma}^{\dagger} \hat{c}_{k,\bar{\sigma}}^{\dagger} \hat{c}_{i,\bar{\sigma}} (1 - \hat{n}_{i,\sigma}) \hat{c}_{j,\sigma} \hat{n}_{j,\bar{\sigma}} + h.c. \right]. \quad (5.2.1)$$

The change in these constants is a few percent. Representative for these three interactions we show the results for the nearest neighbor pair interaction  $V_p$  in the figures 5.16 and 5.17.


 Fig. 5.16.: Pair interaction  $V_p$  for different  $\delta$ 

 Fig. 5.17.: Pair interaction  $V_p$  depending on  $\delta$ 

The coefficients  $V'_n$  defined in Eq. 4.8.6 and  $V''_n$  show a rather strong dependence on the doping constant for larger values of  $W/U$ . As the coefficients show the same behavior we show the coefficient  $V'_n$  describing the density-density interaction between diagonal neighboring sites in Fig. 5.18 and 5.19.


 Fig. 5.18.:  $V'_n$  for different doping concentrations

 Fig. 5.19.:  $V'_n$  depending on  $\delta$

### 5.2.1.3. Results for the hopping terms

The value of the hopping parameter  $t_0$  is increased with increasing  $\delta$ . The increase with  $\delta$  is nearly linear (see Fig. 5.20) and leads to values which are a few percent higher than the undoped ones.

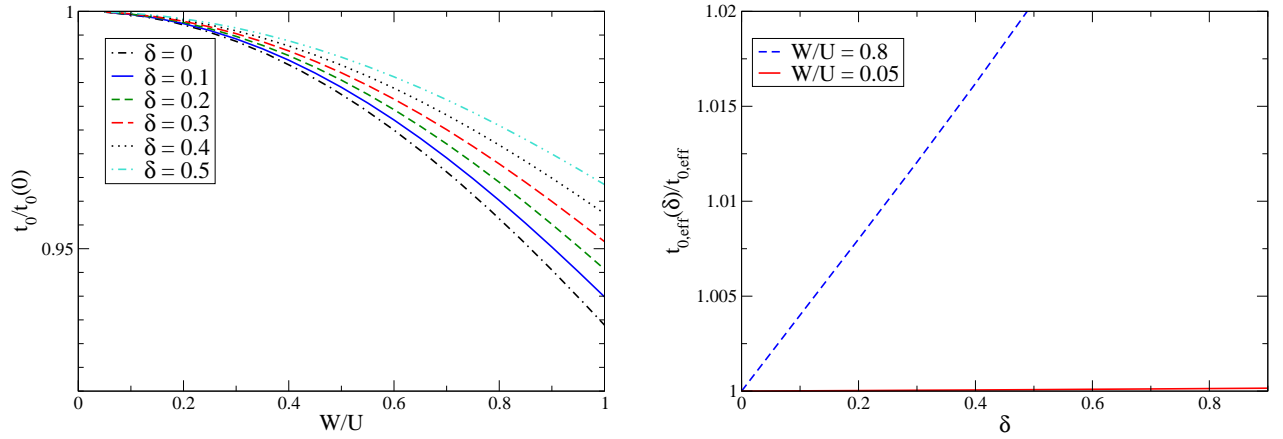


Fig. 5.20.: Dependence of the hopping element  $t_0$  from  $\delta$

The values for the hopping parameters  $t'$  and  $t''$  are according to amount smaller than the undoped values. As both parameter show the same behavior we present only the results for  $t'$ .

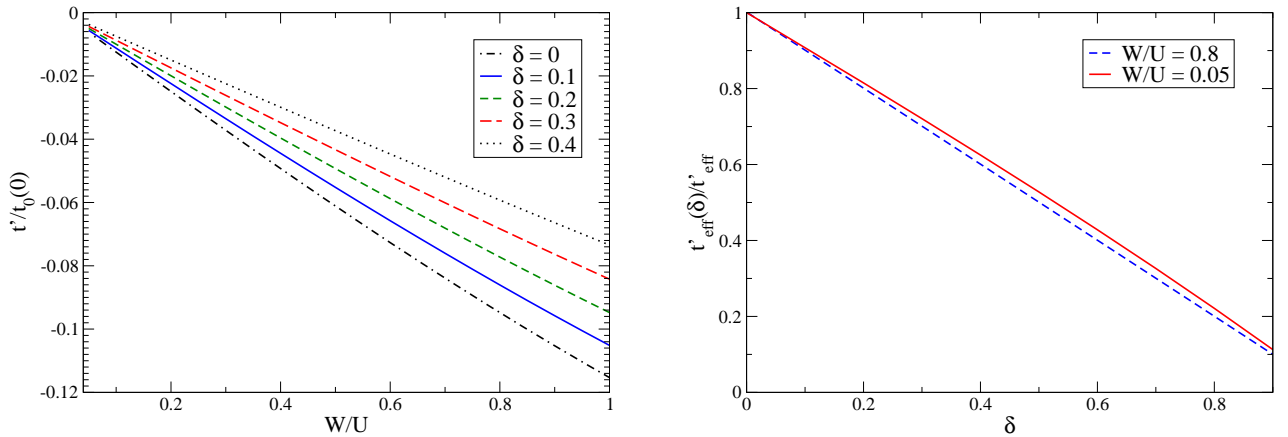


Fig. 5.21.: Hopping element  $t'$  for different  $\delta$

Fig. 5.22.: Dependence of  $t'$  on  $\delta$

Thus inserting holes in the model makes the hopping processes described by  $t'_0$  and  $t''_0$  less important. The coupling  $t''_0$  shows a nearly linear decrease with  $\delta$ .

Representative for the spin dependent hopping elements the results for the spin dependent hopping between diagonal neighbors  $t'_{spin}$  is displayed in Fig. 5.23.

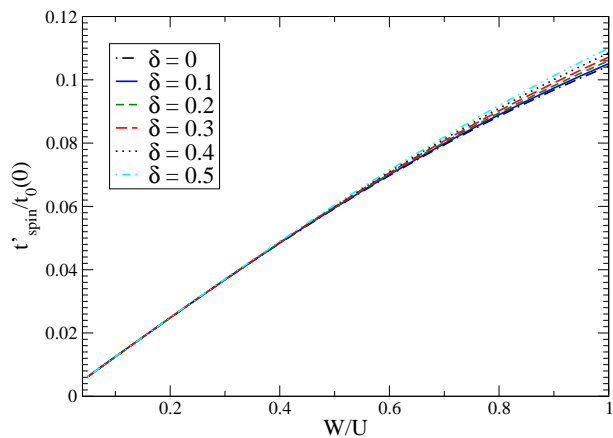


Fig. 5.23.: Spin dependent hopping element  $t'_{spin}$

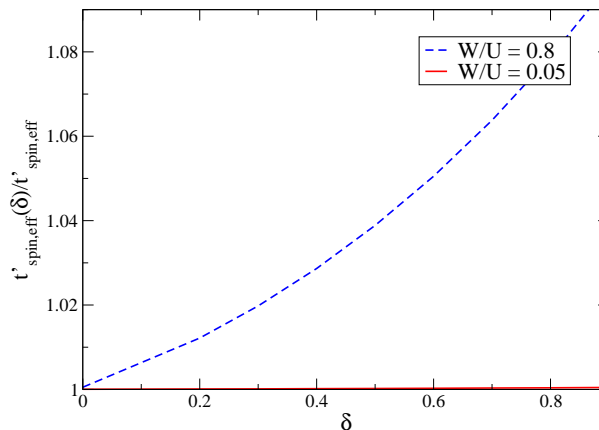


Fig. 5.24.: Dependence of  $t'_{spin}$  on  $\delta$

The coefficient  $t''_{spin}$  behaves similarly. Both coefficients show a change in the range of a few percent for  $W/U = 0.8$ .

### 5.2.2. Results for the $0n$ and the $0n1n$ generator

All calculations for the doped system have additionally been performed with the  $0n$  and the  $0n1n$  generator. As the curves for different truncation schemes behave rather similarly we show a few exemplary results for the upto4 truncation scheme.

At first we study the effect of the different generators on the chemical potential  $\mu$ . Figure 5.25 shows the results for the chemical potential for different generator. Additionally we show the deviation of the results for the  $0n$  and the  $0n1n$  generator from the MKU results in Fig. 5.26.

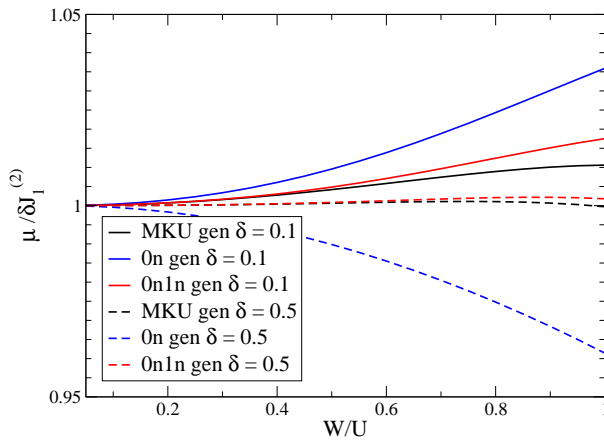


Fig. 5.25.: Chemical potential for different generators

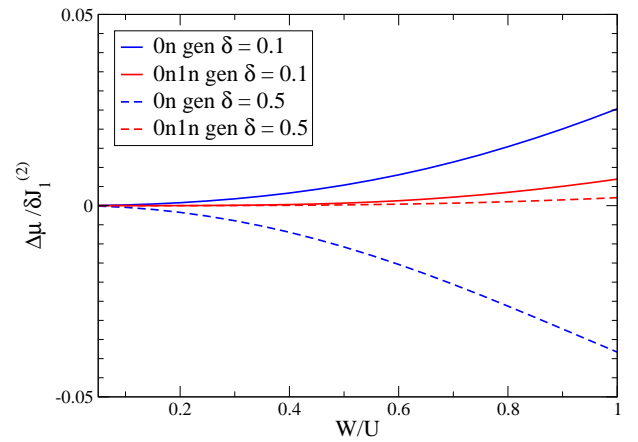


Fig. 5.26.: Deviation from the results obtained by the MKU generator

These figures show that the deviations for the  $0n$  generator are much larger than for the  $0n1n$  generator for both doping concentrations. The deviations increase with increasing values of  $W/U$ .

For  $\delta = 0.1$  both generators lead to higher values of the chemical potential than the MKU generator.

## 5.2.2.1. Spin terms for different generators

The first spin coupling constant we consider is the nearest neighbor Heisenberg exchange  $J_1$ .

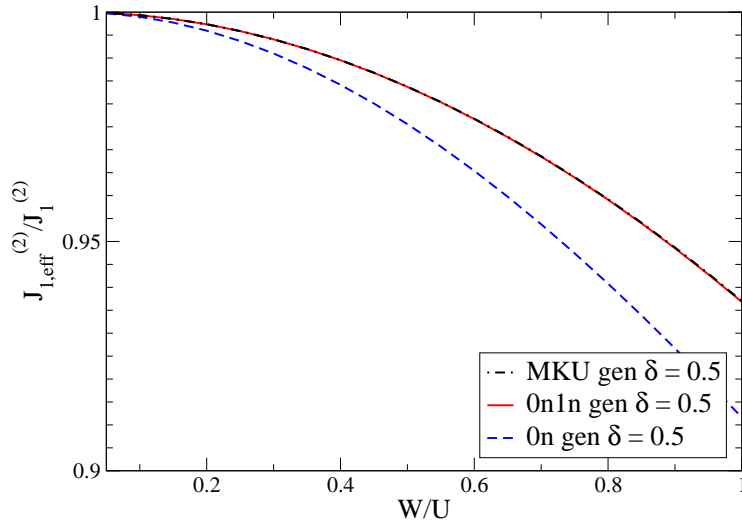


Fig. 5.27.: Heisenberg exchange  $J_1$  for a doping concentration of  $\delta = 0.5$ .

As the curves for the various generators lie close to each other we additionally present the deviation of the results from the results obtained by the use of the MKU generator. The cases of doping with a concentration of  $\delta = 0.1$  and  $\delta = 0.5$  are shown in Fig. 5.28.

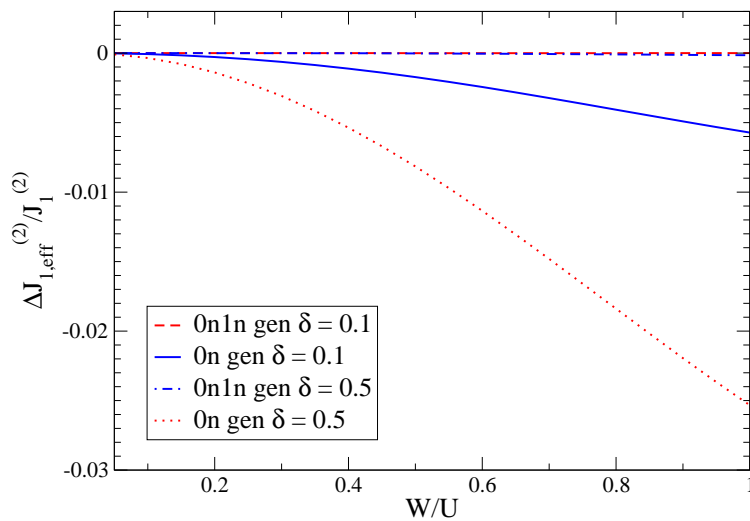


Fig. 5.28.: Deviation of the results for different generators for  $J_1$ .

This plot shows that the deviations of the  $0n$  generator are larger than the one of the  $0n1n$  generator. The deviation increases with the doping concentration. This observation may be explained by the structure of the  $0n$  generator. The  $0n$  generator does not contain interactions of quasiparticles. If the doping concentration is increased holes become more important. Thus the results for the  $0n$  generator differ more from the results of the MKU generator with a higher doping concentration.

In the half-filled case we showed that the second important spin term is the ring exchange between four spins defined in Eq. 4.8.1. The corresponding coupling constant is shown in Fig. 5.29.

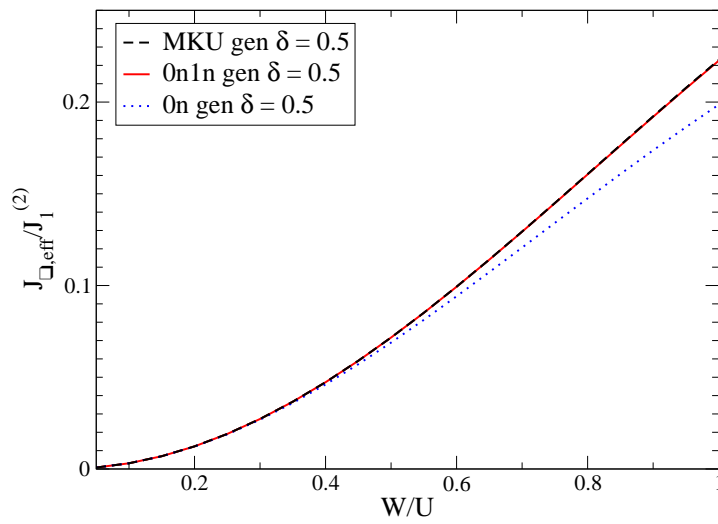


Fig. 5.29.: Deviation of the results for different generators for  $J_{\square}$ .

## 5.2.2.2. Hopping terms

The deviation of the hopping parameter  $t_0$  for the different generators and various concentrations is shown in Fig. 5.30.

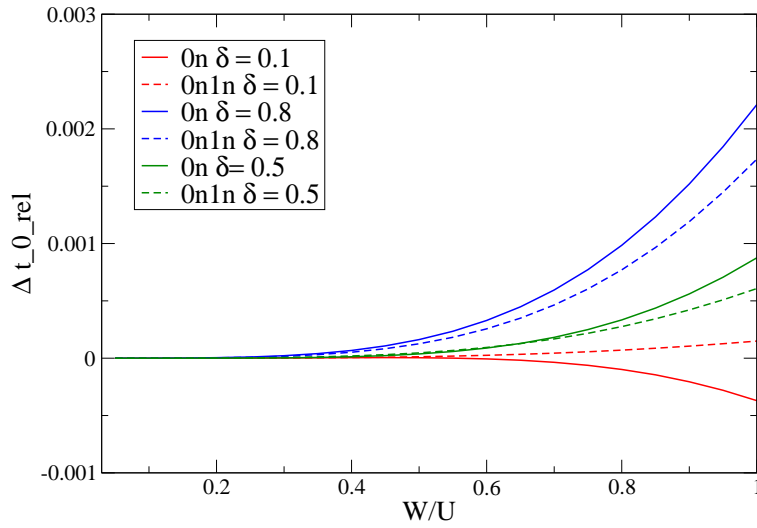


Fig. 5.30.: Deviation of the results for different generators for  $t$  relative to the MKU generator.

Both generators lead to smaller values for  $\delta = 0.1$  and to higher values for doping concentrations of  $\delta \geq 0.5$ . But the changes remain in the range below 1%.

As seen in the half-filled case the deviation of the  $0n$  generator is bigger than the one of the  $0n1n$  generator. Additionally we observe negative values for  $\delta = 0.1$  and positive values for  $\delta = 0.5$ .

For the spin dependent hopping shown in Fig. 5.31 the curves for the  $0n$  generator show a better agreement with the MKU calculations for a doping concentration of  $\delta = 0.8$  than for a doping concentration of  $\delta = 0.5$ .

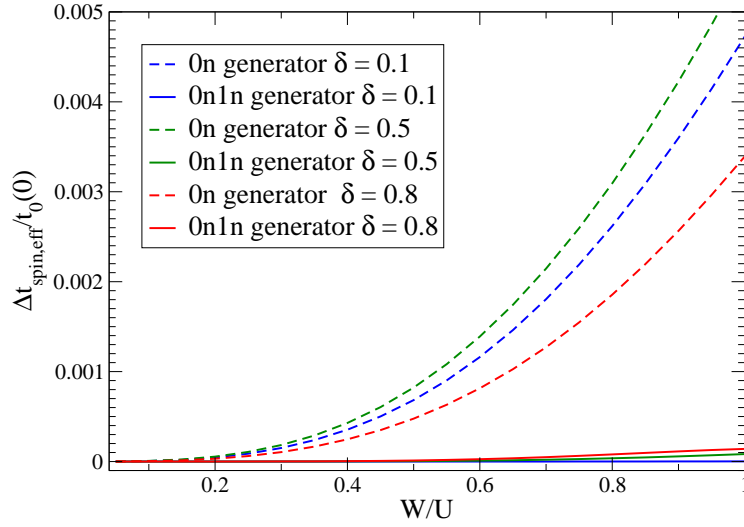


Fig. 5.31.: Deviation of the results for different generators for  $t_{spin}$ .

### 5.2.2.3. Interaction terms

As exemplary results for the interaction terms we show the results for the pair interaction between diagonal neighbors  $V'_p$  given by Eq. 4.8.5 for different generators and different doping concentrations  $\delta$ .

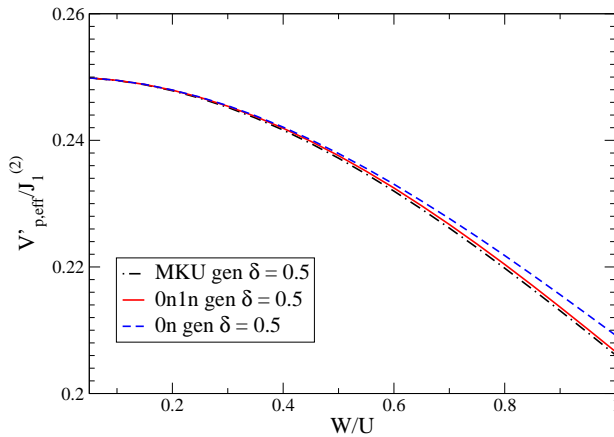


Fig. 5.32.: Results for the pair interaction between diagonal neighbors

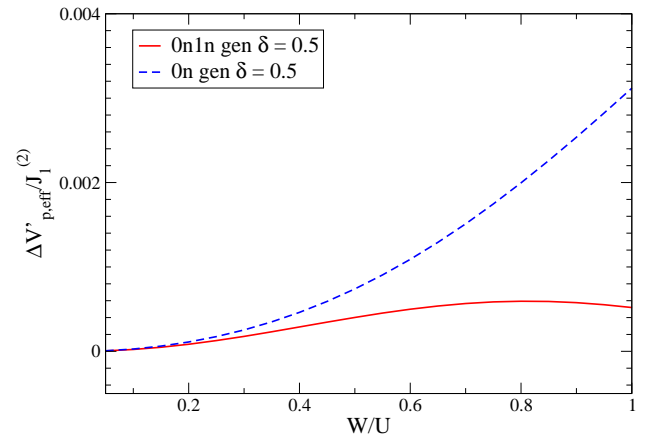


Fig. 5.33.: Deviation of the results from the MKU result

The results for the  $0n$  generator obtained for a doping concentration  $\delta = 0.8$  show a better agreement with the MKU result than the result for  $\delta = 0.5$ . However the deviations

for both generators are small. The results differ about less than three percent.

The density-density interaction between diagonal neighbors  $V'_n$  as defined in Eq. 4.8.6 is shown in Fig. 5.34.

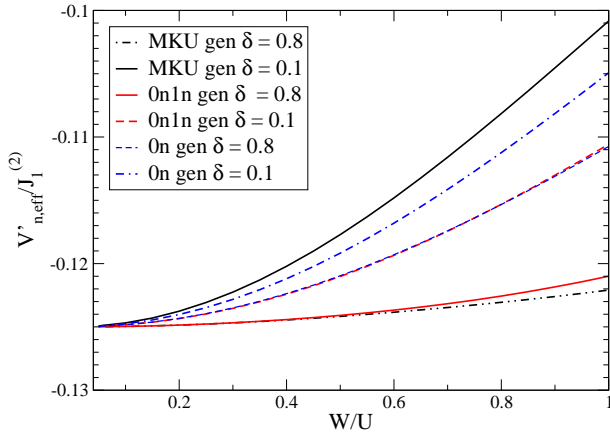


Fig. 5.34.:  $V'_n$  for different doping concentrations  $\delta$

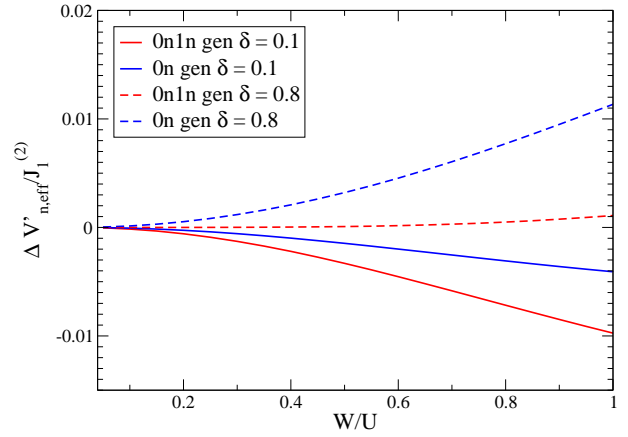


Fig. 5.35.: Deviation of the results from the MKU result

For a doping concentration of  $\delta = 0.1$  the  $0n$  and the  $0n1n$  generator lead to smaller values of  $V'_n$  whereas a higher doping concentration results in larger values for the coupling constant  $V'_n$  obtained with these generators.

### 5.3. Chapter conclusion

In the case of doping a new reference ensemble has to be defined leading to new normal-ordered operators. In accordance to the half-filled case an analytical nearest neighbor calculation leads to a formula describing the chemical potential as function of the doping constant  $\delta$ . In this formula the structure of the lattice is considered by the coordination number  $z$ . All other coupling constants are not altered by the influence of doping.

For the higher truncation schemes we show the effective coupling constants depending on  $W/U$  and on  $\delta$ . The results for the nearest neighbor Heisenberg exchange for various  $\delta$  between  $\delta = 0$  and  $\delta = 0.9$  differ about less than 10%. The dependence of the ring exchange on the doping concentration  $\delta$  shows a similar behavior. Even for the large value  $W/U = 1.6$ , which is already beyond the range of the applicability of the mapping, the change in the Hubbard repulsion  $U$  due to doping effects is less than 3%. In contrast to this the pair interaction  $V_p$  shows a stronger dependence on the doping concentration resulting in deviations of the value in case of doping of about 20%. The remaining interaction terms show differences in the range of a few percent under the influence of doping.

The effective coupling constants in the case of doping are also shown for different generators. These results show that the deviation of the results for the  $0n$  generator from the MKU results are higher than in the undoped case. This may be accounted for by the shift in the weights according to the doping. Due to the doping interaction terms describing holes and doubly occupied sites become more important. Thus the deviations are higher in this case.

It is worthwhile to notice that the results for the  $0n1n$  generator are close to the ones obtained by the MKU generator except for density-density interaction between diagonal neighbors under the influence of doping. For this coupling constant a  $\delta$  of 0.1 leads to a significant difference in the results of the MKU generator from the  $0n1n$  generator of about 10%. In this particular case the results for the  $0n$  generator show a better agreement with the results obtained with the MKU generator which may be accounted for by the change of the sign.

## 6. Charge gap

In this chapter we analyze the conditions which have to be fulfilled for the mapping to be physically reasonable. We give an estimate for the parameter range to which the derivation of the effective model is restricted. A first clue for the breakdown of the mapping is the behavior of the *residual off-diagonality* (ROD) defined in Sect. 3.3.2. Some exemplary results for the behavior of the ROD are depicted in Sect. 4.7.

In agreement with the work done by A. Reischl [RMHU04], we observe a divergence of the ROD in the calculations for the double plaquette truncation scheme. The calculations done by Reischl with the MKU generator as well as our results obtained by the use of the  $0n1n$  generator show this behavior for values of  $W/U$  above a certain threshold. As can be seen in figure 4.40 the ROD diverges for values of  $W/U$  above  $W/U = 1.6$  in the case of the  $0n1n$  generator.

As explained before (see Sect. 3.3.2) a diverging ROD indicates that the mapping to the effective  $t$ - $J$  model breaks down. The basis of the transformation of the Hubbard Hamiltonian to the effective Hamiltonian is the elimination of charge fluctuations. To be able to eliminate these fluctuations, sectors with differing numbers of double occupancies have to be separated in energy.

The density of states for such a case is depicted in Fig. 6.1.

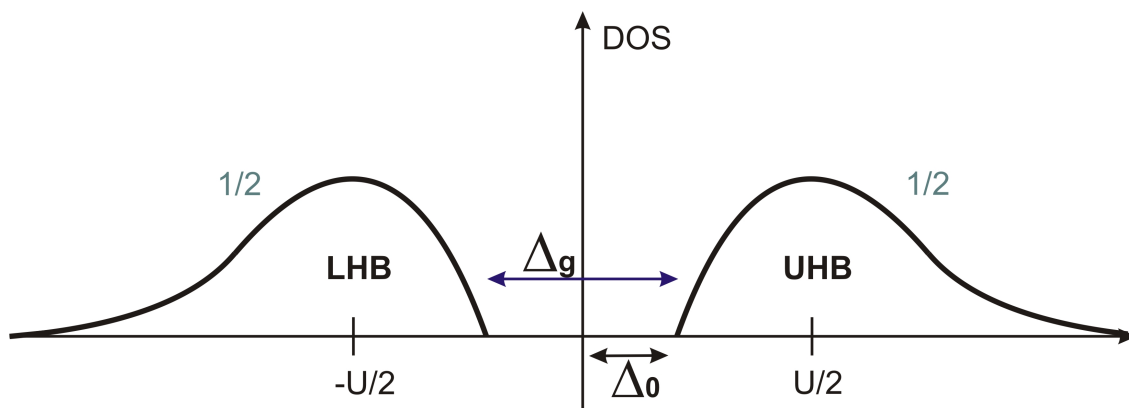


Fig. 6.1.: Density of states for a Hubbard insulator with repulsion strength  $U$ . The density of states exhibits two equally weighted bands, the upper Hubbard band (UHB) and the lower Hubbard band (LHB) [GKKR96].

Such a density of states is found for the insulating regime of a Hubbard model at half-filling and with a large Hubbard repulsion  $U$ . The picture shows two equally weighted bands. The lower Hubbard band (LHB) is situated at  $-U/2$ . This band corresponds to

states without double occupancies. The other band corresponding to states with one DO is denoted as upper Hubbard band (UHB). In the case of a large repulsion  $U$  the bands are separated by a gap  $\Delta_g = 2\Delta_0$ .

If the ratio  $W/U$  is increased the bands begin to approach each other. Eventually they overlap (see Fig. 6.2).

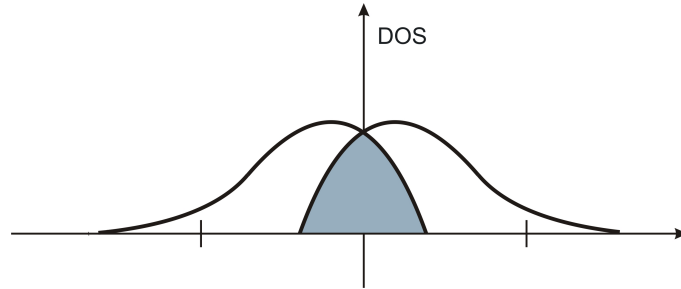


Fig. 6.2.: Density of states for a Hubbard model in the metallic phase, showing the overlap of the bands [GKKR96].

As the bands begin to overlap the model undergoes a transition from an insulator to a metal. An overlap of the bands results in a connection of sectors with differing numbers of double occupancies. As a consequence the gap can be used as a tool to analyze the separation of states with excitations from the ground state sector. Thus a vanishing gap can be seen as indicator for the transition to a metal. Consequently a vanishing gap indicates the breakdown of the mapping.

In this thesis the gap is calculated as a function of the hopping parameter  $t$ . Let  $t^*$  be the value for which the gap vanishes. From  $t^*$  a value of  $W/U$  up to which the results of the mapping are reliable can be determined. If the gap vanishes, the sectors overlap. In the case of a vanishing gap it is not possible to order the states with different numbers of double occupancies according to the corresponding energies. The transformation does no longer yield a model in which the number of double occupancies is a conserved quantity. Results for the coupling constants obtained for this region have to be treated cautiously.

In order to determine the applicability of the mapping quantitatively we compute the charge gap. The calculation of the gap is performed within the effective  $t$ - $J$  model. In the effective model under study the ground state sector does not consist of a single ground state but of a huge subspace of magnetically disordered states. This leads to a considerable expenditure for the calculation of the gap.

We start our considerations by analyzing the half-filled case.

## 6.1. Charge gap in the half-filled case

In the half-filled case the lower Hubbard band is completely filled. Creating an excitation causes the energy cost  $\Delta_g = 2\Delta_0$ .

As a result the gap can be calculated by estimating the lowest energy of a DO in this model. In the effective model the DO moves along the magnetically disordered spin background which is given by the reference ensemble.

Before we describe the calculation of the gap explicitly, we want to highlight that the calculated gap does not correspond to a true gap between two possible states of the system. Starting with a reference ensemble which is not the true ground state of the system the calculated gap might differ from the true gap. To avoid confusion we call the calculated gap the apparent charge gap  $\Delta_g$  in contrast to the true charge gap  $\Delta_{\text{true}}$ .

Brinkman and Rice [BR70], who calculated the propagation of a particle in various spin backgrounds, found that in the density of states of such a system Lifshitz tails [Lif64] may appear. Further calculations considering Lifshitz tails led to the assumption that the weight included in these tails is small [MSV92, Mie92].

Due to the small weight of the Lifshitz tails it is hard to treat their effects appropriately. A local calculation with a restricted extension fails to capture effects from these tails.

This argument also holds for our approach. Although our approach captures most of the weight, we miss the weight in the Lifshitz tails. As can be seen in Fig. 6.3, this results in a larger value for the gap.

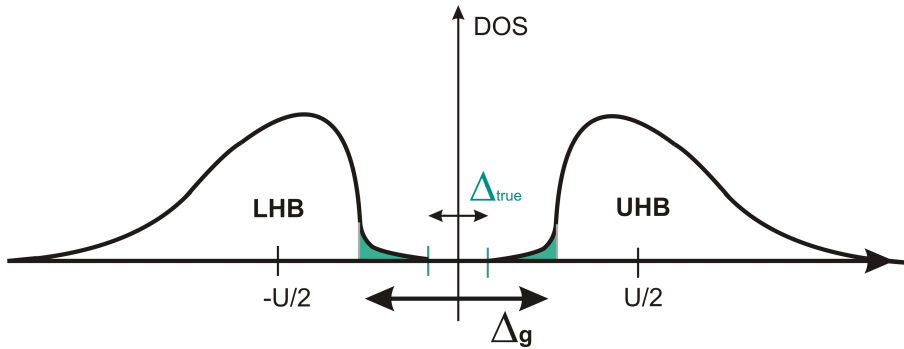


Fig. 6.3.: Effects of Lifshitz tails on the calculated charge gap  $\Delta_g$ .

Even if the apparent charge gap  $\Delta_g$  differs from the true charge gap, the effect of the Lifshitz tails is assumed to be very small. Therefore the behavior of the system can be analyzed by the use of the apparent charge gap. At least the transition from an insulator to a paramagnetic metal should be captured by the considerations presented here. As a significant overlap of sectors with differing numbers of quasiparticles is needed to cause a breakdown of the method, it is assumed that the small weight of the band tails does not influence the results.

For the determination of the apparent charge gap the dispersion of a DO has to be calculated. Due to the complexity of the effective  $t$ - $J$  model a full diagonalization of the

Hamiltonian is not feasible. Therefore we use an approximate method based on the Lanczos method. The Lanczos method was developed to bring large matrices to tridiagonal form without keeping the whole matrix in the storage. Since we have to deal with operators acting on the reference ensemble instead of single states the Lanczos method is not applicable in its original description. Thus we use the Liouville representation of the Lanczos technique [Mor65, Ful91, VM94].

In this representation the evolution of a DO in the spin background is described by the Liouville superoperator. This operator is given by

$$\mathcal{L} = \left[ \hat{H}_{\text{eff}}, \cdot \right]. \quad (6.1.1)$$

The effect of  $\mathcal{L}$  consists of shifting the DO and changing the spin background. Due to the Liouville formulation we use operators as vectors in the superspace [FL82]. Thus the vectors  $v_i$  are given by the operators they contain. The calculation starts with the vector  $v_0$ .  $v_0$  is given by

$$v_0 = \frac{1}{\sqrt{N}} \sum_{\vec{r}} e^{i\vec{k}\vec{r}} \hat{n}_{\vec{r},\downarrow} \hat{c}_{\vec{r},\uparrow}^\dagger \quad (6.1.2)$$

where  $N$  denotes the number of lattice sites and  $\vec{r}$  indicates the position. The action of this operator is to place an electron with spin up on a site  $\vec{r}$  which is occupied by one electron with spin down. Conclusively  $v_0$  creates a single doubly occupied site. The vector  $\vec{k}$  represents the momentum of this DO moving across the lattice.

Starting with  $v_0$  we now construct a Krylov sequence by creating iteratively a set of orthogonal vectors  $v_i$ . Each new vector is calculated from the ones before by applying

$$v_{i+1} = \mathcal{L}v_i - a_i v_i - b_i^2 v_{i-1}. \quad (6.1.3)$$

The prefactors  $a_i$  and  $b_i$  are chosen in such a way that the  $v_i$  are pairwise orthogonal. Thus the  $a_i$  are given by the projection of the Liouville operator onto  $v_i$ .

$$a_i = \frac{(v_i | \mathcal{L}v_i)}{(v_i | v_i)} \quad (6.1.4)$$

The brackets in this formula denote a suitable scalar product of the Liouville formulation [Ful91]

$$\left( \hat{A} | \hat{B} \right) = \text{Tr} \left( \hat{A}^\dagger \hat{B} \hat{\rho}_0 \right). \quad (6.1.5)$$

Here  $\hat{\rho}_0$  stands for the statistical operator of the reference ensemble see Eq. 4.2.12. In the same way the  $b_i$  are determined as

$$b_i^2 = \frac{(v_i | v_i)}{(v_{i-1} | v_{i-1})} \quad (6.1.6)$$

with the starting value  $b_0 = 0$ .

The resulting vectors form a basis  $\{v_i\}$  in which the Liouville operator has tridiagonal

form. To simplify the calculations further we normalize the  $v_i$ . In this normalized basis, the Liouville operator can be written as

$$\mathcal{L} = \begin{pmatrix} a_0 & b_1 & 0 & 0 & & \\ b_1 & a_1 & b_2 & 0 & \dots & \\ 0 & b_2 & a_2 & b_3 & & \\ 0 & 0 & b_3 & a_3 & & \\ & & \dots & & & \end{pmatrix}. \quad (6.1.7)$$

Having created a matrix representation of  $\mathcal{L}$  we can now determine the energy eigenvalues of the Liouville operator. The lowest energy value is used to calculate the apparent charge gap

$$\Delta_g = 2 \min_{\vec{k}} E_k. \quad (6.1.8)$$

As the effective Hamiltonian conserves the number of DOs we can restrict the whole calculation to the one DO subspace. It is clear that we can not use the results obtained with the  $0n$  generator in this context because it does not decouple the sector with one DO from the ones with more DOs. For a calculation using these results we would have to consider additionally all subspaces with more than one DO. This is impossible as it would result in an overwhelming number of terms. Therefore we restrict ourselves to the results for the MKU and the  $0n1n$  generator.

However even for the simplified calculations within the one DO subspace only a few iterations were feasible. Starting with the simple vector  $v_0$  the commutation leads to complicate terms for the following vectors. Consequently the effort for the calculation grows exponentially with the number of iterations.

Due to the complexity of the vectors a large subspace is created within a few iterations.

Each iteration extends the considered subspace more and more. As we can only perform a few iterations the apparent charge gap  $\Delta_g$  we obtain has to be understood as an upper bound for the realistic charge gap.

Expecting extremal values for the dispersion on points with high symmetries, we calculate the gap for values of the momentum of  $\vec{k} = (0, 0)$  and  $\vec{k} = (\frac{\pi}{a}, \frac{\pi}{a})$  with the lattice constant  $a$  or  $k = 0$  and  $k = \frac{\pi}{a}$  in the one dimensional case.

## 6.2. Charge gap in the case of doping

This section deals with the determination of the apparent charge gap in the case of hole doping.

The effect of doping on the density of states does not only consist in a shift of the Fermi energy. Additionally the doping causes a redistribution of the weight. This weight shift in the density of states of Mott materials has been observed using dynamical mean field theories [ZPB02].

A schematic density of states for this case is shown in Fig. 6.4.

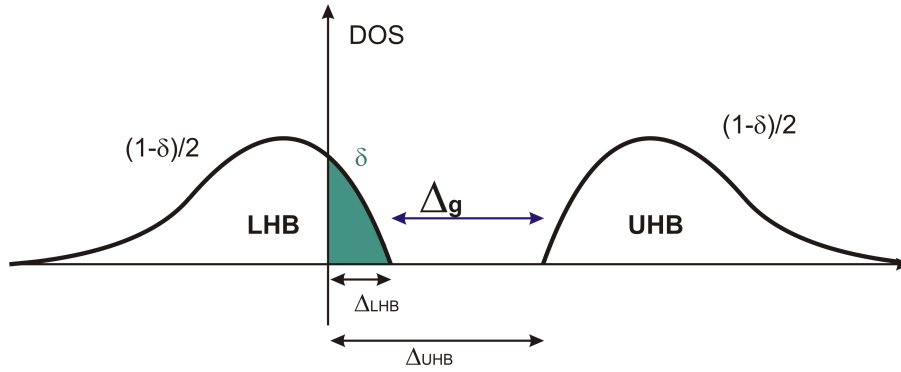


Fig. 6.4.: Density of states in the case of hole doping with the doping constant  $\delta$ .

From this picture the weight of the different states can be deduced. An empty state has the possibility  $\delta$  whereas the two singly occupied states have a possibility of  $\frac{1-\delta}{2}$  each. Note that the total weight in the LHB is  $\frac{1}{2} + \frac{\delta}{2}$  whereas it is  $\frac{1}{2} - \frac{\delta}{2}$  in the UHB. This constitutes a shift in the spectral weight. This shift has been observed in Monte Carlo calculations for the infinite-dimensional Hubbard model [JFP95].

In the doped case the calculation of the gap can be divided into two parts. In the first part the lowest possible energy for a DO  $\Delta_{\text{UHB}}$  is calculated. In the second part we have to calculate additionally the maximal energy for the destruction of a DO  $\Delta_{\text{LHB}}$ . The DO is destroyed by placing a single electron on an empty site.

The apparent charge gap is given by the difference of these two energies

$$\Delta_g = \Delta_{\text{UHB}} - \Delta_{\text{LHB}}. \quad (6.2.9)$$

The first part of the calculation is performed in analogy to the half-filled case [RMHU04]. For the second part a new starting vector

$$v_{0,\text{LHB}} = \frac{1}{\sqrt{N}} \sum_{\vec{r}} e^{i\vec{k}\vec{r}} \hat{c}_{\vec{r},\uparrow}^\dagger (1 - \hat{n}_{\vec{r},\downarrow}) \quad (6.2.10)$$

has to be introduced.

The action of  $v_{0,\text{LHB}}$  is to place an electron with spin up on an empty site  $\vec{r}$ .

By the use of this method we calculate the gap for different degrees of doping. Thus we can draw conclusions concerning the doping dependence of the charge gap.

### 6.3. Implementation

For the calculation of the gap we use the same program structures as before. At the beginning the program loads the effective  $t$ - $J$  model with the  $t$ -dependent coefficients obtained before. Then an outer loop is performed for each iteration. Within this loop the vectors  $v_i$  are commuted. Then we calculate the traces and determine the new vector  $v_{i+1}$ .

Having determined the new basis we just have to calculate the eigenvalues of  $\mathcal{L}$ .

The most time consuming part of this program is the calculation of the commutator and the determination of the traces. As explained before the computational effort grows exponentially with the number of iterations. Already the calculations for the one-dimensional nearest neighbor model with three iterations took 24 hours of CPU for each data point whereas calculations with two iterations are performed within a few minutes.

## 6.4. Results for the charge gap

### 6.4.1. One-dimensional linear chain

As explained in Sect. 6.1 we calculate the apparent charge gap for values of the momentum of  $k = 0$  and  $k = \pi/a$  with the lattice constant  $a$ . As we are looking for an upper bound for the gap, the following figures show the minimal value obtained for energy of a moving DO.

#### 6.4.1.1. Results for the half-filled case

For the half-filled case Fig. 6.5 shows the results obtained for the gap in dependence of the quotient  $W/U$ .

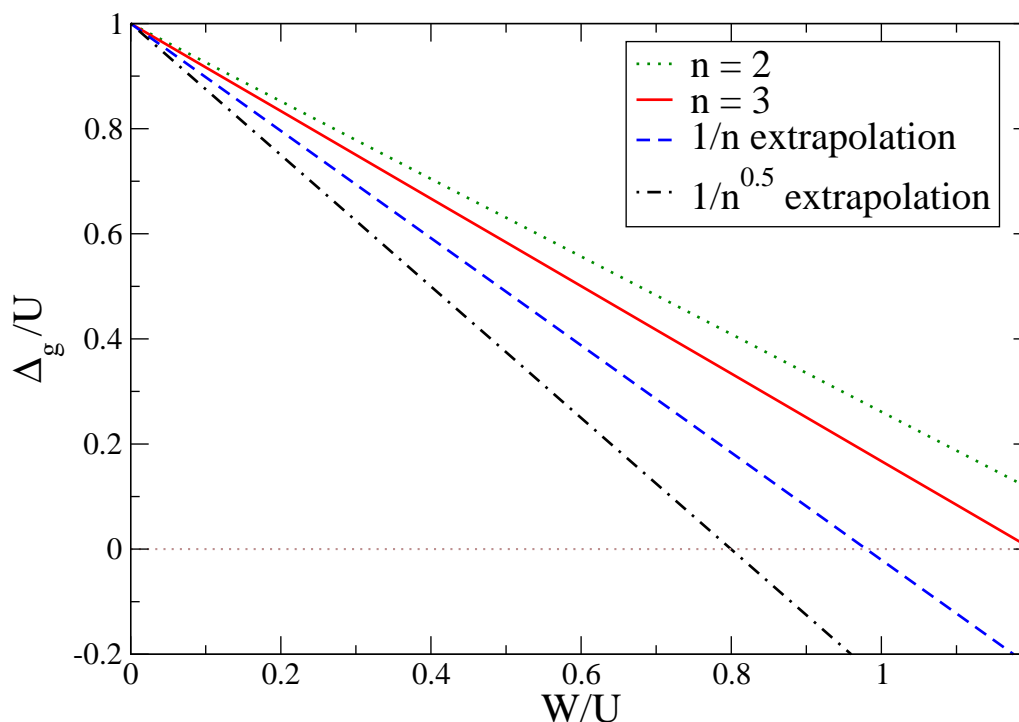


Fig. 6.5.: Behavior of the apparent charge gap  $\Delta_g$  for a one dimensional linear chain in the case of half-filling for the NN calculation.  $n$  denotes the number of iterations performed.

In the case of a vanishing hopping parameter  $t = 0$  the model is governed by the repulsion  $U$ . In this case the gap has the value  $\Delta_g = U$ . Thus the shown curves start at  $\Delta_g/U = 1$  for  $W/U = 0$ . This observation serves as a check for the program.

Due to the vast number of terms in the effective model the first iteration in the nearest neighbor calculation leads to a vector consisting of about 900 terms. As a result of this the numerical calculations were restricted to small truncation schemes. All results obtained in the context of this thesis correspond to nearest neighbor NN calculations.

A. Reischl [RMHU04] observed that the differences obtained for different truncation schemes are rather small. But there are sizeable differences in the results obtained for differing numbers of iterations.

As the terms become more complex the more iterations are performed, only a few iterations (up to four) were feasible in this work. Restricting the calculations to the nearest neighbor truncation, we are not able to analyze the influence of the choice of the generator on the results up to now.

As can be seen in figure 6.5 the gap decreases linearly from a values of  $U$ . The difference between the results obtained after two iterations and the results obtained after three iterations is rather large. As we only performed a few iterations we extrapolated the results for the case of infinitely many iterations  $n \rightarrow \infty$ . Following Zhong and Sorella [ZS95] a linear extrapolation in  $\frac{1}{n}$  with  $n$  as the number of iterations is performed. Additionally we extrapolate the results in  $\frac{1}{\sqrt{n}}$ . These extrapolations are performed for the momentum  $k = \pi/a$  for which we find the minimal energy in all calculations. The obtained curves are shown in 6.5.

In the case of  $n = 3$  iterations a closure of the gap is found at  $W/U \approx 1.2$ . The results for the extrapolations point towards an earlier closure. The curve for the  $\frac{1}{n}$  extrapolation shows a vanishing gap for  $W/U = 1$  and the  $\frac{1}{\sqrt{n}}$  extrapolation induces a closure of the gap at  $W/U \approx 0.8$ . Let us highlight again that the obtained values for the gap have to be seen as upper bound to the real charge gap. The influence of the Lifshitz tails might only be observed in calculations with a high number of iterations, which were not feasible. Negative values of the gap imply the breakdown of the mapping. The gap is just a measure for the separation of the energy scales. If the gap vanishes the whole mapping breaks down. Thus results obtained in the parameter range where the gap is zero or even smaller than zero are not reliable anymore.

From the vanishing of the gap we can conclude that the mapping to the effective model is valid for values of  $W/U < 0.8$  in the half-filled case. Values obtained for the coupling constants for  $W/U \geq 0.8$  have to be treated cautiously.

#### 6.4.1.2. Results for the doped case

Due to the redistribution of the weight for the doped Hubbard model (see section 6.2), an earlier closure of the gap is expected for the doped case. This feature can be observed in the curves of figure 6.6. This figure shows the results of the  $\frac{1}{n}$  extrapolation for different doping concentrations  $\delta$ .

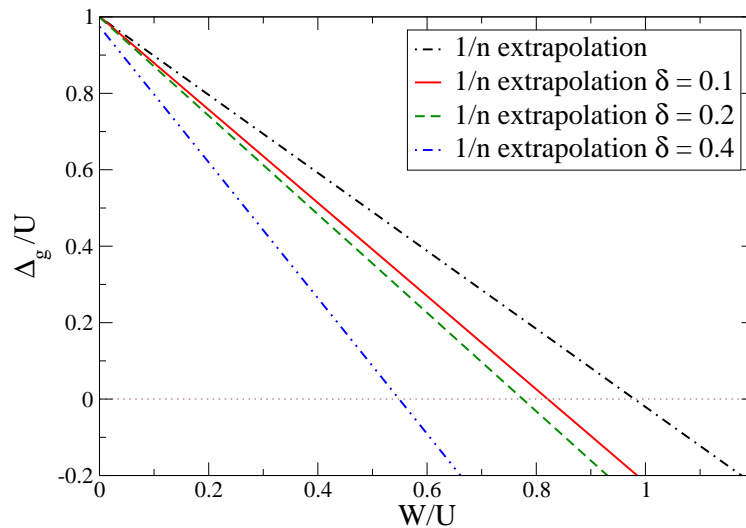


Fig. 6.6.:  $1/n$  expansion for the apparent charge gap  $\Delta_g$  for a one dimensional linear chain in the case of hole doping with dopant concentration  $\delta$ .

There a clear decrease of the gap with the doping concentration  $\delta$  is seen. For  $\delta = 0.2$  the extrapolation shows a closure of the gap for  $W/U$  about 0.8. Increasing  $\delta$  to  $\delta = 0.4$  leads to a closed gap for  $W/U \geq 0.55$ .

The curves for the  $\frac{1}{\sqrt{n}}$  extrapolation, which are shown in figure 6.7, point towards smaller values of the gap.

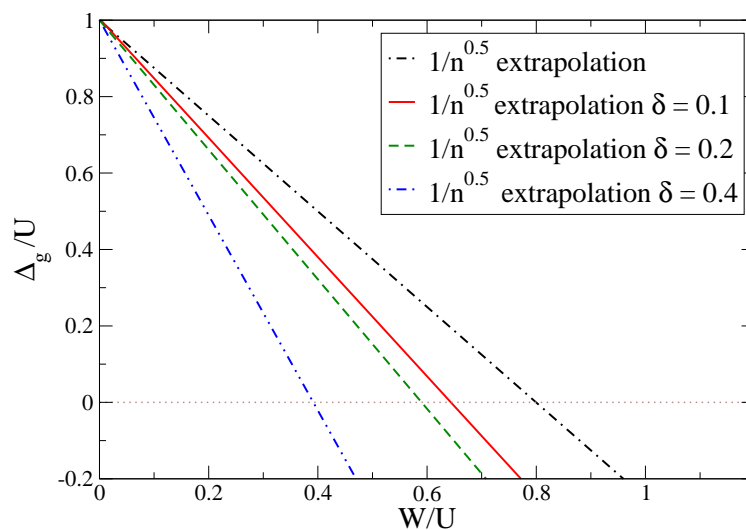


Fig. 6.7.:  $1/\sqrt{n}$  expansion for the apparent charge gap  $\Delta_g$  for a one dimensional linear chain in the case of hole doping

This leads to a value for the apparent charge gap of  $W/U \approx 0.4$  for  $\delta = 0.4$ . With the apparent charge gap also the parameter range where mapping stays controllable decreases with the doping concentration. This is in agreement with the results obtained by Millis and Coppersmith [MC90,MC91] who studied the phase diagram of the Hubbard model in dependence of the doping concentration  $\delta$ .

Figure 6.8 summarizes the results obtained in the doped case. It depicts the values of  $W/U$  for which a closure of the gap is found in dependence on the doping concentration  $\delta$ .

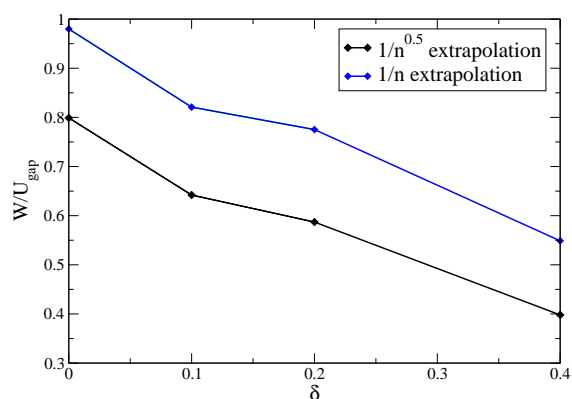


Fig. 6.8.: Results of the extrapolations for the apparent charge gap for the doped one-dimensional linear chain

### 6.4.2. Results for the two-dimensional square lattice

In analogy to the one-dimensional case we show a few results for the nearest neighbor calculations on a two dimensional square lattice. The resulting curves for two and three iterations are shown. Additionally we improve the estimation for the gap by the use of a linear  $\frac{1}{n}$  and a linear  $\frac{1}{\sqrt{n}}$  extrapolation for the results.

For the two-dimensional square lattice at half-filling A. Reischl showed, that the results obtained with different truncation schemes are close to each other. Therefore we assume that we can draw conclusions concerning the gap from the nearest neighbor calculation.

#### 6.4.2.1. Results for the half-filled case

The results obtained for a two-dimensional square lattice are depicted in Fig. 6.9. As explained before the curves show a linear decrease from  $\Delta_g/U = 1$  for  $W/U = 0$ . This linear decrease has been observed before by Gebhard [Geb97], who predicted a closure of the gap at  $W/U = 1$ . In contrast to this linear approach a downward curvature was found for higher truncation schemes [RMHU04]. This curvature induced an earlier closure of the gap. Consequently the linear curves obtained for the nearest neighbor calculations serve as an upper bound to the gap.

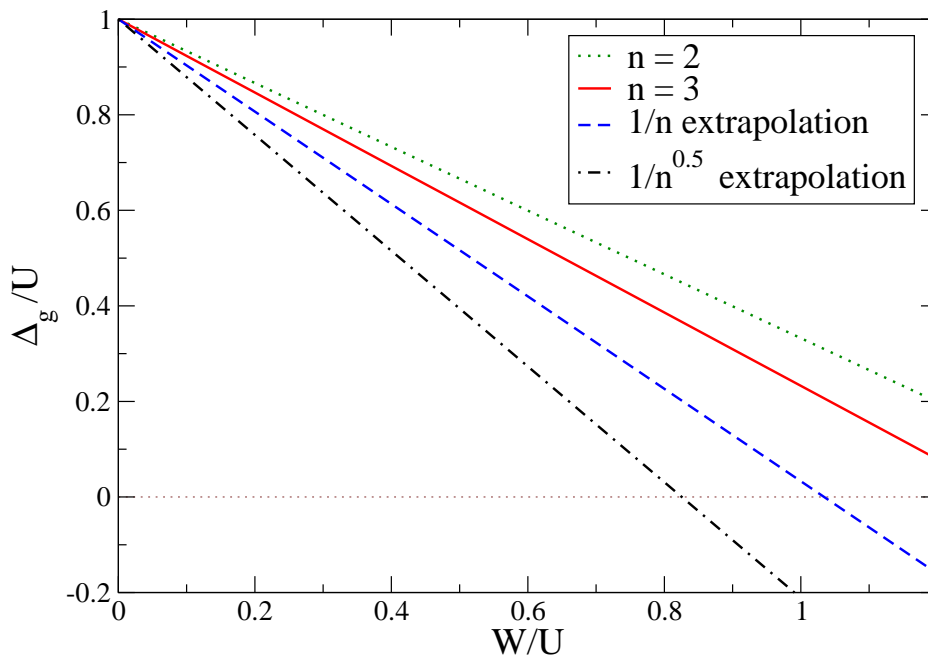


Fig. 6.9.: Results for the apparent charge gap in the case of a half-filled square lattice

From Fig. 6.9 a closure of the apparent charge gap is found for  $W/U \geq 1.25$  for  $n = 3$ . A  $\frac{1}{n}$  extrapolation leads to a close around  $W/U = 1.05$ . The  $\frac{1}{\sqrt{n}}$  extrapolation pushes this value even lower to  $W/U = 0.83$ .

For a Hubbard model on a Bethe lattice with  $z \rightarrow \infty$  a closure of the gap is found for  $W/U \approx 0.89$  [NGJ03]. A  $\frac{1}{U}$  expansion of this model led to a closure of the gap at  $W/U \approx 0.9$  [EGK<sup>+</sup>03].

Due to the closure of the gap results for the effective coupling constants for  $W/U \geq 0.83$  have to be treated cautiously. If the apparent charge gap closes a controlled mapping to an effective  $t$ - $J$  model preserving the number of quasiparticles is not possible anymore. This may lead to a diverging ROD as it was observed in the double plaquette calculation for  $W/U = 1.6$  (see Fig. 4.40). This value lies far above the limit for  $W/U$  above which the mapping to the effective model breaks down. This may be accounted for by the fact that the DOs are created as pairs with strongly restricted distance in the present approach. Thus an independent motion is not possible.

Assuming that the gap closes at about  $W/U \approx 0.83$ , we have to admit that the coupling constants shown before are only valid in the range  $W/U < 0.83$ . Although the gap closes thus making the mapping impossible, we do not observe effects on the coupling constants for  $W/U > 0.83$ . Besides there is no divergence of the ROD except for  $W/U = 1.6$  in the case of the  $0n1n$  generator. These effects may be originated in band tails. Even if the gap closes it might be the case that most of the weight is situated in regions where the gap still exists. Thus the influence of the small weighted tails is too small to cause effects on the coupling constants.

A. Reischl followed a slightly different approach [RMHU04]. In analogy to the approach presented in this thesis the Lanczos technique was used to create the vectors  $v_i$ . But in contrast to our approach he split the vectors  $v_i$  into the terms of which they consist and calculated the action of the Liouville superoperator on these terms. This results in a much larger matrix representing  $\mathcal{L}$ . Thus a smaller value for the closure of the gap was found by this approach. The  $\frac{1}{n}$  extrapolation lead to a closure of the gap at  $W/U \approx 0.9$  whereas we found a value of  $W/U = 1.05$  in this case.

### 6.4.2.2. Results for the two-dimensional hole doped square lattice

We show some exemplary results for the two-dimensional hole doped lattice.

First of all the curves obtained after  $n = 3$  iterations are shown for various doping concentrations  $\delta$  (see figure 6.10).

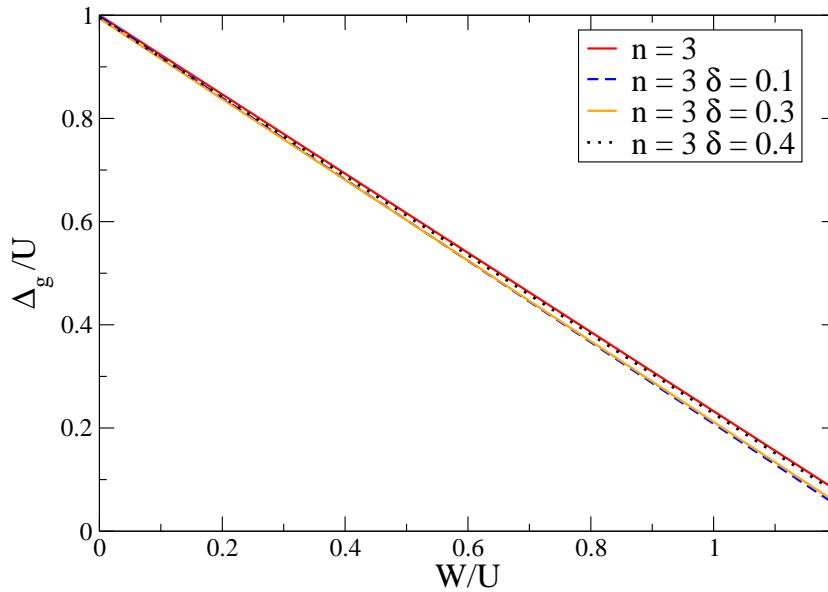


Fig. 6.10.: Results for the gap obtained in the case of doping for a calculation with 3 iterations

While the curves for differing doping concentrations  $\delta$  nearly lie above each other for the  $n = 3$  calculation, the results obtained by extrapolations show a strong dependence on  $\delta$ . The curves for the  $\frac{1}{n}$  extrapolation show an earlier closure of the gap with higher doping concentrations  $\delta$  (see Fig.6.11).

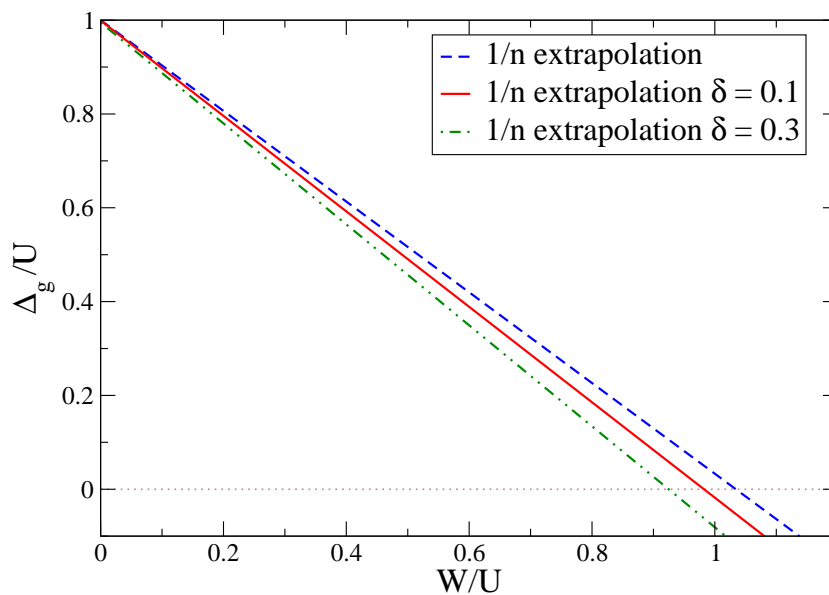


Fig. 6.11.:  $1/n$  expansion for the apparent charge gap  $\Delta_g$  for a two-dimensional square lattice in the case of hole doping

A doping concentration of  $\delta = 0.1$  leads to a value of  $W/U = 0.99$  instead of  $W/U = 1.05$  in the undoped case.  $\delta = 0.3$  leads to a value of  $W/U = 0.92$ .

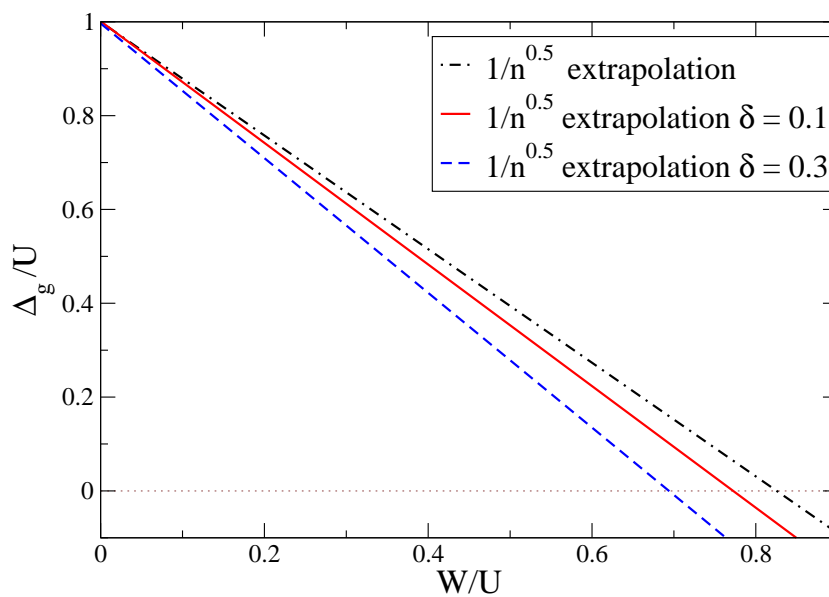


Fig. 6.12.:  $1/n$  expansion for the apparent charge gap  $\Delta_g$  for a two-dimensional square lattice in the case of hole doping

For the  $\frac{1}{\sqrt{n}}$  extrapolation smaller values are obtained. Doping the system with  $\delta = 0.1$  leads to a closure of the gap at  $W/U = 0.78$ . This value goes down for  $\delta = 0.3$  to  $W/U = 0.7$ .

Thus doping causes a decrease of the gap in this region. These results are supported by the work of Millis and Coppersmith ([MC90] [MC91]), who showed that the breakdown of the insulator takes place for smaller  $W/U$  under the influence of doping.

This behavior is accounted for by the density of states in the doped case. According to the probabilities of the single states (section 6.2) the probability to find two electrons on the same site decreases with  $\delta$ . If the doping concentration is too high it is unlikely to find two interacting electrons on one site. As a result the repulsion can be neglected and the system has to be understood as a system of itinerant electrons thus the system has to be seen as a metal.

In analogy to the one-dimensional case Fig. 6.13 displays the values of  $W/U$  for which a closure of the gap is found depending on the doping concentration  $\delta$ .

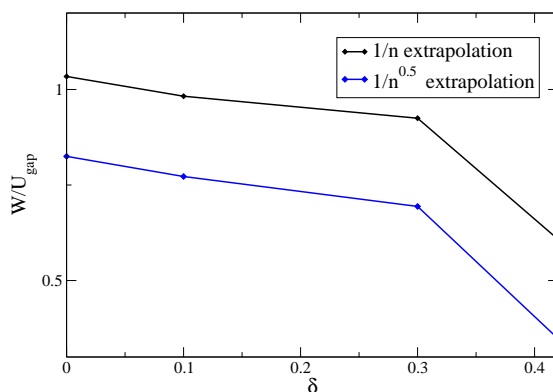


Fig. 6.13.: Results of the extrapolations for the apparent charge gap for the doped two-dimensional square lattice

For doping concentrations  $\delta < 0.3$  there is nearly no dependence of the range of validity on the doping concentration. For higher doping concentrations the range of validity of the mapping decreases rapidly with  $\delta$ .

Compared to the one-dimensional case, it seems that these effects set in earlier in one dimension.

## 6.5. Chapter conclusion

In the chapters before we presented results for the effective coupling constants obtained in the half-filled and in the doped case. In this chapter the limitations of a mapping to a DO conserving effective model are analyzed.

The mapping is possible in the non-metallic regime of the phase diagram 2.1 of the Hubbard model, which corresponds to a doped insulator. As the mapping is possible as long as the sectors which should be decoupled from each other are separated in energy the *apparent charge gap*  $\Delta_g$  was introduced as a measure for this separation. Thus a value for the apparent charge gap  $\Delta_g > 0$  is a prerequisite of a well-controlled mapping, whereas  $\Delta_g = 0$  indicates the breakdown of the mapping.

In this case a transition to a metal takes place, in which charge excitations do not cause energy costs and thus can no longer be eliminated.

The apparent charge gap is calculated within the Liouville formulation of the Lanczos technique. Due to the fact, that we can only perform a few iterations the apparent charge gap has to be understood as an upper bound to the real gap. Although the results presented in this chapter are restricted to nearest neighbor calculations we obtained good results for the limit of an infinite number of iterations  $n$  by extrapolation. For this the results were linearly extrapolated in  $\frac{1}{n}$  and additionally in  $\frac{1}{\sqrt{n}}$ . Up to now we performed too little iterations to decide which of these extrapolation schemes describes the behavior of the gap most accurately.

All results presented in this chapter have in common that they show a linear decrease of the gap with  $W/U$ . Compared to the two-dimensional case the gap calculated for the one-dimensional linear chain closes earlier. In this case the  $\frac{1}{\sqrt{n}}$  extrapolation yields the value  $W/U = 0.799$  for the closure of the gap. For the two-dimensional square lattice the  $\frac{1}{\sqrt{n}}$  extrapolation leads to a value of at about  $W/U = 0.83$ .

As a result we state that the effective coupling constants obtained for  $W/U < 0.83$  in the two-dimensional case are reliable whereas the results obtained for  $W/U \geq 0.83$  have to be treated cautiously. This threshold lies above the parameter range in which one is interested in the context of cuprates [Dag94].

The breakdown of the mapping can not be seen in the behavior of the calculated coupling constants. Besides the only diverging ROD we observed corresponds to the  $0n1n$  generator and a value of  $W/U$  of 1.6. Although the gap closes earlier we do not find a diverging ROD in this parameter range. This effect may be accounted for by tails in the density of states.

The gap is also calculated in the doped case in dependence of the dopant concentration  $\delta$ . These calculations point towards an earlier closure of the gap under the influence of hole doping.

In further calculations one could determine the value  $\delta_{crit}$  above which the mapping is not possible by the use of this method. This values serves as a threshold under which the system can still be seen as a doped insulator. For values of  $\delta$  above this threshold the system has to be seen as metallic electron system for which the mapping breaks down.

## 7. Summary and outlook

In this thesis the method of *self-similar continuous unitary transformations* is applied to the Hubbard model in real space. Due to the local approach the extension of a term is used as a measure for its relevance. Using the MKU generator this leads to an effective generalized  $t$ - $J$  model, in which the number of double occupancies is conserved.

In a nearest neighbor calculation a universal formula describing the effective coupling constants for all types of lattices and all coordination numbers  $z$  is derived analytically. For higher truncation schemes numerical methods have to be used.

The effective  $t$ - $J$  model describes spin interactions between two spins as well as four spin terms. For the two spin terms we find that the coefficients of interactions between two diagonally neighboring spins  $J_2$  and between two third nearest neighbor spins  $J_3$  are much smaller than the nearest neighbor Heisenberg interaction  $J_1$ . This is valid for the  $J_3$  in the one-dimensional as well as for  $J_2$  and  $J_3$  in the two-dimensional case. Consequently these terms may be neglected in simplified models. In contrast the ring exchange which appears in the two-dimensional calculation turns out to be rather important. Thus this term has to be included in an appropriate description of high- $T_C$  cuprates.

Besides the spin terms the generalized  $t$ - $J$  model contains various hopping terms and the interaction and motion of holes and doubly occupied sites. For the two-dimensional square lattice we observe that the spin dependent hopping term between diagonal neighbors is as important as its spin independent equivalent.

The sCUT is performed using different generators. In contrast to the MKU generator the  $0n$  and the  $0n1n$  generator only decouple certain subspaces from the rest. The  $0n$  generator is restricted to the ground state sector. Although this generator includes a significantly smaller amount of terms, it seems to capture the most important contributions to the spin terms. Even for the interaction terms the results of the  $0n$  generator show a good agreement with the results of the other generators although this sector is not part of the  $0n$  generator. The results for the density-density interaction term  $V_n''$  obtained by the  $0n$  generator stay below 7 percent even for larger values of  $W/U$ . Conclusively we can state that it is sufficient to use the  $0n$  generator when only the dominant parts of the effective model should be considered. Using the  $0n$  generator instead of the MKU generator simplifies the calculation as less terms are created during the flow.

The deviations of the results obtained with the  $0n1n$  generator from the results obtained with the MKU generator are even smaller. The relative deviations stay below a few percent. The relative deviation for the coupling constant  $V_n''$  stays below 1.2 percent for  $W/U = 1$ .

In the case of hole doping a new term is introduced describing the chemical potential

$\mu$ . In leading order this coefficient is proportional to  $\frac{t^2}{U}$ . For this coefficient a universal formula describing  $\mu$  in dependence of the coordination number  $z$  and the dopant concentration  $\delta$  is found analytically for a nearest neighbor calculation. Besides this the coefficients of higher truncation schemes are calculated in dependence on  $\delta$ . Under the influence of doping the most important coefficients show a deviation from results in the undoped system about a few percent.

The different generators are also applied to the doped case. There we find that the deviations of the coupling constants derived by the use of the  $0n$  generator are bigger than the ones obtained by the  $0n1n$  generator. The deviations of the  $0n$  generator increase with higher values of  $W/U$  and with the doping concentration  $\delta$ . With a higher  $\delta$  the interaction of holes becomes more important. Thus the results of the  $0n$  generator show higher deviations for higher values of  $\delta$ .

For the  $0n1n$  generator even the double plaquette calculation can be performed. During this calculation the ROD shows divergent behavior for values of  $W/U \geq 1.6$ . As a diverging ROD indicates the breakdown of the mapping we examine the limitations of the transformation in section 6. The mapping is possible as long as the apparent charge gap is positive. An estimate for the gap is found by the use of the Liouville formulation of the Lanczos method. In the one-dimensional case smaller values for the gap are found than in the two-dimensional case. Thus the gap seems to close earlier in one dimension than in two.

Due to the vast amount of terms only a few iterations were feasible. Linear extrapolations in  $\frac{1}{n}$  and  $\frac{1}{\sqrt{n}}$  with  $n$  denoting the number of iterations provide additional estimates for the gap.

The results obtained in this context induce that the mapping is valid for values of  $W/U \leq 0.8$ .

We were also able to study the influence of doping on the apparent charge gap. In this case we observe an earlier closure of the gap under the influence of doping.

By the use of this method one could calculate the value of  $\delta$  above which the system is no longer governed by the interactions between the electrons. If  $\delta$  is too high the insulator is no longer the appropriate reference. In this case the system has to be seen as a system of itinerant electrons for which a mapping to an effective model conserving the number of DOs is not possible. This would be seen in a gap that closes for very small values of  $W/U$ .

Additionally further calculations including more iterations for the Lanczos method could be performed. The results obtained in such a calculation can be used to decide which of the extrapolation schemes used in this thesis is most appropriate.

Besides the results of the gap for higher truncation schemes and different generators could be examined.

Furthermore the program structures developed in this work can be used to describe other models containing interacting fermions and bosons in real space. The only condition to be fulfilled is that the most important processes have to be local.

## 8. Abstract

In this thesis the Hubbard model is studied in the half-filled case as well as in the case of hole doping. The model is analyzed in real space on a one dimensional linear chain and on a two dimensional square lattice. For this purpose *self-similar continuous unitary transformations* (sCUTs) are used. Applying this method to the original model an effective Hamiltonian is derived, whose structure is imposed by the chosen generator. During the transformation with the generators used in this work charge fluctuations are eliminated. The self-similar approach to the flow equation method relies on classifying terms according to their structure. In contrast to a perturbative treatment the results obtained in this thesis are valid also for larger values of the Hubbard repulsion  $U$ .

The truncation scheme which is meant to limit the amount of new terms is based on the representation of the terms in real space. In order to decide whether a term should be kept or not its spatial extension has to be determined. Therefore the terms are normalordered with respect to a predefined reference ensemble. As this reference ensemble represents magnetically disordered phases, the effective model does not favor a certain spin direction.

Applying the sCUT method to the Hubbard model an effective generalized  $t$ - $J$  model can be derived. The derivation of the  $t$ - $J$  model is not based on perturbation theory. Consequently the  $t$ - $J$  model is not restricted to a particular parameter range. Beyond the usually considered spin terms and hopping terms of various expansions the generalized  $t$ - $J$  model provides a systematic treatment of the motion and interaction of holes or doubly occupied sites.

The choice of the generator is decisive for the structure of the effective model. In a first approach we use the MKU generator, which preserves the block diagonality and leads to an effective model conserving the number of doubly occupied sites and holes. In the second approach we use the  $0n$  and the  $0n1n$  generator. These choices of the generator are accounted for by the fact, that the  $t$ - $J$  model describes the low energy sectors best. By the use of the  $0n$  ( $0n1n$ ) generator we obtain an effective model in which only the sector without quasiparticles (and the sector with one quasiparticle) is decoupled from the other sectors.

In the case of a nearest neighbor calculation a universal formula describing the coupling constants for all types of lattices and all coordination numbers  $z$  can be derived analytically. This formula is also valid in the limit of a coordination number  $z = \infty$ . In the doped case a similar calculation yields the dependence of the coupling constants on the doping concentration  $\delta$ .

For the other truncation schemes we obtain values for the effective coupling constants as

function of  $W/U$  for different doping concentrations. From these coefficients the relevance of a term for the effective model can be estimated. Besides, the influence of the different generators on these coefficients are studied.

The program written for the present project can be applied to systems of interacting fermions and bosons in the half-filled and in the doped case. The only restriction imposed to the system is that the physics has to be governed by local processes.

In the last part of this thesis we examine the limitations of the mapping to the effective  $t$ - $J$  model. On this account the dispersion of a doubly occupied site moving above the spin background is determined. As the ground state sector of the  $t$ - $J$  model is a highly degenerate subspace we use the Liouville formalism for this purpose. In this way an upper bound for the charge gap is derived depending on the value of  $W/U$ . This results in an estimate for the transition of a doped insulator to a metal. In the doped case we obtain the dependence of the transition on the doping concentration.

## A. Additional results for the coupling constants in 2d for different generators

Coefficient of the density-density interaction between next nearest neighbors  $V'_n$  defined in Eq. 4.8.6 ( figure A.1) and the deviation of the results for different generators from the MKU results.

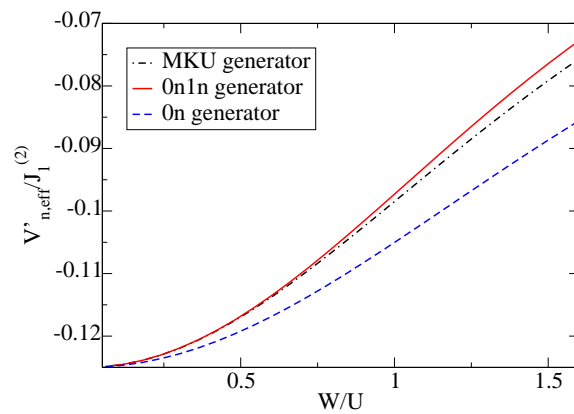


Fig. A.1.: Results for  $V'_n$  for different generators

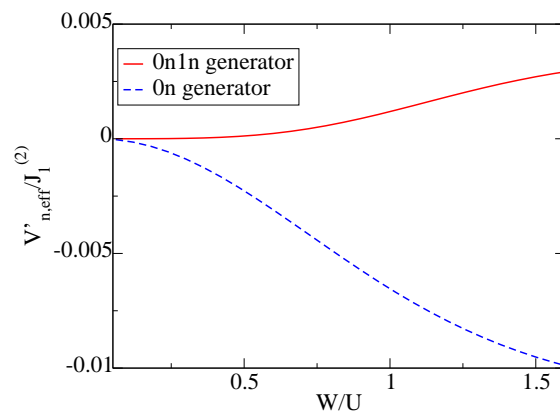


Fig. A.2.: Deviation of the results for different generators from the MKU result.

The cross exchange

$$H_{\times} = J_{\times} \sum_{\langle i,j,k,l \rangle} (\vec{S}_i \vec{S}_k) (\vec{S}_j \vec{S}_l). \quad (\text{A1})$$

for different generators is shown in Fig. A.3.

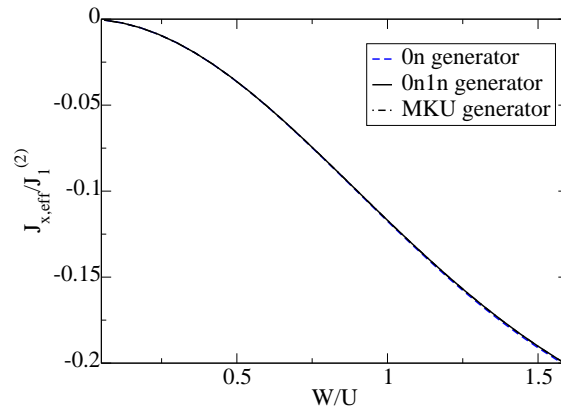


Fig. A.3.: Deviation of the results for different generators from the MKU result.

Figure A.4 depicts the deviation of the results for the  $0n$  and the  $0n1n$  generator from the result obtained by the use of the MKU generator.

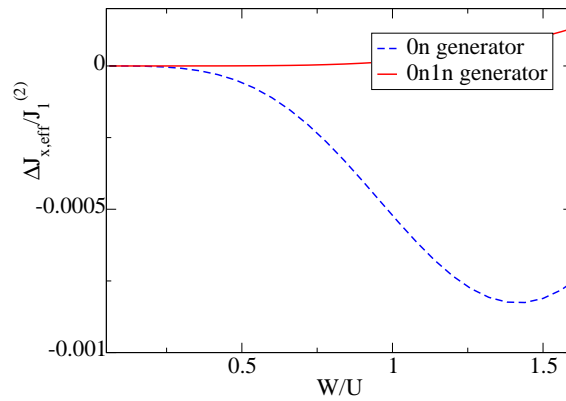


Fig. A.4.: Deviation of the results for different generators from the MKU result.

## Bibliography

- [And87] P.W. Anderson. The Resonating Valence Bond State in  $\text{La}_2\text{CuO}_4$  and Superconductivity. *Science*, **235** 1196, 1987.
- [BM86] J.G. Bednorz and K.A. Müller. Possible high- $T_c$  superconductivity in the Ba-La-Cu-O system. *Z. Phys. B*, **64** 189, 1986.
- [BR70] W.F. Brinkman and T.M. Rice. Singe-Particle Excitations in Magnetic Insulators. *Phys. Rev. B*, **2** 1324, 1970.
- [Dag94] E. Dagotto. Correlated lectrons in high-temperature superconductors. *Rev. Mod. Phys.*, **66** 763, 1994.
- [DEO08] C.M. Dawson, J. Eisert, and T.J. Osborne. Unifying variational methods for simulating quantum many body systems. *Phys. Rev. Lett.*, **100** 130501, 2008.
- [DHS03] A. Damascelli, Z. Hussain, and Z.-X. Shen. Angle-resolved photoemission studies of the cuprate superconductors. *Rev. Mod. Phys.*, **75** 473, 2003.
- [DU04] S. Dusuel and G.S. Uhrig. The quartic oscillator: a non-perturbative study by continuous unitary transformations. *J. Phys. A: Math. Gen.*, **37** 9275, 2004.
- [EGK<sup>+</sup>03] M.P. Eastwood, F. Gebhard, E. Kalinowski, S. Nishimoto, and R.M. Noack. Analytical and nuemrical treatment of the Mott-Hubbard insulator in infinite dimensions. *Eur. Phys. J. B*, **35** 155, 2003.
- [Eme87] V.J. Emery. Theory of high- $T_c$  superconductivity in oxides. *Phys. Rev. Lett.*, **58** 2794, 1987.
- [FDU] T. Fischer, S. Duffe, and G.S. Uhrig. *to be published*.
- [Fis07] T. Fischer. Beschreibung von Quantendimermodellen mittels kontinuierlicher unitärer Transformationen. *diploma thesis*, 2007.
- [FL82] P. Fulde and W.-D. Lukas. On the Computation of Electronic Excitations in Solids. *Z. Phys. B*, **48** 113, 1982.
- [Frö52] H. Fröhlich. Interaction of Electrons with Lattice Vibrations. *Proc. Roy. Soc. A*, **215** 291, 1952.
- [Ful91] P. Fulde. Electron Correlations in Molecules and Solids. *Solid-State Sciences, Springer Verlag Berlin Heidelberg*, , 1991.
- [Geb97] F. Gebhard. The Mott Metal-Insulator Transition. *Springer Tracts in Modern Physics*, **137**, 1997.
- [GKKR96] A. Georges, G. Kotliar, W. Krauth, and M.J. Rozenberg. Dynamical mean-field theory of strongly correlated fermion systems and the limit of infinite dimensions. *Rev. Mod. Phys.*, **68** 1, 1996.

- [Gut63] M.C. Gutzwiller. Effect of Correlation on the Ferromagnetism of Transition metals. *Phys. Rev. Lett.*, **10** 159, 1963.
- [GW93] S. D. Glazek and K. G. Wilson. Renormalization of Hamiltonians. *Physical Review D*, **48(12)** 5863, 1993.
- [GW94] S. D. Glazek and K. G. Wilson. Perturbative renormalization group for Hamiltonians. *Physical Review D*, **49(8)** 4214, 1994.
- [HDU] S.A. Hamerla, S.-L. Drechsler, and G.S. Uhrig. Nonperturbative Hubbard-Heisenberg model mapping at arbitrary dimension (coordination number): the effective nearest neighbor exchange. *to be published*.
- [HU02] C.P. Heidbrink and G.S. Uhrig. Renormalization by continuous unitary transformations: one-dimensional spinless fermions. *Eur. Phys. J. B*, **30** 443, 2002.
- [Hub63] J. Hubbard. Electron correlations in narrow energy bands. *Proc. Roy. Soc.*, **276** 238, 1963.
- [Hub64] J. Hubbard. Electron correlations in narrow energy bands III. An improved solution. *Proc. Roy. Soc.*, **281** 401, 1964.
- [IFT98] M. Imada, A. Fujimori, and Y. Tokura. Metal-insulator transitions. *Rev. Mod. Phys.*, **70** 1039, 1998.
- [JFP95] M. Jarrell, J.K. Freericks, and Th. Pruschke. Optical conductivity of the infinite-dimensional Hubbard model. *Phys. Rev. B*, **51** 17, 1995.
- [Kan63] J. Kanamori. Electron Correlation and Ferromagnetism of Transition Metals. *Prog. Theor. Phys.*, **30** 275, 1963.
- [Keh06] S. Kehrein. The Flow Equation Approach to Many-Particle Systems. *Springer tracts in modern physics*, **217**, 2006.
- [KK02] A.A. Katanin and A.P. Kampf. Spin excitations in  $\text{La}_2\text{CuO}_4$  : Consistent description by inclusion of ring exchange. *Phys. Rev. B*, **66** 100403, 2002.
- [KM94] S. Kehrein and A. Mielke. Flow equations for the Anderson Hamiltonian. *J. Phys. A: Math. Gen.*, **27** 4259, 1994.
- [KSU03] C. Knetter, K.P. Schmidt, and G.S. Uhrig. The Structure of Operators in Effective Particle-Conserving Models. *J. Phys.:Condes. Matter*, **36** 7889, 2003.
- [KU00] C. Knetter and G.S. Uhrig. Perturbation theory by flow equations: dimerized and frustrated  $s = 1/2$  chain. *Eur. Phys. J. B*, **13** 209, 2000.
- [LES99] J. Lorenzana, J. Eroles, and S. Sorella. Does the Heisenberg Model Describe the Multimagnon Spin Dynamics in Antiferromagnetic CuO Layers? *Phys. Rev. Lett.*, **83** 5122, 1999.
- [Lif64] I.M. Lifshitz. The Energy Spectrum of Disordered Systems. *Adv. Phys.*, **13** 483, 1964.
- [LNW06] P.A. Lee, N. Nagaosa, and X.-G. Wen. Doping a Mott insulator: Physics of high-temperature superconductivity. *Rev. Mod. Phys.*, **78** 17, 2006.
- [Lor] N. Lorscheidt. Systematische Ableitung des allgemeinen t-J Modells aus dem Hubbard-Modell abseits halber Füllung.

- [LW68] E.H. Lieb and F.Y. Wu. Absence of mott transition in an exact solution of the short-range, one-band model in one dimension. *Phys. Rev. Lett.*, **20** 1445, 1968.
- [MC90] A.J. Millis and S.N. Coppersmith. Interaction and doping dependence of optical spectral weight of the two-dimensional Hubbard model. *Phys. Rev. B*, **42** 10807, 1990.
- [MC91] A.J. Millis and S.N. Coppersmith. NONCONVERGENCE OF THE  $t/U$  EXPANSION IN THE METALLIC PHASE OF THE HUBBARD MODEL. *Sol. State Comm.*, **79** 1043, 1991.
- [MGY88] A.H. MacDonald, S.M. Girvin, and D. Yoshioka.  $t/U$  expansion for the Hubbard model. *Phys. Rev. B*, **37** 9753, 1988.
- [Mie92] P.v. Miegheem. Theory of band tails in heavily doped semiconductors. *Rev. Mod. Phys.*, **64** 755, 1992.
- [Mie98] A. Mielke. Flow equation for band-matrices. *Eur. Phys. J. B*, **5** 605, 1998.
- [Mor65] H. Mori. Transport, Collective Motion, and Brownian Motion. *Prog. Theor. Phys.*, **33** 423, 1965.
- [Mot90] N.F. Mott. Metal-Insulator Transitions. *Taylor and Francis, London*, , 1990.
- [MSV92] W. Metzner, P. Schmit, and D. Vollhardt. Hole dynamics in a spin background: A sum-rule-conserving theory with exact limits. *Phys. Rev. B*, **45** 2237, 1992.
- [MVM04] M. Müller, T. Vekua, and H.-J. Mikeska. Ring exchange in low-dimensional spin systems. *J. Mag. Mag. Mat.*, **272** 904, 2004.
- [NGJ03] S. Nishimoto, F. Gebhard, and E. Jeckelmann. Dynamical density-matrix renormalization group for the Mott-Hubbard insulator in high dimensions. *Eur. Phys. J. B*, **35** 155, 2003.
- [RMHU04] A. Reischl, E. Müller-Hartmann, and G.S. Uhrig. Systematic mapping of the Hubbard model to the generalized  $t$ - $J$  model. *Phys. Rev. B*, **70** 245124, 2004.
- [Ste97] J. Stein. Flow equations and the strong-coupling expansion for the Hubbard model. *J. Stat. Phys.*, **88** 487, 1997.
- [Tak77] M. Takahashi. Half-filled Hubbard model at low temperature. *J. Phys. C*, **10** 1289, 1977.
- [VM94] V.S. Viswanath and G. Müller. The Recursion Method; Application to Many-Body Dynamics. *Lecture Notes in Physics, Springer Verlag Berlin Heidelberg*, , 1994.
- [Weg94] F. J. Wegner. Flow-equations for Hamiltonians. *Annalen der Physik*, **3** 77, 1994.
- [ZPB02] R. Zitzler, Th. Pruschke, and R. Bulla. Magnetism and phase separation in the ground state of the Hubbard model. *Eur. Phys. J. B*, **27** 473, 2002.
- [ZR88] F.C. Zhang and T.M. Rice. Effective Hamiltonian for the superconducting Cu oxides. *Phys. Rev. B*, **37** 3759, 1988.
- [ZS95] Q.F. Zhong and S. Sorella. Low-energy and dynamical properties of a single hole in the  $t$ - $j_z$  model. *Phys. Rev. B*, **51** 16135, 1995.



## Danksagungen

An erster Stelle möchte ich Herrn Prof. Dr. Götz S. Uhrig danken ohne den eine Bearbeitung dieses spannenden Themas nicht möglich gewesen wäre. Ich möchte ihm besonders für die hervorragende Betreuung auch während seiner Zeit in Australien danken und für die immer neuen Denkanstöße.

Herrn Prof. Dr. Weber möchte ich dafür danken, dass er die Rolle des Zweitgutachters übernommen hat.

Sebastian Duffe und Tim Fischer möchte ich für die vielen Diskussionen und vor allem auch für das Korrekturlesen von Teilen der vorliegenden Arbeit danken. Desweiteren danke ich meinen Arbeitskollegen für ihre Hilfsbereitschaft und die angenehme Atmosphäre. Besonderer Dank gilt dabei Carsten Raas der mir bei meinem Kampf gegen die Doppelplakete zur Seite stand.

Ganz besonders möchte ich mich bei meiner Familie bedanken, die immer für mich da ist und immer an mich glaubt. Vielen Dank für eure Unterstützung in jeglicher Hinsicht.

Nicht zu letzt möchte ich mich bei meinen Freunden für die schöne Zeit (auch auerhalb der Universität) danken und dafür dass sie immer wieder für Abwechslung gesorgt haben.

## **Erklärung**

Hiermit erkläre ich, dass ich die vorliegende Arbeit selbständig verfasst habe und dabei keine anderen als die angegebenen Quellen und Hilfsmittel verwendet sowie Zitate kenntlich gemacht habe.

Simone Anke Hamerla